UNIVERSITÀ DEGLI STUDI DI PARMA

FACOLTÀ DI FARMACIA

DOTTORATO DI RICERCA IN

BIOFARMACEUTICA-FARMACOCINETICA

MICROPARTICULATE DRUG DELIVERY SYSTEMS BASED ON HYDROPHILIC POLYMERS OBTAINED WITH A SUPERCRITICAL CO_2 PROCESS

Tutore:

Chiar.mo Prof. Ruggero Bettini

Coordinatore:

Chiar.mo Prof. Paolo Colombo

Tesi di Dottorato:

Irene Pasquali

XX CICLO 2005-2007

To my family and Nicola

List of papers discussed

This thesis includes the paper listed below:

1. I. Pasquali, R. Bettini, F. Giordano, Solid-State Chemistry and Particle Engineering with Supercritical Fluids in Pharmaceutics, Eur. J. Pharm. Sci., 27, 299-310 (2006).

2. I. Pasquali, R. Bettini, F. Giordano, Supercritical fluid technologies: an innovative approach for the manipulation of the solid-state of pharmaceuticals, *Adv. Drug Del. Rev*. In press, doi: 10.1016/j.addr.2007.08.030.

3. I. Pasquali, L. Comi, F. Pucciarelli, R. Bettini, Swelling, melting point reduction and solubility of PEG 1500 in supercritical CO_2, *Int. J. Pharm*, in press, doi:10.1016/j.ijpharm.2007.12.048.

4. I. Pasquali, J.-M. Andanson, S. G. Kazarian, R. Bettini, Measurement of CO_2 sorption and PEG 1500 swelling by ATR-IR spectroscopy, *J. Supercrit. Fluids*, accepted.

5. I. Pasquali, J.-M Andanson, S. G. Kazarian, R. Bettini, Solubility of diazepam in PEG 1500 under supercritical CO_2 by FT-IR spectroscopy, in preparation for *Int. J. Pharm*.

6. I.Pasquali, R. Bettini "Are pharmaceutics really going supercritical?" Invited review for *Int. J. Pharm*., in preparation

7. I. Pasquali, L. Pezzini, R. Menabeni, R. Bettini, Diazepam microparticles with improved biopharmaceutical properties obtained with PGSS method, in preparation for *Eur. J. Pharm. Biopharm.*

Contents

1. Introduction

The founders of "Pharmaceutics" brought the science of physical chemistry to drug delivery, recognizing "Pharmaceutics" as the science of rationale dosage form development.

The design and the production of effective, stable, uniform and safe dosage forms that contain exact quantities and specific qualities of active pharmaceutical ingredients (APIs) is the primary mission of the pharmaceutical industry. The quality of a product is strongly related to and influenced by its design in research and development.

In the case of the solid dosage form a great attention has been paid, in recent years, on particle engineering defined as the discipline enabling the scientist to design solid dosage forms tailored to possess optimal physico-chemical characteristics (Pasquali et al., 2006). Specific characteristics of particles (size, shape, surface, crystal structure and morphology) are among the important factors to control technological and biopharmaceutical properties of drug products. In general, morphology (crystal habit) can influence the physical and chemical stability of solid dosage forms, a narrow size distribution is important to obtain content uniformity, while sphericity allows good flowability and tablettability. Furthermore, micronisation increases the surface area with a consequent increase of dissolution rate and bioavailability of the drug, thus promoting the formulation of active principle ingredients which may be insoluble or slightly soluble in aqueous media. Finally, the increase of bioavailability maximizes the efficiency of the drug and hence minimizes the required dosage.

Technological and biopharmaceutical characteristics can also be improved by co-formulation of the API with polymers. Co-formulations are used to increase (fast-release) or decrease (sustained release) the dissolution rate of the drug, for taste-masking, where a drug is co-formulated to remove or disguise an unpleasant taste, and in general to improve technological characteristics such as: sphericity, flowability, tabletability etc.

Formulation of drug delivery systems implies the challenge of producing particles with optimal physico-chemical characteristics, especially in the case of an administration by parenteral or inhalation route. For inhalation route, particles with a size less then 5 μm, narrow particle size distribution, appropriate aerodynamic size, shape and apparent density are required. Whilst is crucial to control the aerodynamic particle size, it is also important to control the surface properties as micronized tend to be highly charged leading to agglomeration. Furthermore, some techniques used to reduce particle sizes (milling, spray-

drying) damage the crystal structure of the drug leading to total or partial amorphisation, which leads to the physical instability of the drug.

Meanwhile, there is a continuous effort to develop processes pollution-free, with low environmental impact. Numerous pharmaceutical processes use volatile organic compound (VOC) as medium for preparation of drug delivery systems, but VOCs emission limit are being reduced in many industrialised countries, for example the European Union legislation came into force in 2000 (Hay et al., 2002). Furthermore, the "green" alternatives has become very important, especially in case of pharmaceutical industries, because the regulatory requirements are more and more restrictive for the residual contents of volatile organic compounds in the API and in the final products. A "green" solvent, alternative to traditional solvents, may lead both to a technical and commercial benefits.

A relatively recent approach for obtaining pharmaceutical microparticles with desired physico-chemical characteristics is represented by technologies based on the supercritical fluids (SCF). By proper adjustment of the operating conditions as well as physical and chemical parameters, (pressure, temperature, drug concentration, flow and nature of supercritical fluid and organic solvent) materials with desired biopharmaceutical and technological characteristics can be generated. Advantages in the use of supercritical fluids technology are the high versatility, the flexibility in offering alternative processing approaches, the possibility to avoid or minimize the use of organic solvents and to reach peculiar process conditions (i.e., change in the pressure and in the rate of solvent evaporation) difficult to obtain with traditional processes (Pasquali et al., in press-b). In fact, the most discernible process parameters that differentiate the SCF technologies from the conventional ones are the high compressibility and diffusivity of the supercritical fluid, the possibility of fine tuning pressure and solvent evaporation rate.

Great attention is given to the SCFs also in the field of polymer processing (Nalawade et al., 2006a). Most of the beneficial effects of SCF in the polymers processing are due to the possible weak interaction of CO_2 with the macromolecular chains of the polymer. As demonstrated by some authors (Kazarian et al., 1996, Nalawade et al., 2006b, Pasquali et al., in press-a), CO_2 is a weak Lewis acid that may interact with the basic sites in the polymer leading to the absorbtion of significant amount of CO_2. The absorption of the gas results in an increase of the inter-chain distances as well as of the degree of chains-segmental mobility causing a polymer plasticization and a decrease of the polymer viscosity. The property of CO_2 to reduce the glass transition temperature and viscosity of

the polymer would be beneficial for enhancing in the processing of composite materials during mixing, homogenization, coating, extrusion and foaming.

Polymer plasticization can be also induced thermally or by means of organic solvents. Major drawbacks of these approaches are the difficulty to process heat-sensitive materials and the possible presence of residues solvent in the final product. By using the SCF, there is no residual solvent in the material produced, in fact, being a gas at ambient condition, it can easily be removed from the final product.

The application of the SFC technology in the control of physico-chemical properties of drug particles (Pasquali et al., 2006, Pasquali et al., in press-b) and the production of controlled-release drug formulations seems to have at the moment a big development, as reflected by the large number of patents granted in this area.

Despite the numerous advantages in the use of SCF, it must be stated that these techniques are not going to replace existing and well-established techniques (solvent coating, granulation, spray-drying, etc.); but more likely they are going to support them.

One of the major drawbacks of the SCF techniques presently represented by the high cost of the equipments. This can be mainly ascribed to the fact that the field is still young and the SCF technologies are not yet widespread.

1.1. Supercritical fluids properties

In 1822, Cagniard de la Tour first put into evidence the existence of a supercritical phase by observing the disappearance of two distinct gas and liquid phases into one visually homogeneous phase by increasing the temperature of a material in a closed glass container (Cagniard de LaTour, 1822).

The first report that describes a process using the supercritical fluid as a medium for obtaining solid materials was published by Hannay and Hogarth: *" We have then, the phenomenon of a solid with no measurable gaseous pressure, dissolving in a gas. When the solid is precipitated by suddenly reducing the pressure, it is crystalline, and may be brought down as snow in the gas, or on the glass as a frost, but it is always easily redissolved by the gas on increasing the pressure"* (Hannay and Hogarth, 1879).

A supercritical fluid can be defined as a dense non-condensable fluid.

A fluid reaches the supercritical status when its temperature and pressure exceed the relevant critical temperature and pressure.

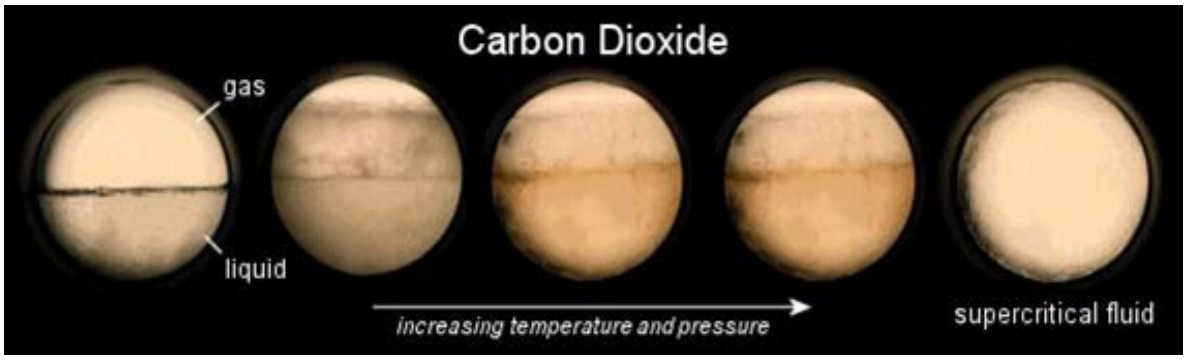

Figure 1: Images of the CO_2 at different pressure and temperature values (http://www.galenotech.org/tecniche_est.htm)

As it can be observed in Figure 1, below the critical point a liquid and a gas phase are separated by a meniscus; with an increase in temperature or pressure the meniscus begins to disappear. Further increase of temperature causes the gas and liquid densities to become similar. The meniscus is less easily observed but still evident. Once the critical temperature and pressure have been reached the two distinct phases (liquid and gas) are no longer visible. The macroscopic appearance of the SCF is a homogeneous and opalescent system without phase separation (single phase) because, at this point, the density of the gas and liquid are identical. Nevertheless, a SCF does not show a specific aggregation state; in fact its physico-chemical properties are intermediate between those of liquid and gas (Table 1).

Table 1. Physico-chemical characteristics of a substance as gas, liquid and SCF.
* standard condition (1 atm, 20 °C)
**at critical pressure and temperature

Physical state	*Density (g / ml)*	*Viscosity (g/cm·s)*	*Diffusivity (cm^2 / s)*
Gas*	10^{-3}	10^{-4}	10^{-1}
Liquid	1	10^{-2}	10^{-6}
SCF**	0.2 –0.8	10^{-4}	10^{-3}

Like a gas the SCF shows a lower viscosity and higher diffusivity relative to the liquid. These properties facilitate mass transfer and all related phenomena, so SCFs can diffuse and impregnate matrices like a gas. Like a liquid, the SCF shows a density value appreciable for the solvation power. Most importantly, the SCF is dense but highly

compressible, thus, any change of pressure alters its density and consequently the solvent power (Brunner, 1994). The greatest change of the solvent density is attained in the vicinity of the solvent's critical point, where the solvent compressibility is large, and small changes in pressure yield a large change in density (Figure 2).

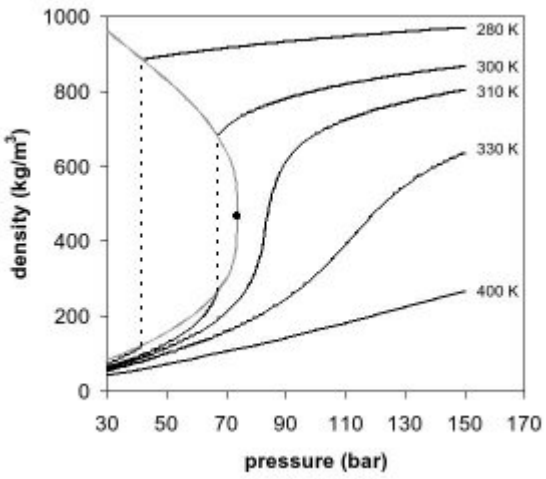

Figure 2. Carbon dioxide density-pressure phase diagram

At the microscopic level, the opalescence observed at the critical point can be interpreted considering the fluctuations of the local density with a correlation length of the same order of magnitude than that of the visible light. The inhomogenity is the most fundamental concept which characterizes the supercritical status, and the density fluctuations is a measure of the inhomogenity in the distribution of the molecules. It has been reported that there is likely a local organization of molecules inside the supercritical region with areas of local densities for both the gas and liquid (Nishikawa and Morita, 2000). This organization is dynamic and these fluctuations of density allow to explain the increase of the fluid compressibility. Inside the schematic phase diagram of CO_2 near the critical point, (Figure 3) it is possible to identify a ridge that separates the more liquid-like and more gas-like regions in the supercritical region.

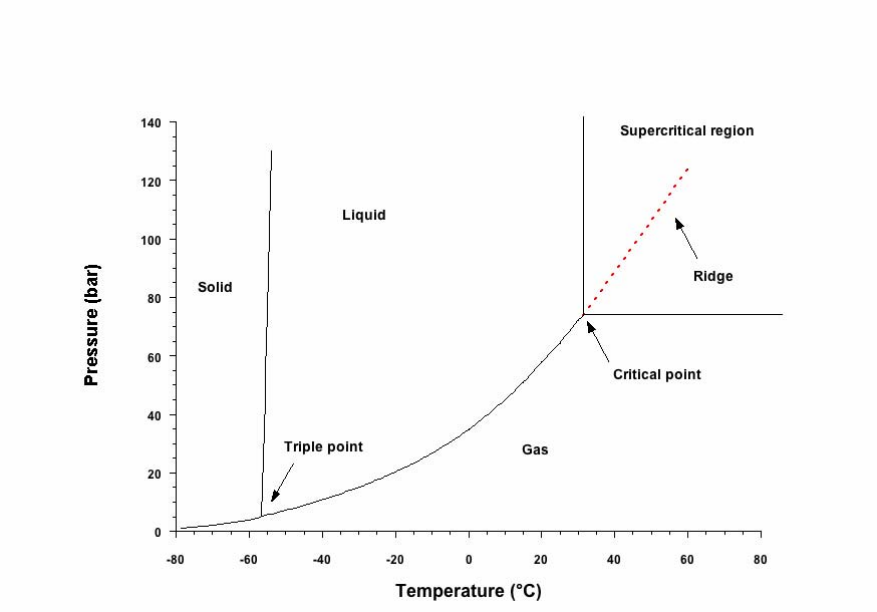

Figure 3. Schematic phase diagram of CO_2

The ridge corresponds to a maximum or minimum of various physical quantities of SCFs, which are related to the second derivates of the Gibbs free energy, such as isothermal compressibility, thermal conductivity, and partial molar volumes (Koga et al., 2006).

Although these unique and complementary physical characteristics allow the development of efficient and versatile processes, it should be underscored that the SCF can not be considered as the universal "super-solvent".

The peculiar characteristics of SCFs lead to a rapidly grown of the field, and of consequence, to important industrial applications (Perrut, 2000, Perrut, 2003). Except for processes applied in the petrochemical industry, supercritical fluids applications are mainly focusing on extraction/fractionation from solid materials for food products (coffee and tea), food ingredients (hops, aromas, coloring agents, vitamins, and unsatured fatty acids) and nutraceuticals/phytopharmaceuticals (Jung and Perrut, 2001, King and Bott, 1993, Perrut and Reverchôn, 2000, Perrut and Subra, 1998, Poliakoff et al., 1999, Rizvi, 1994). At present, supercritical fluids techniques are still expanding and new applications are being investigated. Some of them are listed below:

- *Ceramics manufacture*: preparation of a new generation of inorganic cross-flow membranes (Sarrade et al., 2003);
- *Reactions*: synthesis of complex organic molecules (Prajapati and Gohain, 2004);
- *Preparative Scale Supercritical Fluid Chromatography*: fractionation of very similar compounds, especially lipids;

- *Preparation of foams* (Alavi et al., 2003a, Alavi et al., 2003b) *and aerogels* (Fricke and Tillotson, 1997, Gross et al., 1998). *Various SF-processed nano-systems or nano-structured materials* for applications mainly in the micro-electronic industry; (Perrut, 2000)
- *Polymer processing:* impregnation, extraction of residues (stripping), morphological modifications (foams, particles, and fibers) and particle coating.

Among the new applications of SCFs, *particle engineering* of pharmaceutical materials seems to be at the moment the area with the major development.

All gases can be a SCF above specific sets of critical conditions (P,T), but it should be born in mind also that, for many cases, the transition to the supercritical state occurs at high temperatures not compatible with pharmaceutical compounds (e.g., SC water, Table 2).

Table 2: Critical parameters of selected compounds

	T_c (°C)	P_c (MPa)
H_2O	374	22
Xe	16.6	5.9
SF_6	45.5	3.8
N_2O	36.5	4.1
C_2H_4	9.1	5.1
CHF_3	25.9	4.7
CO_2	31.3	7.4

The critical P, T values increase with the molecular weight or intermolecular hydrogen bonding or polarity (Vasukumar and Bansal, 2003). Not only the mild processing conditions, but also safety and affordable economics are valid criteria to choose the supercritical fluid. For example, Xenon and SF_6 (when sufficiently purified), have low critical values, but they are still too expensive for commercial use. Gases as N_2O or ethane have low critical values, but can generate explosive mixtures and are therefore unsafe to handle. Some authors (Hillmann and Bächmann, 1995, Nakatani et al., 1989, Sako et al., 1989) used as SCF trifluoromethane (CHF_3) which is chemically inert, non-flammable, has

low toxicity and low critical temperature and pressure. Furthermore, CHF_3 has a strong permanent dipole moment (1.56 D) thus it can solubilize pharmaceutical compounds. However, more than 98 % of applications have been developed using carbon dioxide as SCF because of its low critical temperature (31,18 °C) and pressure (7.4 MPa), inexpensiveness, non–flammability, non-toxicity, recyclability and environmental benignity.

1.2. Processes using supercritical fluids

There are several methods based on the supercritical fluids for particles production, which can be divided into four groups.

i) Processes using supercritical fluids as solvent. The rapid expansion of a supercritical solution (RESS) is the process that exemplifies this first group. The supercritical fluid is used as crystallization solvent; in fact, with RESS the solute is first dissolved in a supercritical fluid, then the solution is rapidly expanded by sudden decompression, typically by passing through an orifice at lower pressure.

ii) Processes using supercritical fluids as antisolvent. In this case, the supercritical fluid (antisolvent) comes in contact with the solute dissolved in a suitable organic solvent. The crystal formation is due to the sharp decrease of the solvent power of the organic phase.

iii) Processes using supercritical fluids to assist the spray-drying thechnique. These techniques are close to the classic micronization by spray-drying, where the SCFs is used to assist the nebulization of the solution of the compound to be process.

iiii) Processes using supercritical fluids to precipitate molten material from gas saturated solution. The supercritical fluid is dissolved into a solution of a solute or into a melted material. Then, a rapid depressurization of the mixture, that occurs through a nozzle causing the particles formation.

1.2.1 Processes using supercritical fluids as solvent

RESS (Rapid Expansion Supercritical Solution)

Nearly a century later the discovery of Hannay and Hogarth, Krukonis first applied the concept of producing fine particles with a narrow size distribution using a SCF (Krukonis, 1984). This technique was called rapid expansion of a supercritical solution (RESS). A

typical RESS process is carried out with an apparatus consisting of a pre-heater, a solubilization vessel, and a precipitator (Figure 4).

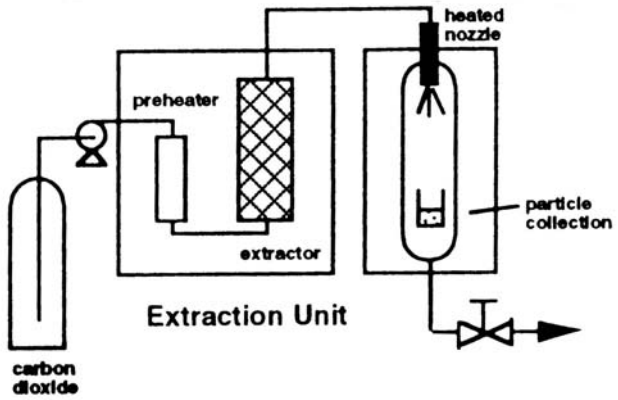

Figure 4. Schematic representation of RESS

The heated gas is pressurized and pumped into the solubilization unit (extractor), containing the solute. The supercritical fluid dissolves the solute; then the solution is rapidly expanded (decompressed) by passing through a heated nozzle at supersonic speed. During the rapid expansion of the supercritical solution, both density and solvent power decrease dramatically leading to a solute supersaturation. The solution reaches almost instantaneously, a highly homogeneous supersaturation with a degree of supersaturation often much higher than that achieved by thermal methods. The combination of large, rapid and uniform supersaturation is the major advantage of RESS and leads to the production of small particles with uniform size (Phillips and Stella, 1993)

The parameters that influence this process can be divided into pre- and post-expansion conditions. The pre-expansion conditions are temperature and pressure of the vessel. These operative parameters influence the kinetics of the crystallization process changing the density of the SCF and, consequently, the pre-expansion concentration. This last depends also on the supercritical fluid, the nature of the solute (crystalline or amorphous, composite or pure), and possible addition of a cosolvent. The higher the pre-expansion concentration, the narrower the particle size range will be (Phillips and Stella, 1993)

The post-expansion conditions depend on the nozzle temperature, geometry and size, distance and angle of impact against the surface of the jet stream (Kayrak et al., 2003) (Figure 5).

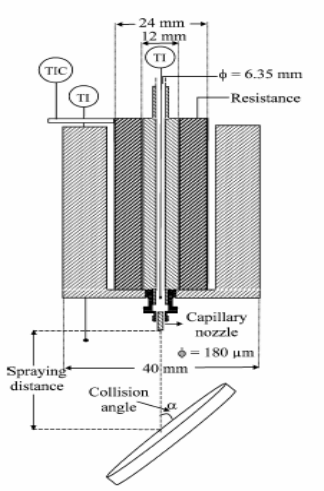

Figure 5. Schematic draw of the nozzle in the RESS process (Kayrak et al., 2003)

The nozzle can be maintained at a suitable pre-expansion temperature to prevent the premature precipitation of the solute.

The advantages of RESS are that it is a simple process, and relatively easy to implement on a small scale when a single nozzle is used. Another attractive characteristic of this process is its environmental benignity: it allows minimization of the use of organic solvent and the reuse the SCF in a continuous process. On the other hand, the main drawback, limiting the scaling of this process, is represented by the poor solubility of most pharmaceutical products in supercritical CO_2. The CO_2 is a non polar molecule with low molecular weight, scarcely able to dissolve drugs that, typically, are weak bases or acids and, therefore, show more or less pronounced polar characteristics. In the RESS technique, the solubility value, for obtaining a reasonable yield, should be in the order of 10^{-4} mole fraction. Otherwise, the low solubility can, in some instances, be overcome with appropriate tuning of the fluid density and/or using an adequate cosolvent. Cosolvents modify the polarity of the solvent phase in favour of the solute, thereby improving the solvent power. Enhancement factors values of 10^4-10^6 (defined as the measured solubility divided by the solubility in the SCF without cosolvent) are common, although even values as high as 10^{12} have been reported (Kompella and Koushik, 2001) Other limitations are poor predictive control of particle size and morphology along with the difficulty of scaling-up the process because of particle aggregation and nozzle blockage caused by cooling due to the rapid expansion of the supercritical solution (York, 1999).

RESOLV (Rapid Expansion of a Supercritical Solution into a Liquid Solvent)

The solution of the drug in liquid CO_2 is prepared inside a high pressure syringe pump. The solution is pumped into a heating unit to attain the desire temperature before the expansion through a laser-drilled orifice. The rapid expansion of the solution occurs into an aqueous medium at ambient pressure. Various water-soluble polymers could be added to the aqueous medium for stabilizing the nanoparticles suspension (Meziani et al., 2005).

1.2.2 Precipitation using supercritical fluids as antisolvent

Gallagher et al. (Gallagher et al., 1989) first proposed a SCF process alternative to RESS to overcome the limitation of poor solubility of most organic compounds in SC-CO_2. This technique was first tested to micronize explosives because milling generates high local temperatures, while the use of CO_2 as an antisolvent allowed to proceed at milder temperature. This method is based on the ability of a liquid to solubilize a large amounts of gaseous CO_2. The antisolvent must show a low affinity for the solute but at least partial miscibility with the organic phase. The nucleation and the consequent growth of crystals from the *solute/organic solvent/antisolvent* system are governed by the diffusion of the antisolvent into the organic phase and the evaporation of the organic solvent into the antisolvent phase (Figure 6).

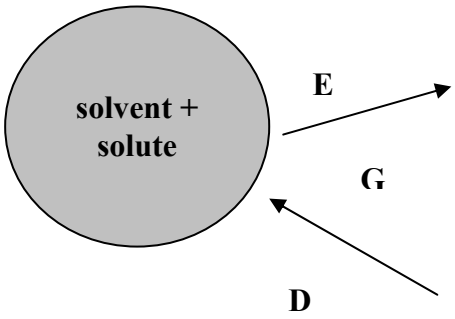

Figure 6. Single droplet (solvent + solute) as the smallest unit where the crystallization occurs. G gas (antisolvent), D diffusion of the antisolvent into the solution, E evaporation of the organic solvent into the antisolvent phase

The volume expansion caused by the antisolvent diffusion lowers the solubility of the solute due to density reduction. On the other hand, the solvent evaporation into the gas

phase increases the solute concentration. The combined phenomena lead to supersaturation, nucleation and particle formation (Bristow et al., 2001).

Contributions from thermodynamics, fluid dynamics, and nucleation kinetics are necessary to describe the antisolvent precipitation. Mass transfer coefficient governs the rate of mutual transport of the SCF into the solvent phase and *viceversa.* The relationship that describes the rate of mutual transport for component (N_i) is represented by a simple solution of the Fick's law,

$$N_i = K_{L,SC}\, a\, (C_{ie} - C) \qquad [1]$$

where, a is the mass transfer area, C_{ie} is the saturated concentration in the respective supercritical (SC) or liquid (L) phase, C is the concentration in the bulk liquid or SC phase, and $K_{L,SC}$ is the overall mass transfer coefficient either in the liquid or SC phase (Bristow et al., 2001).

Since crystallization is the opposite of dissolution, the diffusion theory (Brunner, 1904, Nernst, 1904, Noyes and Whitney, 1897) can be applied. Therefore, equation 2 holds for the solute mass transfer rate (N_{so}) over the crystal surface area, a_c :

$$N_{so} = K_{so}\, a_c\, (C_{ss} - C_s) \qquad [2]$$

here, C_{ss} is the supersaturated concentration and C_s is the solubility (both in the liquid phase), and K_{so} is the solute mass transfer coefficient (Figure 7).

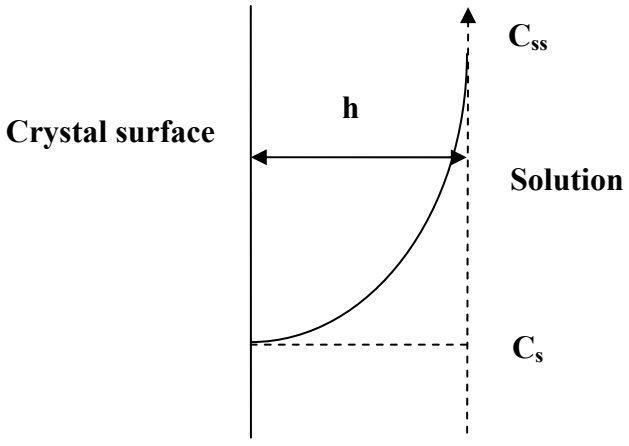

Figure 7. Scheme of the concentration profile at the crystal-supersaturated solution interface; C_s equilibrium concentration, C_{ss} supersaturated concentration, h thickness of the diffusional path lenght

To achieve a high supersaturation and thus particle formation level, the mass transfer rate has to be improved, by increasing the mass transfer area, the concentration gradient, or the SCF/solvent ratio.

As far as the surfacial mass transfer is concerned, it can be increased by spraying a phase into the other. In this case, the nucleation of the particle depends on the efficiency of the droplets generation. The distribution of the droplet size has to be as homogeneous as possible. The Weber number (N_{we}), which is the ratio between disruptive fluid dynamic and inertial forces and the shape maintaining interfacial forces, determines the droplet size.

$$N_{we} = \frac{\rho_A v_A^2 D}{\sigma} \qquad [3]$$

where ρ_A is the density of the antisolvent, v_A^2 is the relative velocity, D is the jet diameter and σ is the interfacial tension (Brunner, 1904). The higher the Weber number, the lower the droplet size and *viceversa.*

Another important factor that must be considered in an antisolvent process is the efficiency of the mixing between the SCF and the solution. The Reynolds number (N_{Re}) describes the mixing efficiency

$$N_{Re} = \frac{\rho v_s L}{\eta} \qquad [4]$$

where, ρ is the density of the fluid, v_s is the mean fluid velocity, L is the characteristic length (equal to the diameter if the cross-section is circular), and η is the fluid viscosity. It is possible to obtain a complete mixing at a high Reynolds numbers (> 10,000) that lead to dry particles with little agglomeration. In this situation, the flow is dominated by inertial forces, producing random eddies, vortices and other flow fluctuations (turbulent flow). At low Reynolds numbers, the viscous forces prevail, and the flow is characterized by smooth, constant fluid motion (laminar flow) (Shekunov et al., 1999). The nozzle geometry, the nature of the solvent and of the SCF are the main factors influencing the parameters described above. However, it must be underlined that the density of the antisolvent, which is one of the more easily tunable parameter (via temperature and/or pressure variation) in a SCF, can be considered the key factor of the process.

Since the driving force for crystallization is the supersaturation, other operative parameters, such as solute concentration, solvent to SCF ratio influence the characteristics of the product (Werling and Debenedetti, 1999).

The antisolvent process is a batch discontinuous process; its main disadvantage is the difficulty to reach a complete removal of the residual solvent. The regulatory authorities clarified that the amount of residual solvent in the crystallized powder must not exceed predetermined concentrations (USP 30, 2007). For this reason, a final washing step of the precipitated particles with supercritical CO_2 alone may be required to remove residual traces of organic solvents and to prevent condensation during depressurization.

Different experimental designs of antisolvent processes are known and can be classified on the basis of different mixing modes between the solution and the SCF.

GAS (Gaseous Anti Solvent)

GAS is a batch technique which entails the gradual introduction of CO_2 inside a vessel filled with the solution of the solute of interest (Figure 8).

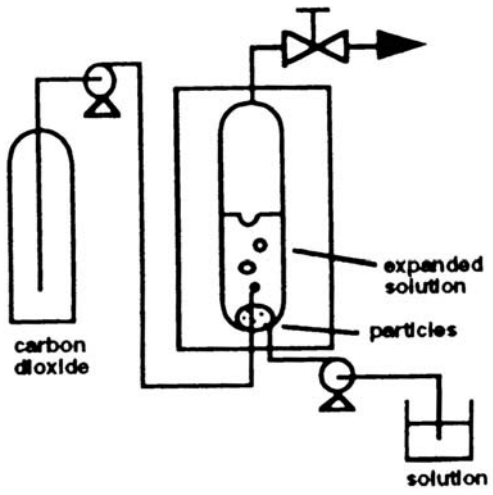

Figure 8. Schematic representation of GAS

The CO_2 is pumped in from the bottom of the vessel, until the fixed pressure is reached. The main advantage of this technique is that, by introducing the SCF through the bottom of the vessel, a good mixing of solvent and antisolvent can be reached.

PCA (Particles by Compressed Antisolvent), SAS (Supercritical Antisolvent), ASES (Aerosol Solvent Extraction System)

In these three arrangements CO_2 (supercritical for SAS, or subcritical for PCA) is first pumped inside the high pressure vessel until the system reaches the fixed conditions (pressure and temperature) Subsequently, the organic solution is sprayed through a nozzle into the SCF bulk and the particles are collected on a filter at the bottom of the vessel (Figure 9). ASES represents a modification implying the simultaneously spraying of the solution and antisolvent.

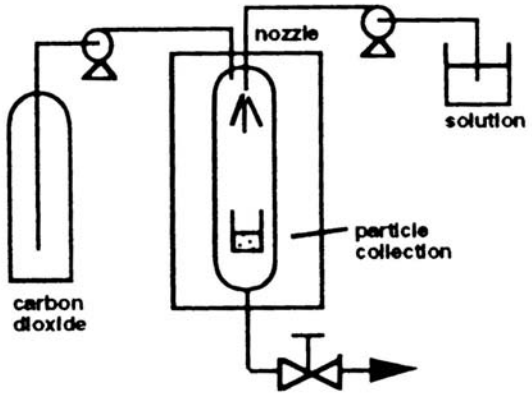

Figure 9. Schematic representation of PCA, SAS and ASES

SEDS (Solution Enhanced Dispersion by Supercritical Fluids)

SEDS is a technique developed by Hanna and York (Hanna and York, 1995). By this process the drug solution and the supercritical fluid are introduced simultaneously into the particle formation vessel through the mixing chamber of a co-axial nozzle (Figure 10 and 11).

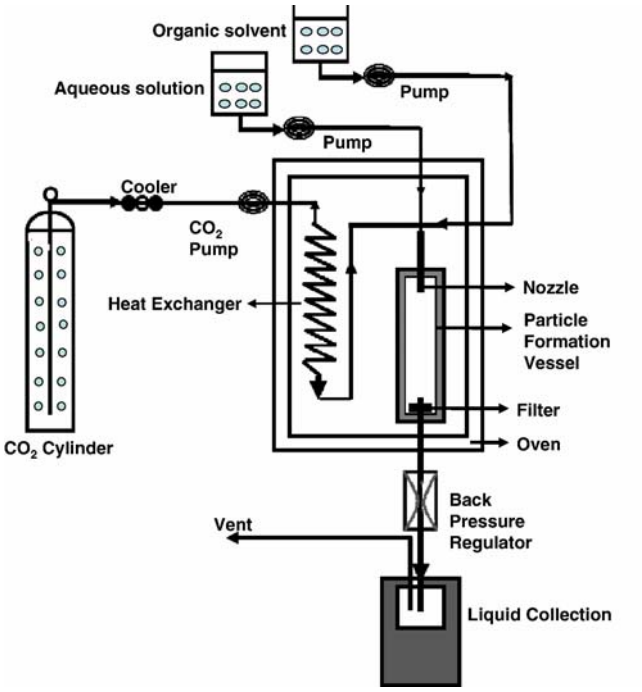

Figure 10. Schematic representation of SEDS (Byrappab et al., in press)

The geometry of the nozzle allows to work at high Reynolds numbers (good mixing) and at low Weber number (small droplet size) by increasing the velocity of the fluid. Moreover, the use of a mixing chamber favors a higher mixing surface area that leads to a increase of the mass transfer (rate of mutual transport N_i in eq. 1). The high mass transfer causes a fast nucleation rate and the production of particles of small size with little agglomeration (Palakodaty and York, 1999).

SEDS has been further developed to process water soluble compounds (e.g. peptides and proteins) by using a co-axial three-component nozzle (Figure 11). The organic solvent, the SCF, and the aqueous solution, as separate streams, are introduced by means of the nozzle inside the vessel. This arrangement helps in overcoming problems associated with limited solubility of water in supercritical CO_2 (Moshashaee et al., 2003).

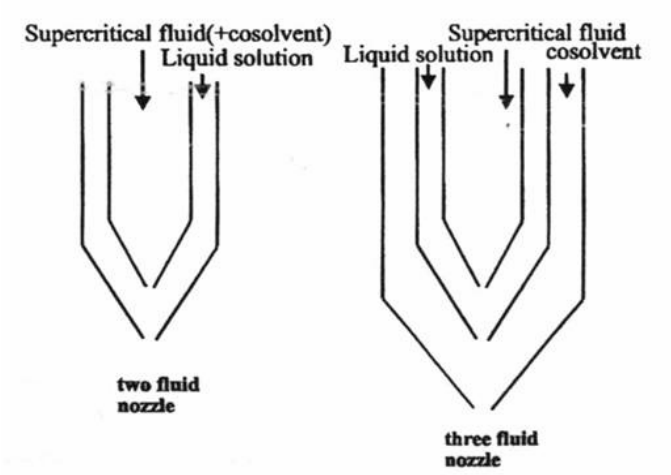

Figure 11. Schematic representation of coaxial two and three fluid nozzle

All these characteristics make SEDS a highly controlled, reproducible technique compared to other antisolvent-based SCF processes. Furthermore, SEDS process proved to be suitable for scaling up and manufacturing according to GMP requirements (York et al., 1998).

1.2.3 CO_2 -Assisted Spray-Drying

These techniques are aerosolization based methods where the supercritical CO_2 is used to assist the nebulization of the solution of the compound to be processed. The mechanism of the process is close to classic micronization by spray-drying: the SCF and the solution are intimately mixed and sprayed in a drying atmosphere. Claimed advantages of this process are: the minimal decomposition of thermally labile drugs, the absence of a high pressure vessel, and the small size of produced particles (below 3 μm in diameter) (Charbit et al., 2004).

CAN-BD (Carbon dioxide Assisted Nebulization with a Bubble Dryer®)

This process (Sievers and Karst, 2000) is particularly useful for substrates that are significantly soluble in water. Three steps are involved in the method. The drug is dissolved or suspended in water or alcohol (or both), and mixed intimately with near-critical or supercritical CO_2 by pumping both fluids through a near zero volume tee to generate an emulsion. The carbon dioxide does not solubilize the compound, but it is soluble in water. The emulsion expands through a flow restrictor into a drying chamber at

atmospheric pressure to generate aerosols of microbubbles and microdroplets that are dried by a flux of warm nitrogen (Figure 12).

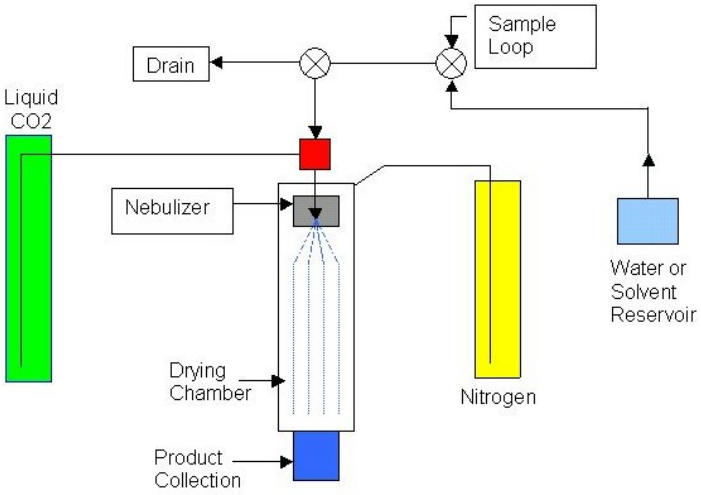

Figure 12. Schematic representation of CAN-BD

SAA (Supercritical Fluid-Assisted Atomization)

In this process (Reverchôn, 2002) supercritical CO_2 and a solution (in water or organic solvent) are mixed and sprayed into a vessel loaded with stainless steel perforated saddles that assures a large contact surface between liquid solution and the SCF, at conditions near the atmospheric pressure under a flow of hot N_2 (Figure 13).

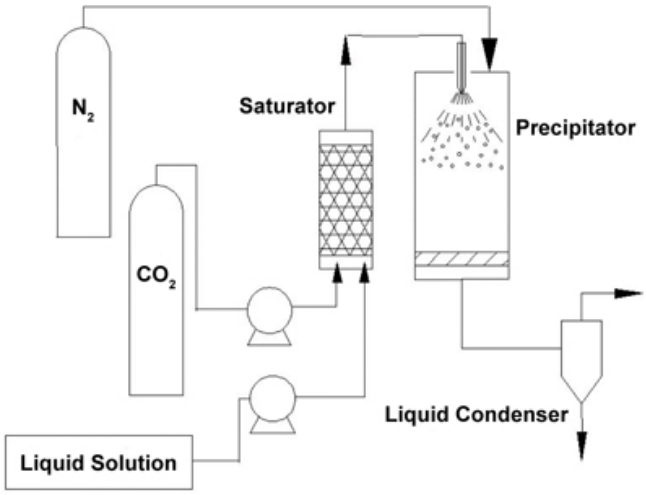

Figure 13. Schematic representation of SAA

The main differences between CAN-BD and SAA processes are the region where the mixing is achieved and the extent of solubilization of SC-CO_2 in the liquid solution where the solute is dissolved.

1.2.4 Precipitation from gas saturated solutions

These processes use the supercritical fluids to obtain a molten material or a ternary mixture solute-solvent-compressed gas that are depressurized by rapid reduction of the system to atmospheric pressure in an expansion chamber. PGSS is the method that exemplifies this group.

PGSS (Particle formation from Gas-Saturated Solutions)

In the PGSS, the compressed gas (super- or sub-critical) is dissolved into a solution of a solute or into a melted material. The gas-saturated solution presents a low viscosity due to an increase in free volume. Moreover, the interfacial tension between gas and the liquid phase is lowered as the surface tension of the gas in the supercritical state is near zero. The solution is then expanded over a nozzle from a supercritical status to ambient pressure. It causes a supersaturation of the gas and an intense expansion of the nucleated gas bubbles leading to explosion of the molten material into fine particles (Graser and Wickenhaeuser, 1982) (Figure 14).

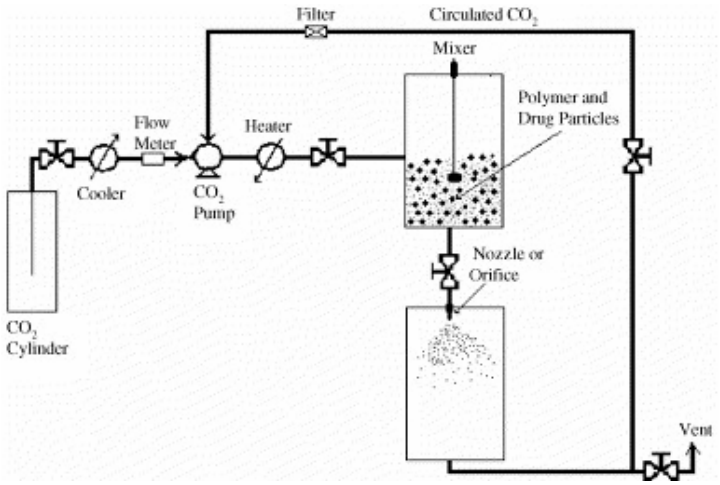

Figure 14. Schematic representation of PGSS

The advantages of this technique are numerous. The pressure used is lower than that used with RESS, the required amount of gas is smaller, no additional solvent is necessary, so no residual solvent traces can be found in the final product, it can work in continuous mode, while the antisolvent technique required a wash-out step to remove the solvent traces. Furthermore, because of the high solubility of the compressed gas, a good process yield can be obtained. An interesting case is represented by the use of the PGSS technique to process the polymers. It is well known that compressed CO_2 can act as a plasticizer and can decrease the melting point and/or glass transition of some polymers, (Kazarian, 2000, Kazarian et al., 2002, Pasquali et al., in press-c) so in this case, it is possible to use PGSS to load active substances on this melted polymer that form composite microspheres after decompression. The concept is simple and the substances both polymer and drug do not have to be soluble in the CO_2. The main drawbacks of this technique are the poor control of the particle size that can, in some cases, leads to a broad particle size distribution, moreover the high temperature that can be required to melt some polymers may damage thermolabile compounds. Anyway, the balance between advantages and drawbacks is positive, and the technique is promising, several plants are running with capacities of some hundred kilograms per hour (Natex, Austria, Thar Technologies, USA, Uhde HPT, Germany).

DELOS (Depressurization of an Expanded Liquid Organic Solution)

In the DELOS technique, the compressed gas acts as a cosolvent. In fact the CO_2 expands in an autoclave where a organic solution of the solute that has to be micronized is dissolved. Then the ternary mixture solute-solvent-compressed gas is depressurized by rapid reduction of the system pressure to atmospheric pressure in an expansion chamber (Ventosa et al., 2001, Ventosa et al., 2003) (Figura 15).

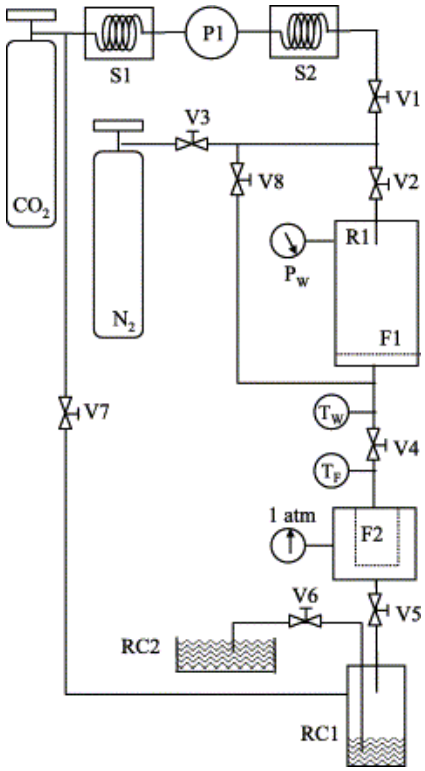

Figure 15. Scheme of the equipment used for DELOS experiments. P: pump; S: heat exchanger; V: valve; F: filter; R: high-pressure vessel; RC: recycling collector.

CPCSP (Continuous Powder Coating Spraying Process)

The CPCSP was proposed by Weidner et al., as an alternative technique for powder coating based on the PGSS (Weidner et al., 2001). In the CPCSP, the main components (binder and hardner) are melted in separated vessels to avoid a premature reaction of the polymers. The molten polymer are fed to a static mixer, here, the melts are homogenised with compressed carbon dioxide under pressure up to 220 bar. In the static mixtures, the three flows are not only intensively mixed, but a part of compressed gas dissolves in the polymer mixture. Then, the solution formed in the mixer expands via a nozzle to a spray tower.

A qualitative technological assessment of the different supercritical fluids based techniques is reported in the table 3.

Table 3. Technological features of different supercritical fluids based techniques

	RESS	GAS/SAS/PCA	PGSS
Process	Discontinuous	Semicontinuous	Continuous
Gas demand	High	Medium	Low
Pressure	High	Low to medium	Low to medium
Solvent	None	Yes	None
Volume of pressurized equipment	Large	Medium to large	Small
Separation gas/solid	Difficult	Easy	Easy
Separation gas/solvent	Not required	Difficult	Not required

1.3 Phase behaviour

When supercritical fluids based processes are used, it is important to take into account both the solid-fluid phase behaviour (solubility) and liquid-fluid phase behaviour (miscibility) to understand and be able to govern the process.

For a full understanding of the phase equilibria for mixtures, it is important to consider the geometric constraints on their topology imposed by the phase rule:

$$f = c-p+2 \qquad [5]$$

where f is the degree of freedom, c the number of components, and p the number of phases. This equation (Gibbs's phases rule) provides the number of independent variables that must be set in a equilibrium system. For example, for a two-phase binary mixture the regions of the equilibrium of the phases can be obtained either by experiment or calculation if the temperature and pressure are fixed. In a two-phase ternary mixture, one more variable, usually the overall mixture composition, must also be fixed.

1.3.1 Unitary system (one component)

A substance can exists in three different states: solid, liquid and gas depending on the two variables temperature (T) and pressure (p), as shown in Figure 3.
Equilibrium between different phases is along the saturation curves and the three phases co-exist in equilibrium at the triple point. The evaporation curve (equilibrium between liquid and vapour phases) ends at the critical point.

1.3.2 Binary system (two components)

Liquid-vapour/SCF

In the case of the binary system, the phase boundary can be represented on a T-*x* (temperature plotted against the mole fraction of the mixture at a constant pressure) or P-*x* diagram (pressure plotted against the mole fraction of the mixture at a constant temperature), then the locus of the critical points are represented on a P-T space.
In Figure 16 a P-*x* diagram of CO_2 and ethanol at 70 °C is reported. The phase diagram was calculated using the PE-2000 software developed by the Technische Universität Hamburg-Harburg (Germany). The program was developed to model phase equilibria with a variety of equations of state. In particular for this diagram, the binary systems was calculated with the Peng-Robinson Equation of State (PR-EOS) using quadratic mixing rules. The binary interaction coefficients (k_{ij}) and critical parameters (Tc, pc, ω) for the pure components are taken from the literature.

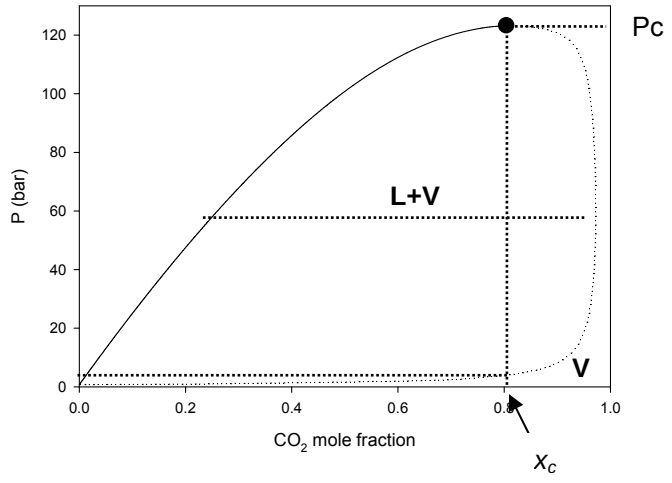

Figure 16. P-*x* diagram of ethanol and CO_2 at 70 °C

At low pressures the mixture only shows a homogeneous vapour phase. With pressure increase the mixture exhibits a dew point (at this point the liquid phase shrunk to an infinitely small droplet which is in equilibrium with a vapour phase). With a further pressure increase, a region where both the liquid and gas phase are present is reached. The composition of the vapour and liquid phase can be obtained by the length of the tieline (virtual connections between co-existing phases). The increase of the pressure leads, contrary to the case of a pure component system, not only to a volume change, but also system composition. At the composition lower than x_c, with a further pressure increase, the mixture crosses first the bubble point curve (at the bubble point the vapour phase shrunk to an infinitely small bubble which is in equilibrium with a liquid phase) and then it reaches a single homogeneous liquid phase. At the composition x_c the mixture does not cross the bubble point, but it reaches the critical point. Above Pc at that temperature (70 °C) all mixtures are supercritical (homogeneous region where ethanol and CO_2 are completely miscible). Note that the critical point in a binary mixture is always at the maximum of the bimodal curve. Furthermore, the critical point is the point where dew and bubble curve meet; therefore the critical point is a dew and a bubble point at the same time. At compositions higher then x_c the mixtures crosses the dew point curve twice with increasing pressure. It appears that the mixture is vaporizing again with increasing pressure. This phenomenon is called *retrograde condensation*.

Another way to plot the binary phase equilibria is a T-*x* diagram. In this case, the change in temperature are plotted against the composition at a constant pressure. The resulting diagrams are usually very similar to the corresponding P-*x* diagrams, but appear to be upside down.

A third way to represent fluid phase equilibria is the P-T diagram at constant composition. Van Konynenberg and Scott (van Konynenburg and Scott, 1980) had grouped the possible phase diagrams of liquid-fluid phase behaviour in five major schematic classes which are represented in Figure 17.

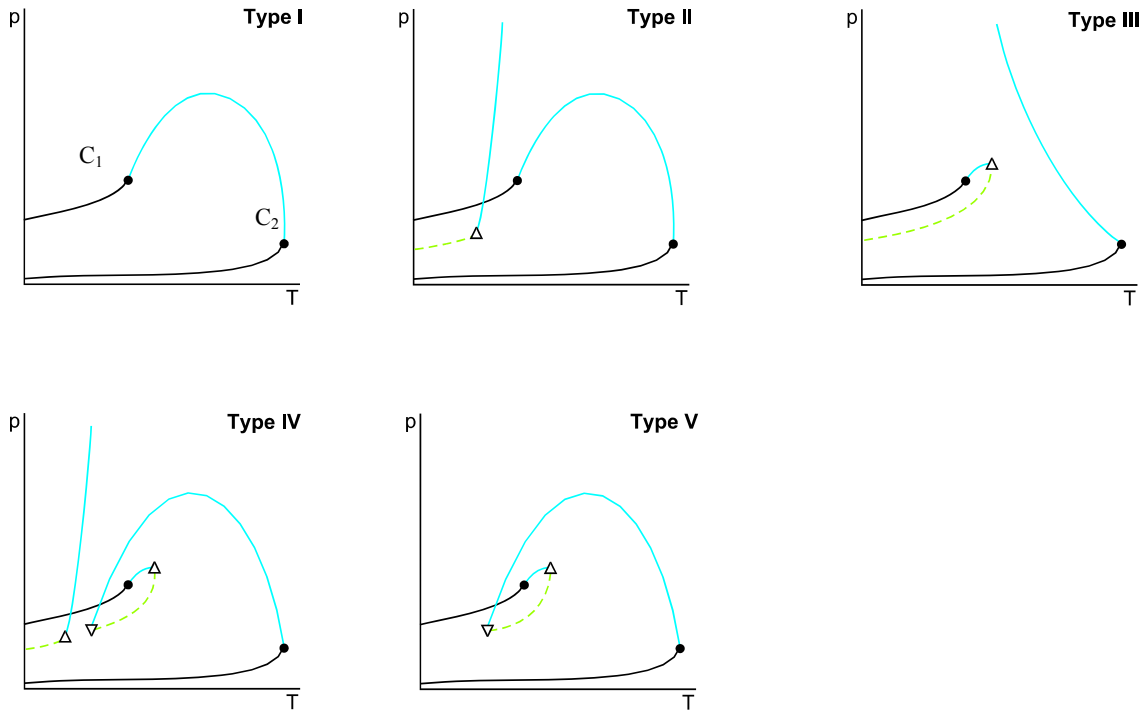

Figure 17. Phase Behaviour Classification for Binary Mixtures according to Van Konynenburg and Scott

The simplest binary mixture is the Type 1. The dark lines represent the vapour-liquid line of the pure components that terminate in the critical point (C_1 and C_2), while the critical curve runs continuously from the critical point of the more volatile component (C_1) to that of the less volatile component (C_2). Above the critical line the fluids are completely miscible. Type II behaviour is similar to Type I with an additional liquid-liquid critical line that commences at low temperatures rising steeply to high pressures from an Upper Critical End Point (UCEP). At this point, the liquid and gaseous phases of one component become identical critical in the presence of the liquid phase of the second component (liquid-liquid-vapour three-phase line). This indicates that, at low temperature, an immiscibility region between fluid and liquid is present.

Type V fluid phase behaviour is characterised by two critical lines. The critical line from the component with the lower critical temperature terminates in an Upper Critical End Point (UCEP) whereas the other critical line ends in a Lower Critical End Point (LCEP). At temperatures between LCEP and UCEP three phases co-exist (liquid 1 + liquid 2 + vapour), but above the UCEP the fluids become completely miscible mimicking Type I behaviour, although with significantly higher mixture critical pressures than Type I systems.

The difference between Type IV and Type V is identical to Type I and Type II. In Type IV a liquid-liquid critical line commences at low temperatures from an Upper Critical End

Point (UCEP) and rises steeply to high pressures, leading to similar operating restrictions as Type II.

In Type III phase behaviour, the vapour-liquid critical line commencing from the critical point of the component with the higher critical temperature only extends partly to the critical point of the other component before rising to high pressures. Furthermore, this critical locus displays a continuous transition between vapour-liquid and liquid-liquid equilibrium. The vapour-liquid line commencing from the critical point of the component with the lower critical temperature ends again in an UCEP. Fluids that show this kind of phase behaviour are completely immiscible with solvents.

The P-T projection are useful for a rationale design of those processes that use the SCF as antisolvent. Potential antisolvents can be classified into three categories according to their phase behaviour with solvents:

- Category I (Type I or Type II fluid phase behaviour)

CO_2, N_2O, CHF_3, CH_2F_2, HFAs, C_nH_{2n} ($4<n<12$), C_nH_{2+n} ($4<n<12$), etc.

- Category II (Type V or Type IV fluid phase behaviour)

C_nH_{2n} ($1<n<5$), C_nH_{2+n} ($1<n<5$), Xe, etc.

- Category III (Type III fluid phase behaviour)

He, Ar, N_2, H_2, CO, SF_6, CH_4, etc.

Fluids belonging to category I do not introduce limitations to the process, and are probably the least potent antisolvents. Fluids of category II are non-polar and therefore good antisolvent for solids. However they have the restriction on the antisolvent process of a limited range of operating temperature and pressure. Fluids of category III are immiscible with solvents and therefore are also good antisolvent for solids, but the immiscibility creates processing problems that might be difficult to overcome (The solvent can not to be extracted from the processed material).

It has to be remembered that it is possible to represent the whole P-T-*x* space in three dimensional diagram. But, usually binary phase diagrams are not represented in this way for two reasons: normally there are not enough data available to support the graph, and these diagrams tend to be very complicated. Anyway, it is possible to derive P-*x* and T-*x* projections of the mixture from the P-T diagram.

Solid-fluid

As stated before, unlike gases at low pressure, supercritical fluids show a remarkable solvent power for the solids. As an example, Figure 18 shows the solubility changes of nifedipine in supercritical carbon dioxide as function of the pressure (Knez et al., 1995). The solubility decreases with increasing temperatures up to pressures below the cross over region, which is about 220 bar for this system, and then increases. This is explained taking into account two different aspects: an increase of the temperature leads to a increase of molecular mobility and so at higher solubility, but on the other hand, an increase in temperature decreases the CO_2 density and therefore its solvent power. At low pressure a decreasing of the solubility with the increase of temperature, due to the density change, is observed, while above the cross over pressure the kinetic aspects become more important.

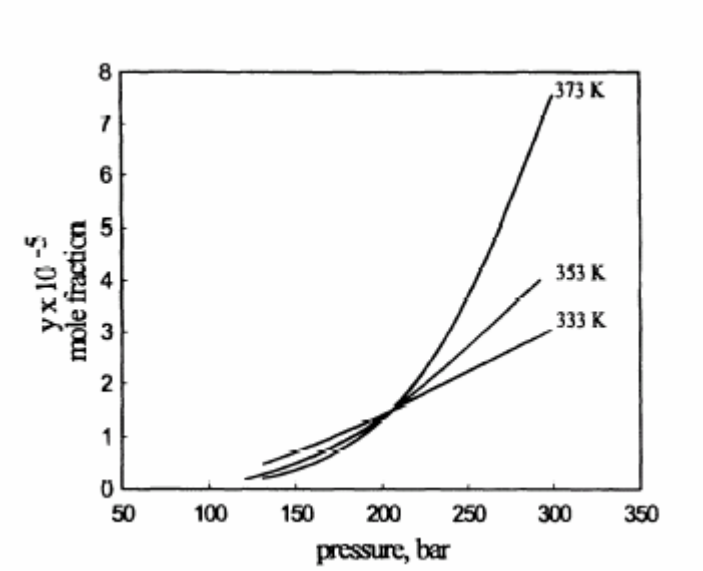

Figure 18. Solubility of nifedipine in the supercritical CO_2 (Knez et al., 1995)

A schematic diagram for a SCF and solid system is represented in Figure 19, where the P-T diagram is reported with the P-*x* sections at three different temperatures.

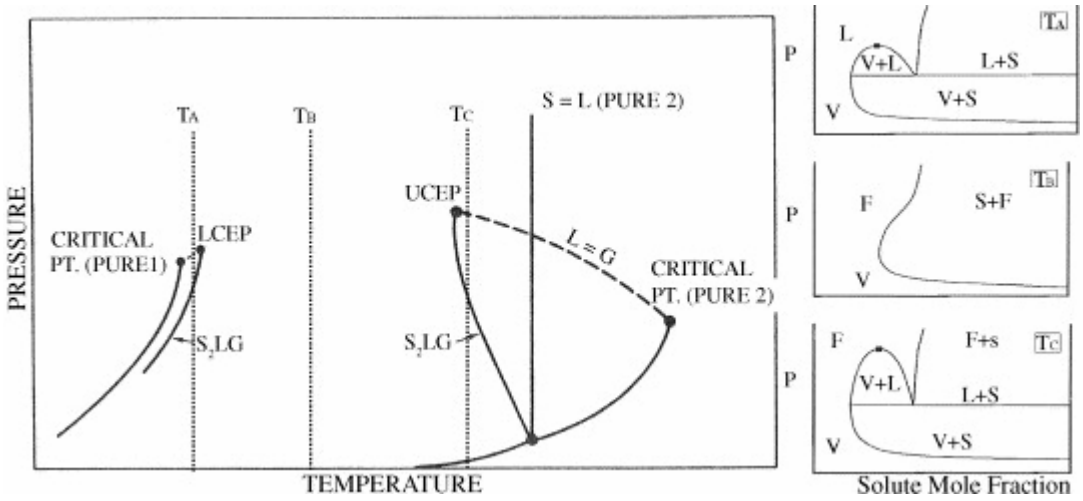

Figure 19. Representative diagram for a SCF+solid system

The diagram generalizes the phase behaviour for systems in which the melting point of the solid is significantly higher then the critical temperature of the fluids. This diagram represents a system where the solid and the SFC are very dissimilar in molecular size, polarity, structure etc, namely when the SFC is not very soluble in the molten solute.

The critical curve shows two branches. One branch runs in the P-T projection from the critical point of the more volatile component to a point of intersection with a three-phase curve S_2LG which is called Lower Critical End Point (LCEP). The second branch of the critical curve runs from a point of intersection with a second branch of the S_2LG (Upper Critical End Point, UCEP) and the critical point of the less volatile component. The three phase line S_2LG starts in the triple point of the pure less volatile component. From the same point commences also a line that rises steeply to high pressures; this represents the liquid-solid line of the pure component.

In the same Figure also a P-*x* sections at three different temperature are reported. At temperature T_A, above the critical temperature of the more volatile component and below the temperature of the LCEP, a two phase region S_2G is separated from a S_2L region, a homogeneous liquid region and a LG region by three-phase equilibrium S_2LG. Furthermore the LG region ends at high pressure in a L=G critical point.

At temperature T_B the LG region disappears and the S_2G region and S_2L region merge into one solid-fluid two phases region, which exhibits a horizontal tangent at the UCEP. This results in a sharp increase of the solubility of the solid in SCF.

For the temperature T_C between the UCEP and the triple point of the less volatile component, the P-*x* projection is given in the same Figure.

As underlined before, for this type of binary mixtures, the melting point of the solid is higher than the critical temperature of the SCF. Sometimes, in the presence of SCF, the melting point of the solid decreases with the increase of pressure. The reason of this depression is that, as the pressure increases, more and more as the gas dissolves into the solid (usually polymers) decreasing its melting point. In this case the phase diagram changes in shape and the right side branch of the diagram becomes close to the branch referred to the SCF critical line (Figure 20 a,b,c). In Figure 20 a, it is possible to note that the three phase curve L_2L_1G ends at low temperature in a quadruple point SL_2L_1G where four phases coexist. In the quadruple point three other three-phase curves terminate. The SL_2L_1 curve runs steeply to high pressure and ends in the UCEP where this curve intersects the critical curve. The SL_2G curve runs to the triple point of the less volatile pure component and the SL_1G curve runs to lower temperature. When the melting point of the less volatile component increases (e.g. in the case of the polymer with higher molecular weight) the melting curve of the solid shifts to higher temperature; and also the quadruple point shifts to higher temperature (b) and eventually coincides with the LCEP of the more volatile component (c).

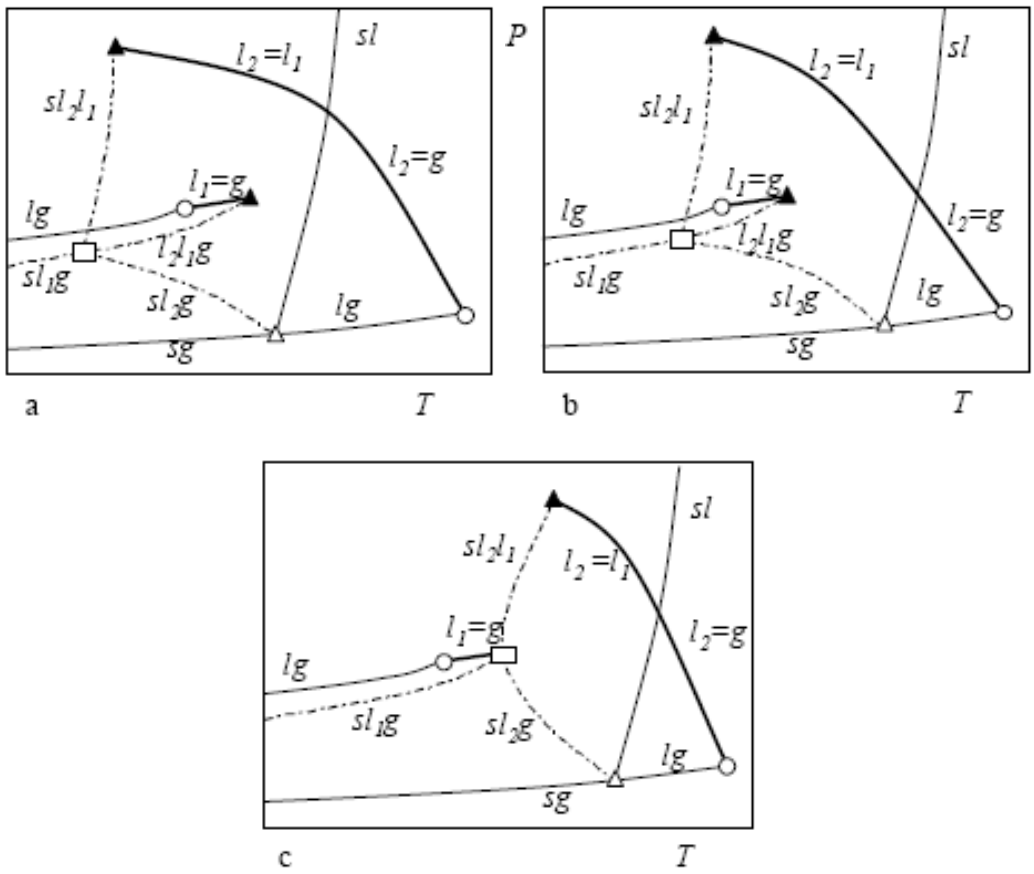

Figure 20. P-T diagrams for SCF+solid system when the SFC decreases the melting point of the solid

1.3.3 Ternary system (three components)

A two phase ternary system has three degrees of freedom and it is usually represented in so-called Gibbs-triangles, where compositions is plotted at constant pressure and temperature.

A typical three component system of CO_2-methanol-water is drawn in Figure 21.

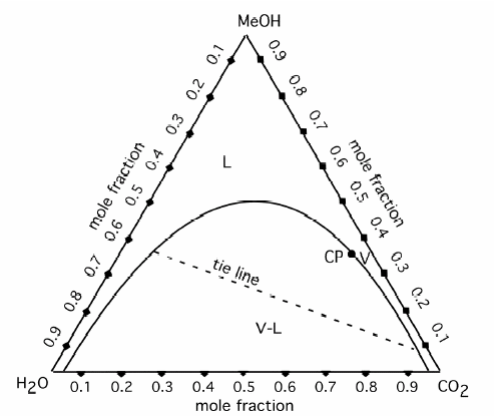

Figure 21. Gibbs-triangle for an arbitrary ternary mixture

The corners of a Gibbs-triangles represent the pure components, the edges the three binary systems (H_2O-CO_2, CO_2-CH_3OH, CH_3OH-H_2O), so any ternary mixture lies inside the borders of the triangle. The binodal curve (defined as the line which envelopes the region where liquid and vapour phases are present) is large indicating a large region of the immiscibility in this ternary system. The bottom of the triangle represents the binary system CO_2-H_2O, it is possible to see that only a small amount of either component is miscible with the other, while CH_3OH and water and CH_3OH and CO_2 are miscible in all proportions. The tielines inside the binodal curve are not parallel to each other as for the binary system (Figure 16), and consequently, the critical point does not lie at any extreme point. Anyway, also in this case, the critical point is the point where dew and bubble curves meet each other, here, at fixed temperature, pressure and composition the three fluids are completely miscible. The non-parallelity of the tielines offers good possibility for the antisolvent process because only changing the flow ratios of the three fluid components, and without changing temperature and pressure it is possible to influence the obtained product.

1.4 Polymers processing using SC-CO_2

SC-CO_2 is used in the area of polymer processing such as polymer modification, blending, foaming, and formation of polymer composites due to its unique properties. CO_2 is able to plasticize many polymers owing to its capability to solubilize into them. This property causes an increase of chain mobility resulting in a decrease either of the glass transition temperature, in the case of amorphous polymers, or of melting point, in the case of semicrystalline polymers. Both in the rubbery or in the liquid state the polymer can be easily manipulated.

A peculiar characteristic is that CO_2 is a "temporary" plasticizer, CO_2 is a gas under standard conditions so it is easily removed from the final product at the end of the process. Furthermore, for the intrinsic properties of the CO_2, the processing of polymeric material is possible at mild operative conditions and the enhancement of the solute diffusion is possible by changing the process parameters.

1.4.1 Polymer-CO_2 phase behaviour (Liquid-Liquid phase behaviour)

In Figure 22, the T-x, phase diagrams typical of an amorphous and monodisperse polymer-CO_2 system at three different pressure are reported.

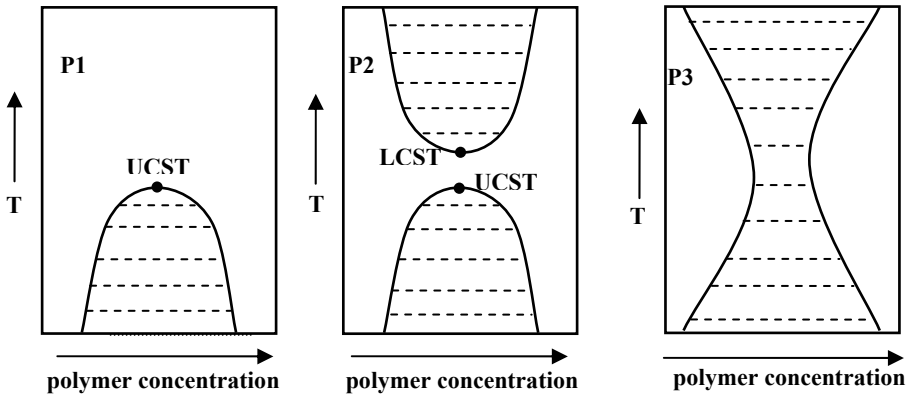

Figure 22. T-x phase diagram typical of an amorphous and monodisperse polymer-CO_2 system

The T-x sections of the L-L phase equilibria indicate the miscibility region of the polymer-CO_2 system, and, on the basis of different pressure, they may show upper critical, lower critical or hourglass-type demixing behaviour.

In particular, at elevated pressure (P1) the section shows a LL miscibility gap in continuous with a maximum that represents the upper critical solution temperature (UCST); at intermediate pressure (P2) the miscibility gap becomes discontinuous with a maximum at UCST and a minimum called lower critical solution temperature (LCST); at pressure lower than critical pressure (P3) the miscibility gap becomes an hourglass-shaped without the critical point. The absence of the critical point underlines that in this case the system is immiscible at all temperatures within a limited concentration range (Folie and Radosz, 1995).

It has to be underlined that the reported diagrams are idealised, because, in the real system, the curve is highly asymmetric with the maximum shifted toward the CO_2-rich phase. Furthermore, for the polydispersity of polymers, the UCST does not coincide with the maximum of the phase boundary, but it is shifted to higher polymer concentrations (Folie and Radosz, 1995).

1.4.2 Pressure Induced Phase Separation (PIPS)

In polymer processes based on SCF such as blending, formation of polymer composites without the use of organic solvents, extrusion, etc., the concentration of CO_2 into the polymer might be kept below the saturation limit to avoid the phase separation and to work in a homogeneous phase. (Nalawade et al., 2006a). If the homogeneous polymer solution is necessary condition for the process, the pressure reduction is an integral step in the recovery of the end product; for this reason, there is a great interest in the study of how a homogeneous polymer solution may undergo phase separation as a result of a change in pressure (Zhuang and Kiran, 1998).

In Figure 23, a more detailed schematic representation of the L-L phase behaviour is reported to explain the phenomenon of PIPS.

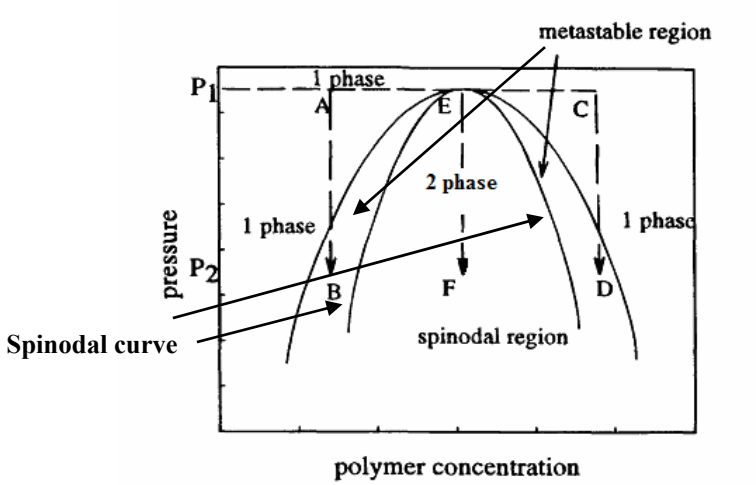

Figure 23. Schematic representation of pressure-induced phase separation in the pressure-composition phase diagram at fixed temperature, modified from (Palakodaty and York, 1999)

The phase diagram shows the binodal curve which, as stated before, is defined as the line which divides the stable one phase region from the region in which two phase coexists in equilibrium, and the spinodal curve, which divides the two phases region into metastable and unstable portions. The region between the spinodal and binodal curves is the metastable region.

If the system is at pressure higher than P1, is in a stable one phase region (above the critical point of the mixture), then, by decreasing the pressure, the system goes into two phases region at a pressure P2. As indicated in Figure 23, three different pressure reduction paths are possible (AB, EF, CD) for solutions at three different polymer concentrations, all starting at an initial pressure P_1 and ending at a final pressure P_2. The reduction in pressure creates a new phase formation that proceeds in two different paths (AB=CD) and leads to a different microscopic separation mechanism: i) *nucleation and growth mechanism* in the case of paths AB and CD (when metastable regions are entered) and ii) *spinodal decomposition mechanism* in the case of EF path (the unstable region is entered).

In the case of nucleation and growth mechanism, the system is brought into the metastable region and so energy-intensive demixing occurs, consequently, the nuclei of the new phase form and grow into dispersed droplets in a continuous polymer-rich phase.

In the case of the spinodal decomposition mechanism, the system is brought into thermodynamically unstable region and the system demixes spontaneously, forming two cocontinuous phases.

The spinodal decomposition mechanism can occur also in the case of paths AB and CD when the pressure is rapidly decrease and therefore, the system goes quickly in the unstable region.
The different mechanisms of the phase separation, as well as the kinetic are very important parameters because they can lead to final product with different morphologies, ranging from powders, to porous structures of different size and distributions (Zhuang and Kiran, 1998).
Interesting experimental works about the kinetics of PIPS in solutions of polymer and gas at high pressure using time- and angle-resolved light scattering were carried out by Kiran and co-workers (Liu and Kiran, 1999, Xiong and Kiran, 2000, Zhuang and Kiran, 1998).

1.4.3 Solubility of CO_2 in polymers and *viceversa*

The solubility data of CO_2 into polymer and polymer in SC-CO_2 at various temperatures and pressures provide a very useful criteria to determine the operative conditions for all type of polymer processing.
The solubility of CO_2 is largely based on its ability to weakly interact with functional groups present along the molecular chains of the polymers. The CO_2 molecule can be seen as a weak Lewis acid that can interact with the basic sites of the polymer; this can be considered the main contributor to its solubility. The evidence of this interaction was obtained spectroscopically by studying interactions between CO_2 and polymers containing basic functional groups (carbonyl group or phenyl rings) (Kazarian et al., 1996).

In the last decade, many experimental methods have been applied to investigate the solubility of CO_2 in polymers at elevated pressure. The most commonly used are: phase separation method, pressure decay method, gravimetric method, chromatographic method and spectroscopic method.

In the *phase separation method*, a molten polymer is exposed to the CO_2 at desired pressure in an autoclave. After reaching the polymer/CO_2 equilibrium system (typically few hours), samples are taken from the two phases: a polymer-rich and a CO_2-rich phase. The amount of CO_2 in the polymer-rich phase is determined with a flowmeter (Weidner et al., 1997), or by measuring the volume of CO_2 corresponding to the displacement of water level in an inverted graduated tube which is immersed in CO_2 saturated water (Daneshvar

and Gulari, 1989a). This method is mainly applicable to low viscosity polymers where mixing and sampling are relatively easy. However, this method can be criticized with respect to the suitability and correctness of the sampling procedure.

In the *pressure decay method*, CO_2 and polymer are placed in a closed autoclave at a fixed pressure and temperature. The sorption of CO_2 into the polymer causes a reduction in pressure until the equilibrium of the system is reached. The initial pressure and temperature values, the volume of the system (without polymer), and the volume occupied by the polymer are used to calculate the amount of gas present initially. The values of temperature and pressure after equilibration and the volume occupied by the polymer are used to calculate the amount of free CO_2 present. The difference between the initial and the final amounts of CO_2 gives the amount of CO_2 in the polymer (Morel and Paul, 1982). Suitable equations of state have to be used to calculate the density of the fluid phase. Furthermore, the swelling of the polymer must to be taken in account, but it can not be measured by these techniques. The Sanchez-Lacombe equation of state is generally used to predict the swelling of the polymer.

Another experimental technique has been proposed to measure *in-situ* the amount of gas dissolved into polymer: the *gravimetric method.* By this method, the weight difference between the CO_2-free and the CO_2-sorbed polymer is used to calculate the solubility. The simplest approach is based on the use of a quartz spring method, originally adopted by Wissinger and Paulaitis. In this technique, the amount of gas absorbed is evaluated from the length extension of the quartz spring (where the sample was suspended), provided that its elastic constant k is known (Wissinger and Paulaitis, 1987). Also with this technique, the density of the CO_2 at the operative pressure and temperature, and the swelling of the polymer have to be known.

A substantially similar approach is based on the use of an electro- or microbalance to perform the weighting of the polymer sample directly in the dense fluid atmosphere (Kamiya et al., 1986).

An improvement of the gravimetric technique is the magnetic suspension balance developed by Kleinrahm and Wagner. By using this approach, the measuring strength is transmitted without contact by a magnetic coupling from the pressurized chamber, containing the polymer sample, to the microbalance (Kleinrahm and Wagner, 1986). The microbalance can be located outside the high-pressure chamber, under standard conditions.

The c*hromatographic method* is another method used to determine the solubility of CO_2 in the polymers. The solubility measurements are carried out with a very thin film of polymer (few micrometers) as a stationary phase and CO_2 as mobile phase. The measurement of the specific retention volume of a tracer determines the CO_2 solubility (Parcher, 1982).
More recently also a gas chromatographic method was used to measure sorption of dense gases into polymers (Galia et al., 2006).

The polymer swelling in the solubility calculation is very important, therefore an experimental set-up capable to measure in situ, the swelling and the solubility at the same time is sought.
Kazarian et al. pioneered the use of the FTIR spectroscopy to measure in-situ the solubility and swelling of the polymer under SCF.
These authors combined a FT-IR apparatus with a high-pressure unit putting into evidence the interactions, at molecular level, of a series of polymers with SC-CO_2. This apparatus can be considered a powerful tool to study the interactions of the polymeric materials with pressurized CO_2, and to simultaneously determine the solubility and the swelling under SCF, by measuring the intensity of the relevant IR bands, directly in-situ, without the need of sampling the system (Kazarian, 2002).

Data about the solubility of CO_2 in the polymers are available in the literature, while a very few data on the solubility of polymer in CO_2 are reported, likely because the solubility concentration of the polymers, especially the solid one, in the pressurized gas is very low, so very difficult to quantify. Often, to study the phase behaviour of the polymer/CO_2 system, the supercritical phase (CO_2-rich) can be assumed to remain pure and only the polymer-rich phase is sampled.
Noteworthy, the accurate quantification of the CO_2 concentration in the polymer and of the polymer in the SC-CO_2 represents still a challenging issue.

1.4.4 Polymer plasticization

The interaction between CO_2 and the polymer reduces the interchain polymer bonds; this results in enhanced segmental mobility of the polymer and a consequent decrease of its glass transition or melting point. The extent of the glass transition or melting point depression depends on the amount of CO_2 dissolved in the polymer.

In the rubbery or liquid state the polymer can be used as coating agent, to produce foams, or to incorporate drugs giving rise to a molecular dispersion that can be extruded or sprayed at lower pressure to obtain drug loaded microparticles.

The polymer plasticization is accompanied by change in the mechanical and physical properties such as swelling foaming, crystallization and viscosity or density reduction (Bae, 1996, Funami et al., 2007, Guadagno and Kazarian, 2004, Kazarian, 2000).

The knowledge of this phenomena is crucial for processing development. For example, in the case of spraying or extrusion, where the particles are formed by forcing molten polymers through an orifice, it is easy to understand that characteristics such as density, or viscosity etc. influence the texturisation of the material and so they are key parameters of the process.

The reduction of the viscosity of the polymer bulk is associated with plasticization, as it was demonstrated by Bae, who studied the viscosity reduction of polymer melts by dynamic light scattering technique (Bae, 1996). This reduction is due to an increase in free-volume of the polymer (swelling), steaming from CO_2 absorption. The viscosity is reduced on the basis of the different operative conditions; therefore, the processing temperature and pressure need to be optimised to obtain a desired viscosity reduction. This provides a route to process, even at low temperature, high molecular weight polymers.

Another important consequence of the CO_2 absorption and plasticization is the possibility to obtain foamed material, in fact, high-pressure CO_2 offers an attractive alternative to traditional blowing agents. The foams are defined as a porous structure formed by non-connected (closed) cells of about 10 μm or less in diameter and cell density larger than 10^9 cells/cm^3 (Baldwin et al., 1996). The foam material serves as an important tool in the preparation of sponge scaffolds used for tissue engineering. The method to produce foams and porous structure concerns the saturation of the polymer with SC-CO_2 at constant temperature and pressure, then the system is brought to the supersaturated state either by reducing pressure or by increasing temperature. These last creates a phase separation resulting in the nucleation and growth of pores.

The plasticization and swelling effect of CO_2 dissolved in the polymer can accelerate the diffusion of additives into the matrix. In fact, if the polymer is in the molten state, it can incorporate or solubilize drugs, and after depressurization, it would be possible to obtain microparticulate drug delivery systems. Another way to obtain microparticulate drug delivery systems is by impregnation. The impregnation mechanism, upon which the solute diffuses into the polymer matrix, may occurs via deposition or portioning. In the case of

deposition, the drug is soluble in CO_2, and it can be carried into the matrix and precipitated during depressurization. Partitioning occurs when the affinity of the solute dissolved in the CO_2 stream is higher for the matrix then for the SCF. A favourable partition coefficient results in a successful loading.

A thorough understanding of the mutual solubility and behaviour of the SCF/compound system is the necessary prerequisite to set-up pharmaceutical processes dealing with polymer in the molten state. By the knowledge of the system properties and the manipulation of the operative conditions, it is in principle possible to achieve the process control to obtain materials with tailor made properties.

1.5 Polyethylene glycols (PEGs)

Polyethylene glycols are stable hydrophilic polymers with general formula $HOCH_2(CH_2OCH_2)nCH_2OH$; where n represents the average number of oxyethylene groups. Synonyms of PEG are: Carbovax, Macrogol, Breox PEG, Hodag PEG, and Lutrol E.

These polymers are manufactured by a reaction of ethylene oxide and water under pressure in the presence of a catalyst. PEGs comprise a class of compounds varying in molecular weights between 200 and over 10000 (Table 4). At standard condition, PEGs up to molar mass 600 Da are liquid, while those with higher molar masses are solid (Kibbe, 2000).

Table 4. Structural formula and molecular weight of typical polyethylene glycol polymers

Grade	n	Average molecular weight
PEG 200	4.2	190-210
PEG 300	6.4	285-315
PEG 400	8.7	380-420
PEG 600	13.2	500-600
PEG 900	15.3	855-900
PEG 1000	22.3	900-1000
PEG 1450	32.5	1100-1500
PEG 1540	28.0-36.0	1300-1600
PEG 2000	40.0-50.0	1800-2200
PEG 3000	60.0-75.0	2700-3300
PEG 3350	75.7	3000-3700
PEG 4000	69.0-84.0	3000-4800
PEG 4600	104.1	4400-4800
PEG 8000	181.4	7000-9000

Due to their biocompatibility (Fruijtier-Pölloth, 2005) they are widely used in cosmetics and in pharmaceutical formulations including parenteral, topical, ophthalmic, oral and rectal preparation.

PEGs are essentially non-irritant to the skin, and they are therefore useful as ointment bases. Solid grades are generally employed in topical ointments with the consistency of the base being adjust by the addition of liquid grades of PEG.

Mixtures of PEGs are used also as suppository bases where they have the following advantages over fats: the melting point of the suppository can be made higher to withstand exposure to warmer climates; release of the drug is not dependent upon melting point; physical stability on storage is better; suppositories are readily miscible with rectal fluids. Disadvantages are that they are chemically more reactive than fats; the rate of release of water-soluble compounds decreases with the increasing molecular weight and the PEGs tend to be more irritant to mucous membranes than fat.

Aqueous PEGs solutions can be used either as suspending agents or to adjust the viscosity and consistency of other suspending vehicles. When they are used with other emulsifier, PEGs can act as emulsion stabilizers.

Liquid PEGs are used as solvents of the contents of soft gelatine capsules.

In concentrations up to approximately 30 %v/v PEG 300 and 400 are used as vehicles for parenteral dosage form.

In the solid-dosage formulations, PEGs with high molecular weight can be used to enhance the effectiveness of tablet binders and impart plasticity to granules.

These polymers can also be used to enhance the aqueous solubility or dissolution characteristics of poorly soluble compounds by making solid dispersions.

Another use of PEGs is in the film coating. Solid grades of polymer can be used alone for film coating or can be useful as plasticizer in conjunction with film-forming polymer. The presence of PEGs in the film coats tends to increase their water permeability. Currently, the PEG is the most popular material used to modify the surface of the biodegradable nanoparticles in order to reduce their plasma protein absorption and so, to avoid their recognition by the reticuloendothelial system (Gref, 2001, Gref et al., 1995).

PEG with molecular weigh of 6000 and above can be used as lubricants.

The antibacterial activity of certain antibiotics such as penicillin, and bacitracin, is reduced in the PEG bases. Also the preservative efficacy of the parabens may also be impaired due to binding with polyethylene glycols.

Polyethylene glycols are described in many pharmacopeias. Some of them such as the USP, have a single monograph describing various different grades; other pharmacopeias have individual monographs.

According to the European Pharmacopeia 6.0 the PEG 1500 is defined as "*white or almost white solid with a waxy or paraffin-like appearance. It is very soluble in water and in methylene chloride, freely soluble in alcohol, practically insoluble in fatty oils and in mineral oils*".

The PEG 4000 is defined as "*white or almost white solid with a waxy or paraffin-like appearance. It is very soluble in water and in methylene chloride, practically insoluble in alcohol, and in fatty oils and in mineral oils*".

1.6 Diazepam

Diazepam is a long-acting benzodiazepine derivative drug which possesses anxiolytic, anticonvulsant, sedative, skeletal muscle relaxant and amnestic properties (Goodman and Gilman, 2001). It is commonly used for treating anxiety, insomnia, seizures, alcohol withdrawal, and muscle spasms. It may also be used before certain medical procedures (such as endoscopy) to reduce tension and anxiety, and in some surgical procedures to induce amnesia (Martindale, 2002).

The mechanism of action of the diazepam is mediated by the enhancement of the activity of gamma-aminobutyric acid (GABA), a major inhibitor neurotransmitter in the brain. Two subtypes of GABA receptors have been identified: A and B. Benzodiazepines interact with GABA receptor (benzodiazepine receptors) that is an integral membrane chloride channel (Martindale, 2002).

Diazepam can be administered orally, intravenously, intramuscularly, or as a suppository.

When diazepam is administered orally, it is rapidly absorbed from the gastrointestinal tract, peak plasma concentrations occurring about 30-90 minutes of oral administration. The onset of action is 1-5 minutes for IV administration and 15-30 minutes for IM administration. Diazepam is highly lipid-soluble and crosses blood-brain barrier; it acts promptly on the brain, and its initial effects decrease rapidly as it is redistributed into fat depots and tissues (Martindale, 2002).

Diazepam is metabolised via oxidative pathways in the liver by the cytochrome P450 enzyme system. It has a biphasic half-life of 1-2 and 2-5 days, and has several pharmacologically active metabolites including oxazepam, and temazepam. These metabolites are conjugated with glucuronide, and are excreted primarily in the urine.

Diazepam is 98.5% bound to plasma proteins.

The dosage of diazepam for healthy adults ranges from 2 to 30 mg depending on the severity of the indications. For severe anxiety diazepam is given P.O. in doses of 2 mg generally three times daily; in case of mild anxiety or insomnia also lower doses are used. When given by intravenous injection the dose is usually 100 to 200 μm per kg body-weight.

The chemical structure and physico-chemical data of the drug are reported in Figure 24.

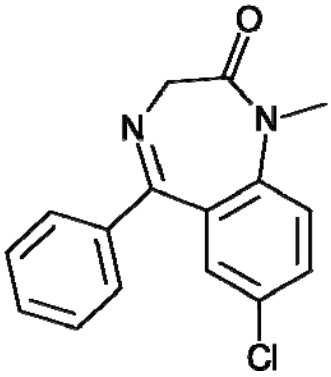

Chemical structure: $C_{16}H_{13}ClN_20$

Molecular weight: 284.7 g/mol

Physical state: white or almost white crystalline powder

Melting point: 131.5 to 134.5 °C

Solubility: slightly soluble in water, soluble in alchol, and free soluble in chloform

Figure 24. Chemical structure of Diazepam. Systematic (IUPAC) name: 7-chloro-1,3-dihydro-1-methyl-5-phenyl-2*H*-1,4-benzodiazepin-2-one

As mentioned before, and also as it can be deduced from the chemical structure, diazepam is a hydrophobic molecule and on the Biopharmaceutics Classification System (BCS) it is classified as class II: higly permeable, but low soluble drug.

2. Aim

Aim of this thesis was to set-up a supercritical process, based on the PGSS technique, for the production of the microparticulate polymeric drug delivery systems without the use of organic solvents. This aim was pursued trough the preliminary study of the phase behaviour of the binary systems polymer/CO_2, drug/CO_2, and the ternary system polymer/drug/CO_2.

The experimental work was carried out in three steps:

i) preformulation studies;
ii) microparticulate drug delivery systems production;
iii) biopharmaceutical and technological characterization of the obtained microparticles.

Polyethylene glycols and diazepam were selected as model polymer and drug, respectively.

In the first part of the work, the solubility, the swelling, the melting point variation of PEG in supercritical CO_2, as well as the solubility of SC-CO_2 in PEG, the solubility of diazepam in PEG in presence of CO_2, and the solubility of diazepam in SC-CO_2 were measured.
The knowledge of the PEG/CO_2 and PEG/CO_2/diazepam phase behaviour allowed to fix the operative conditions to set-up the PGSS process.
Diazepam was chosen as a model drug that can be administered at low dosage to treat pathologies such as mild anxiety, panic attack, or insomnia. Diazepam is a higly permeable hydrophobic molecule. The high permeability can be exploited for its administration via transmucosal or transepitelial route, namely buccal, nasal or pulmonary. However, the low solubility negatively influences the absorption rate; for this reason the incorporation of this drug into a hydrophilic polymer (such as PEG) potentially would lead to an improved drug dissolution rate which would result in a rapid onset of action.
In the third part of the work, the obtained microparticles were characterized for physico-chemical properties.

3. Materials and Methods

3.1 Materials

PEG 1500 and 4000 with degree of polydispersivity of 1.02 and 1.1 respectively, were purchased from A.C.E.F. (Italy); while diazepam was provided by Cambrex (Italy). These products were used as received from the supplier, or after micronization by means of a vibration mill.

CO_2 (99.99% pure) was supplied by Sapio (Italy) and used without any further purification. Methanol, acetonitrile, cyclohexane, glacial acetic acid HPLC grade (VWR, International s.r.l., Italy), distilled water, 1-heptanesulfonic acid sodium salt (Sigma Aldrich, Germany) sodium acetate (Merk, Germany) were also used in this study.

3.2 Methods

3.2.1 HPLC assay

PEG 1500

A HPLC (LC-10 ATvp, Shimadzu, Japan) equipped with Refractive Index detector (RID 10A, Shimadzu, Japan) was used to quantify the PEG 1500. The peak areas were integrated using the Cromatoplus software. The analyses were carried out using a size-exclusion column OHpak, SB-802.5 HQ (Shodex, Japan), and distilled water as mobile phase at the flow of 1 mL/min. The injected volume was 100 µL (Rheodyne injector 7725i) and the PEG 1500 retention time was 7.6 min. PEG 1500 was quantified by comparing the sample signal with that of a standard solution of the polymer.

Diazepam

The HPLC system used to quantify diazepam was composed of a multisolvent delivery unit (LC-10 ATvp, Shimadzu, Japan), an autosampler (Waters 2487) and a diode-array detector (SPD-10Avp, Shimadsu). The peak areas were integrated using the Cromatoplus software. The stationary phase was a Merck octyl derivative silica column (250 × 4.0 mm, 5-µm particle size) thermostated at 50 °C (CTO-10ASvp, Shimadzu). The mobile phase

consisted of 0.5 M sodium acetate tri-hydrate buffer containing 5 mM 1-heptanesulfonic acid monohydrate sodium salt and methanol (30:70 v/v), adjusted to pH 6.0 with glacial acetic acid. The flow rate was 1 mL/min. Diazepam was monitored at 230 nm.

The HPLC methods used in this work were validated for linearity, accuracy, precision, limit of detection and quantification. Furthermore, the number of theoretical plates and tailing factor were also calculated. The validations of the analytical procedures were carried out according to the guidelines of the international conference of harmonisation, ICH Q2 (R1).

Linearity

Linearity shows the method's ability to obtain results which are proportional to the concentration of the analyte within a given range. Linearity is determined by calculating the regression line in the plot peaks area obtained by integration *vs* analyte concentration.

Precision or Relative Standard Deviation (RSD)

ICH defines the precision of an analytical method as " the degree of agreement among the individual test results obtained when the method is applied to multiple sampling of a homogeneous sample". In other words, the precision indicates the reproducibility of the analytical method, and it can be determined by using the equation:

$$RSD\% = \frac{s.d}{mean} \cdot 100 \qquad [6]$$

where RSD is the relative standard deviation defined as the percentage ratio between the standard deviation (s.d) and the mean value. The USP requires that unless specified by a method:

- if a relative standard deviation of < 2%, is required then five replicate injection should be used
- if a relative standard deviation of > 2%, is required then six replicate injection should be used

Limit of detection

The limit of detection is the lowest concentration in a sample that can be detected, but not necessarily quantitated, under the stated experimental conditions. The limit of detection is generally quoted as the concentration yielding a signal-to-noise ratio between 3 or 2.

Limit of quantitation

This is the lowest concentration of analyte in a sample that can be determined with acceptable precision and accuracy. It is quoted as the concentration yielding a signal-to-noise ratio of 10.

Number of theoretical plates (n)

This is a measure of the sharpness of the peaks and therefore the efficiency of the column. It can be calculated in various ways, for example the USP, equation 7, uses the peak width at the base (W_b) and the BP, equation 8, at half of the height (W_h).
In Figure 25, the theoretical plate number calculations are reported.

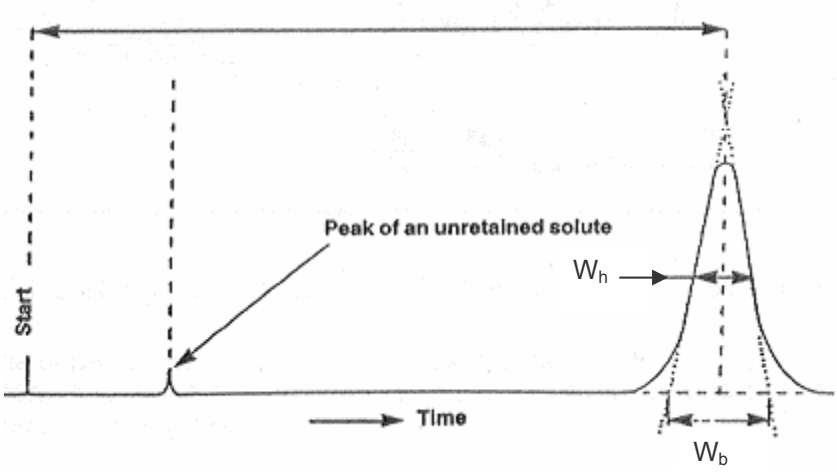

Figure 25. Plate number calculation

$$n = 5.545 \cdot \left(\frac{t}{W_h} \right)^2 \qquad [7]$$

$$n = 16 \cdot \left(\frac{t}{W_b} \right)^2 \qquad [8]$$

where W_h is the peak width at ½ peak height, W_b is the peak width at base, and t is the retention time.

In this work, the number of theoretical plates was calculated as described in the USP 30.

The plates number depends on column length (i.e. the longer the column the larger the plate number). Therefore, the column's efficiency can also be quoted as, the height equivalent to one theoretical plate (HETP):

$$HETP = \frac{L}{n} \qquad [9]$$

where L is the length of the column.

Tailing factor

The tailing factor is a measure for the symmetry of the peak (Figure 26).

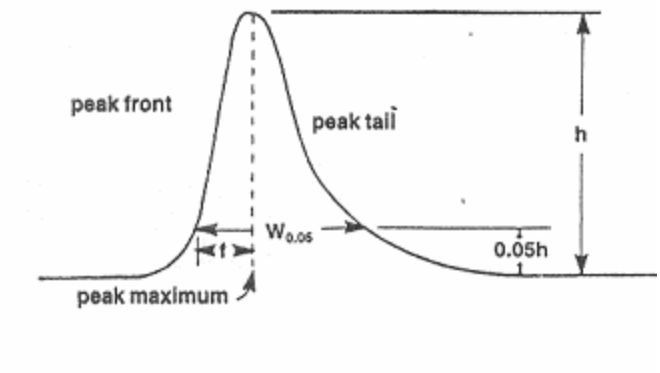

Figure 26. Tailing factor calculation

The tailing factor is quoted as:

$$T = \frac{W_{0.05}}{2f} \qquad [10]$$

where $W_{0.05}$ is the width at 5 % of the peak height, and *f* is the distance between maximum and the leading edge of the peak.

3.2.2 Measurement of the density of PEG 1500 and CO_2

The density values of the PEG 1500 were calculated at 35 and 55 °C at atmospheric pressure. The value at 35 °C was measured by means of a helium pycnometer (Multivolume Pycnometer 1305, Micromeritics, USA) as to 1.28 g/mL. PEG 1500 melts at ambient pressure between 44 and 48 °C (see DSC), therefore, its density at 55 °C was measured by means of calibrated (2 mL) glass pycnometer for liquid; the measured value resulted 1.11 g/mL.
The density values of CO_2 at given pressures and temperatures was calculated by means of the Refprop software (NIST, MD, USA) (http://www.nist.gov/data/nist23.htm).

3.2.3 High-pressure view cell

A high-pressure view cell (SITEC-Sieber Engineering AG, Zurich, Switzerland) (internal volume 74 mL) was used to visualize the behaviour of the PEG 1500 in the presence of CO_2 at fixed temperature and pressure. The cell is equipped with two sapphire windows (diameter 18 mm) facing to each other. The temperature was imposed by a heating jacket to within ± 1K (SITEC-Sieber Engineering AG, Zurich, Switzerland) and the pressure by a high pressure pump (Teledyne ISCO 260D, Nebraska, USA) with a ± 0.5 % pressure gauge monitoring (series D pump controller, Teleodyne ISCO).
By means of the view cell, the melting point and the swelling of the polymer under SC-CO_2 were measured.

Melting point under SC-CO_2

The measurement of the melting points of the PEG 1500 and PEG 4000 under pressure was based on a modified capillary method. The polymer (nearly 1 g) was introduced in a glass cylinder and placed in the high-pressure view cell. Vacuum was created inside the cell (membrane pump KNF, Italy), then, the pressurized CO_2 was introduced and heated.
The melting of the polymer was observed through the sapphire windows and registered with a photo camera (Finepix S602 Zoom, Fujifilm).

For each analyzes the temperature value was fixed while the pressure increased until the polymer melting onset (appearance of the first liquid drop). Each experiment was replicated at least twice.

Polymer swelling under SC-CO_2

PEG 1500 (1.28 g) was placed in a calibrated glass cylinder (2 mL) and introduced inside the high-pressure view cell. After vacuum application, the pressurized CO_2 was introduced into the cell and heated at the desired temperature. The polymer was kept in contact with the CO_2 until the attainment of the equilibrium (typically 24 hours). Pictures of the polymer containing cylinder were recorded at fixed time until a constant volume was reached.
The obtained images were analyzed by means of Image J software (NIH, Bethesda, USA) (http://rsb.info.nih.gov/IJ/) to quantify the polymer volume increase.
Measurements were carried out at least in triplicate at 35 and 55 °C in the 30-250 bar pressure range.

3.2.4 PEG 1500 solubility in SC-CO_2

The solubility of PEG 1500 in supercritical CO_2 was assayed by means of a laboratory scale extractor (Spe-ed SFE, Applied Separation, Allentown, PA, USA) operating under dynamic conditions at low CO_2 flux (about 4.5 10^{-3} mol/min) according to the validated method described by Stassi et al. (Stassi et al., 2000) and modified by Bettini et al. (Bettini et al., 2001) (Figure 27).

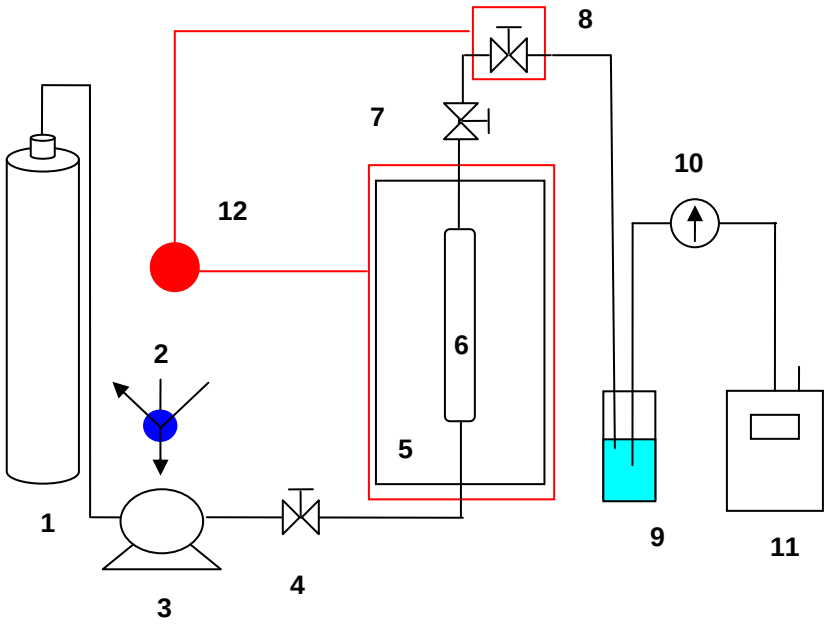

Figure 27. Schematic representation of the apparatus used for the measurement of PEG 1500 in SC CO_2: 1 CO_2 reservoir; 2 chiller; 3 pump; 4 inlet valve; 5 thermostatic chamber; 6 saturation column; 7 outlet valve, 8 micrometric valve; 9 collecting flask; 10 flow-meter; 11 gas-meter; 12 temperature controller

A stainless steel column with internal volume of 1.2 mL was loaded with 200 mg of polymer and placed in a thermostatic chamber at 35 or 55 °C. The CO_2 was introduced into the column and pressurized to the desired pressure in the 100-400 bar range. The CO_2 flow rate was tuned by a micrometric valve.

In a typical isothermal solubility determination, the CO_2 flowed through the polymer to remove the air, then, the pressure inside the column was raised up to the desired value holding the outlet valve closed. After reaching the pressure value, the outlet valve was opened and the CO_2 passed through the column. The run was stopped when about 0.9 moles of CO_2 had flowed through the column.

The PEG 1500 dissolved in CO_2 was collected in 25 mL distilled water after gas expansion. To avoid the risk of missing portion of the solute, at the end of each measurement, the micrometrics valve and the connection tubing were repeatedly washed with portion of distilled water. The amount of polymer dissolved in CO_2 was quantified by HPLC (see 3.2.1). Each measurement was performed at least in triplicate.

The average uncertainty for the solubility experiments was calculated from the contribution of error for each parameter (e.g. pressure, temperature, etc.) applying the rules of the independent variables; the obtained figure resulted above 3.5 %.

3.2.5 CO_2 solubility in PEG 1500

Solubility measurements of CO_2 in PEG 1500 were performed in static conditions at two temperatures (35 and 55 °C) and in the 30-250 bar pressure range. The equipment used is schematically represented in Figure 28.

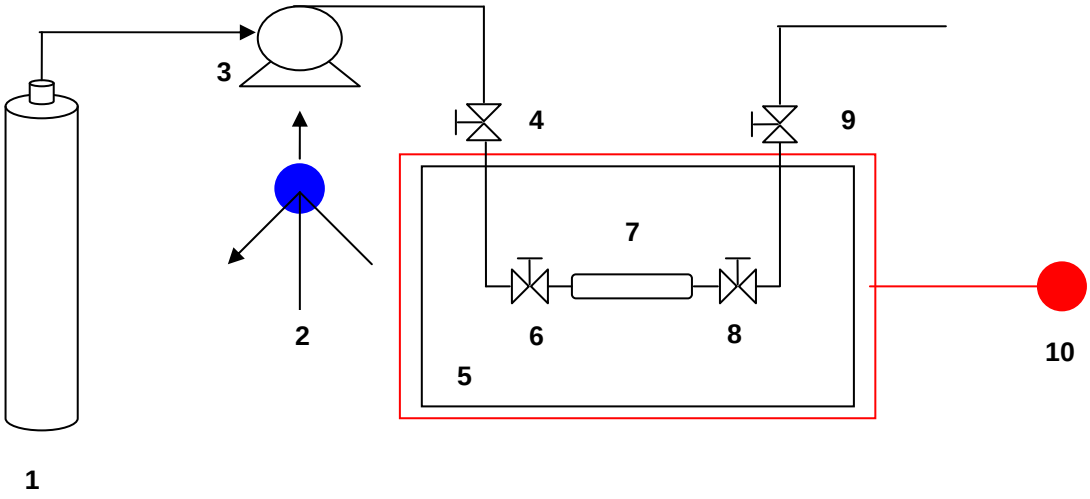

Figure 28. 1 CO_2 reservoir; 2 chiller; 3 pump; 4 inlet valve; 5 thermostatic chamber; 6 needle valve; 7 saturation cell; 8 needle valve; 9 outlet valve, 10 temperature controller

An accurately weighted amount of PEG 1500 (about 1.5 g) was placed into a stainless steel column (internal volume of 9.7 mL) (7) equipped with 2 needle valves (6 and 8). Prior to run, the system was weighted (BEL engineering, Monza, Italy, sensitivity, 0.01g), introduced in the oven (5) and heated at the desired temperature. Then, the column was submitted to vacuum from valve 9 by keeping the valve 6 closed. The valve 6 was opened and the CO_2 was pumped in with the outlet valve closed to reach the desired pressure (Teledyne ISCO 260D, Nebraska, USA).

After 4 hours system equilibration the valve 6 was closed. Then, the sealed vessel along with the two valves was removed and reweighed.

The weight difference between the PEG 1500 inside the vessel before and after equilibration with CO_2 gave the amount of CO_2 inside the vessel (W_{CO2c}). Part of this last was dissolved in the polymer while another amount occupies the empty space in the column (V_e).

The weight of PEG 1500 loaded in the vessel ($W_{PEG1500}$), and the true density of the polymer ($\rho_{PEG\ 1500}$) were known, thus it was possible to calculate the space in the column that was not occupied by the polymer, namely V_e by the equation:

$$9.7\text{-}\ (W_{PEG1500} \cdot \rho_{PEG\ 1500}) = V_e \qquad [11]$$

while the amount of CO_2 not dissolved into the polymer (W_e) was calculated as:

$$(V_e - S)\ \rho_{CO2} = We \qquad [12]$$

where S is the swelling defined as % of volume variation upon exposure to CO_2, and ρ_{CO2} is the CO_2 density at the given pressure and temperature.
From the difference between the total mass of the CO_2 (W_{CO2c}) and W_e, the amount of CO_2 dissolved in the PEG 1500 was calculated. The solubility of CO_2 in the PEG 1500 was expressed as weight %.
The average uncertainty for the solubility experiments was calculated from the error contribution for each parameter (e.g. pressure, temperature, etc.) applying the rules of the independent variables; the value resulted above 2 %.

3.2.6 ATR-FTIR spectroscopy

For the spectroscopic measurements under pressurized CO_2 a heatable Golden Gate™ (Specac, ltd. UK) support equipped with a specially designed high pressure cell was used (Figure 29).

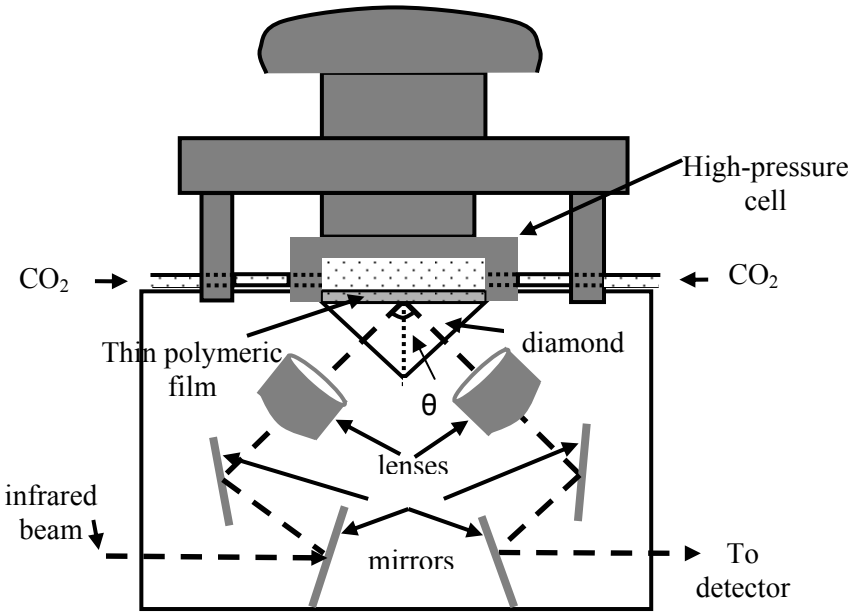

Figure 29. Schematic representation of the Golden Gate™ support equipped with a specially designed high pressure cell

Briefly, the Golden Gate™ was used to hold a diamond crystal (ZnSe focusing lenses) with an incident angle of 43° (± 1°) and the molten solid polymer specimen in form of film. The specimen was positioned on the top of the crystal mounted in the heating plate connected with a temperature controller. The temperature imposed by the heating plate was to within ± 1K.

The high pressure unit comprised a cell sealed to the tungsten carbide plate of the Golden Gate™ and a syringe pump (Teledyne 500D, Isco, USA) imposing the desired pressure, that was measured by a pressure transducer (Swagelok, Germany). The accuracy of the pressure measurement was ± 0.5%. A Teflon® O-ring positioned between the cell and the surface of the tungsten carbide plate ensured a good contact between the cell and the surface of the Golden Gate ™ avoiding CO_2 leaking.

The ATR-IR spectra were collected by means of Bruker Equinox 55 FT-IR spectrometer with a Mercury-Cadmium-Telluride (MTC) detector. The resolution was 2 cm^{-1}, spectra were obtained with 16 scans and were recorded in the 3850-590 cm^{-1} wavenumber range.

The FTIR images were collected with an IFS 66/S step-scan FTIR spectrometer (Bruker, Germany), and a 64 x 64 focal plane array MCT detector. All images were collected with a nominal spectral resolution of 4 cm^{-1}. Sixtyfour scans were co-added and averaged giving a total acquisition time of ca. 360 s. This macro-ATR imaging approach gives an area image

of 1140 x 820 μm^2. The rectangular image shape comes from the incident angle of the infrared light at the surface of the diamond surface (Chan and Kazarian, 2003).

Measurement of CO_2 sorption and PEG 1500 swelling

A small amount of the PEG 1500 (nearly 4 mg) was put onto the crystal surface of the Golden Gate™ and the temperature was raised up to the melting point. The obtained liquid film was slightly pressed against the crystal with a spatula to ensure a uniform surface and a good contact between the film and the crystal. Then, the surface of the crystal was cooled down to obtain the solid film.

The high pressure cell was heated at the desired temperature and the spectrum of the polymer without CO_2 was collected.

Thereafter, the CO_2 was introduced into the cell; then the outlet valve was closed and the pressure was raised up to the desired value. The polymer was kept at fixed temperature and pressure until the equilibrium was reached (typical time ranging from few minutes up to two hours). During this interval spectra were collected at predetermined time: constant absorbance of CO_2 and PEG bands indicated the attainment of equilibrium.

The analyses were carried out at 35 and 55 °C in the pressure range 1-200 bar. Spectra of pure CO_2 in the same conditions were recorded as well. All analyses were performed in triplicate and statistical differences were determined by Student's t-test (two tails, unpaired).

Solubility of diazepam in PEG 1500 under SC-CO_2

Different polymeric films were prepared to carry out the experiments.

A mixture of 10 % w/w of diazepam/PEG 1500 was heated up to 55 °C in order to liquefy the polymer and stirred until complete diazepam dissolution. Then, after cooling to room temperature, a portion of this mixture (nearly 4 mg) was put on the top of the ATR diamond. To guarantee an intimate contact between film and the diamond the temperature was raised up to 50 °C, and the liquid sample was slightly pressed against the crystal, then the surface of the crystal was cooled down.

A second mixture containing 75 % w/w of diazepam was heated up to 55 °C in order to liquefy the polymer and stirred until uniform diazepam dispersion. Then, it was cooled and treated as above reported for the mixture containing 10 % w/w of diazepam.

To obtain the spectrum of pure drug, a thin powder layer was pressed against the crystal using the punch of the golden gate system.

Both pure materials and the films, prepared as described above, were placed onto the diamond surface, and covered with the high-pressure cell. As stated above, the films were heated at the desired temperature and the CO_2 was introduced into the cell and the pressure was raised up to a predefined value. The specimen was kept at the desired temperature and pressure until the equilibrium was reached (typical time ranging from few minutes to two hours). During this interval spectra were collected at fixed time until constant absorbance of the relevant bands which indicated the attainment of equilibrium. The analysis were carried out up to 200 bar, at 35 and 55 °C with the ATR-IR (single element) and between 35 and 95 °C with ATR-IR imaging.

All experiments were performed in triplicate.

The quantitative analysis in the FT-IR spectroscopy are usually performed by using the Lambert-Beer law, that expresses the relation between the absorbance, A, the concentration, c, the beam path length, l, and the absorptivity, ε:

$$A = \varepsilon c l \qquad [13]$$

In the case of diazepam the characteristic C=O (ketone) stretching band (1680 cm^{-1}) can be exploited for the drug quantification. However, the molar absorptivity of the diazepam in PEG under SC-CO_2 is not known. For this reason, diazepam in PEG 1500 was quantified by comparing the absorbance of the sample with that of known concentration solutions, taking advantage from a previously established linear relationship between absorbance at 1680 cm^{-1} and diazepam concentration in PEG (%w/w) (see section 4.5.1).

3.2.7 Solubility of diazepam in SC-CO_2

The solubility of diazepam in SC-CO_2 at 35 and 55 °C, in the 30-180 bar range was measured by Near Infrared (NIR) spectroscopy in transmission. A transmission cell, designed for IR spectroscopic studies under pressure, made in stainless steel, sealed with two windows in CaF_2, with 0.5 cm path length was used. The IR spectra were recorded using a Equinox 22 FT-IR spectrometer (Bruker, Germany) with a deuterated triglycine sulfate (DTGS) detector. The spectral resolution was 2 cm^{-1} number of scans, scanning range with an accumulation of 32 scans between 7000 and 950 cm^{-1}.

The concentration of diazepam in SC-CO_2 was determined from equation 13 using as absorbance the height of the peak at 1485 cm^{-1} (Figure 30).

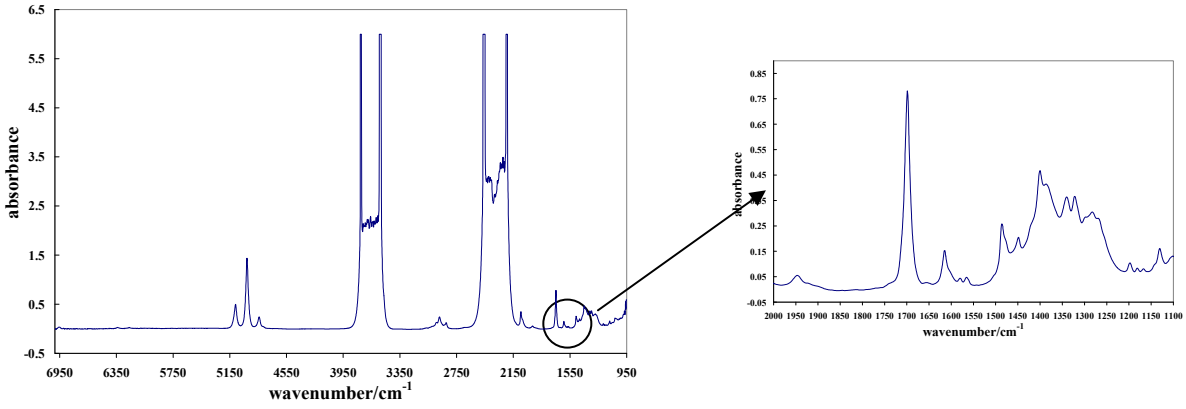

Figure 30. NIR spectra of diazepam in SC-CO_2

This last was selected because, contrary to the band at 1680 cm^{-1}, it did not shift or change in shape passing from ethanol to CO_2 (Figure 31).

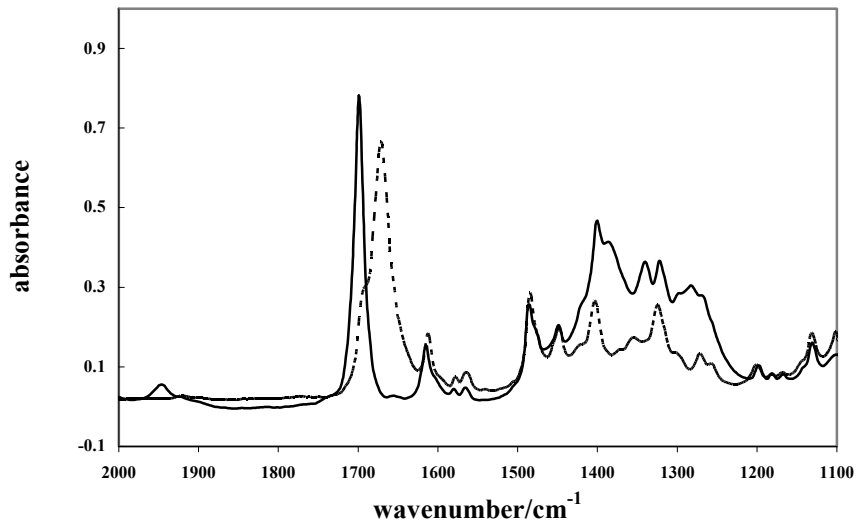

Figure 31. NIR spectra of diazepam in SC-CO2 at 35 ° and 175 bar (dashed line) and diazepam in ethanol (solid line)

In fact, the molar absorptivity coefficient (ε) of diazepam was measured in ethanol by assuming that the perfect overlapping of the spectra in the two solvents (CO_2 and ethanol) indicates no change in absorptivity (Liu and Parsons, 1969).

Linearity between drug concentration in ethanol and absorbance at 1485 cm^{-1} was verified (see section 4.6.1).

3.2.8 Preparation of PEG microparticles loaded with diazepam

A schematic diagram of the PGSS apparatus to prepare the PEG microparticles loaded with diazepam is drawn in Figure 32.

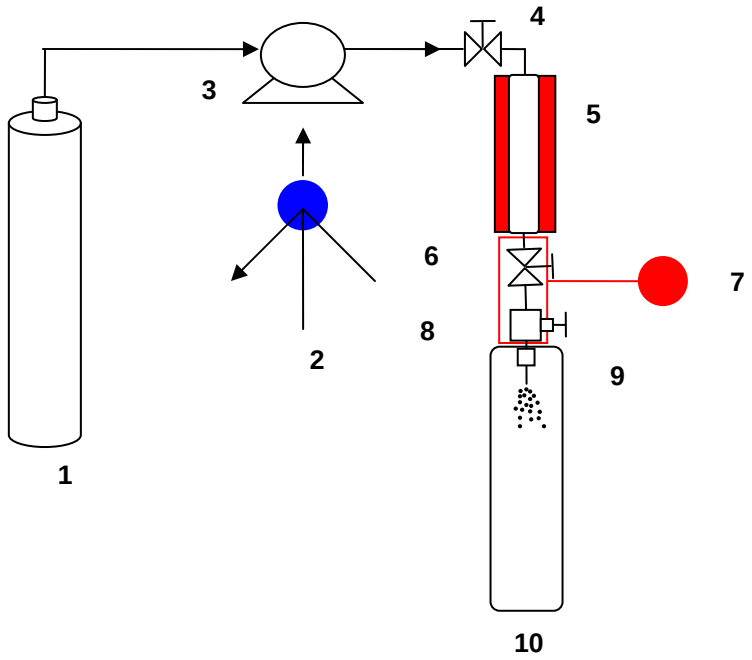

Figure 32. 1 CO_2 reservoir; 2 chiller; 3 pump; 4 inlet valve; 5 thermostatic chamber; 6 needle valve; 7 temperature controller; 8 micrometric valve; 9 nozzle; 10 precipitation chamber

The equipment consists in two main units: a thermostatic chamber (5) wrapped with a heating jacket (Falc instruments S.r.l., Italy) connected with a temperature controller; and a precipitation chamber (10) equipped with a nozzle (0.4 mm diameter).

An accurately weighted amount (nearly 2 g) of a mixture of PEG and diazepam (drug concentration ranging from 9.1 to 15.5% w/w) was placed in the thermostatic chamber. Then the CO_2 was pumped at the desired pressure.

Upon interaction with CO_2, PEG liquefied allowing the diazepam dissolution into the CO_2/liquid PEG mixture. After 4 hours equilibration, the solution was expanded through the nozzle in a glass precipitation chamber at ambient pressure. This caused a supersaturation of the PEG/diazepam system with CO_2 and an intense expansion of the gas

bubbles which lead to an explosion of the molten material into fine droplets which solidified as a consequence of the sudden decrease of temperature and pressure.
The microparticles were obtained both with PEG 1500 and 4000 at operative conditions (75-250 bar and 35 and 55 °C) which were chosen on the basis of the PEG/CO_2 and PEG/diazepam/CO_2 phase equilibria.

3.2.9 Vibration mill

Diazepam, PEG 1500 and 4000 were ground by means of a vibration mill for 10 minutes. Diazepam was ground to compare the dissolution behaviour and pulmonary deposition with the raw material and the diazepam embedded in the microparticles; while the polymers were ground to prepare homogeneous physical mixtures with a particle size comparable with those of the microparticles.

3.2.10 Drug content uniformity in the microparticles

In order to evaluate the drug content uniformity of the obtained microparticles. Three samples randomly taken for each batch were analyzed upon dissolving 30 mg of microparticles in a 50 mL of acetonitrile/water mixture (60:40 v/v). The obtained solution was analyzed by HPLC (see section 3.2.1).

3.2.11 Powder x-ray diffraction (PXRD)

The X-ray powder diffraction is a technique using the electromagnetic radiation of wavelength about 1 Å (10^{-10} m) on powder for structural characterization of the materials.
X-rays are generated within a sealed tube that is under vacuum. A current is applied that heats a filament within the tube; this creates the electron emission. The high voltage of the current applied within the tube accelerates the electrons which then hit a target (generally Cu). When these electrons hit the targets the X-rays are produced. X-rays are collimated and directed onto the flat specimen, and then diffracted at angles that satisfy the following condition of Bragg's equation 14.

$$n\lambda = 2d \sin\theta \qquad [14]$$

where n is the diffraction order, d is the lattice interplanar spacing of crystal (specimen), θ is the X-ray incident angle (Bragg angle) and λ is the wavelength characteristic of the X -rays (due to the X -ray tube).

The powder diffraction data are usually presented as a diffractogram in which the diffracted intensity I is shown as function of the scattering angle 2θ.

X-ray diffraction patterns on powder, reported in this work, were recovered on a Rigaku MiniFlex diffractometer (Japan) using CuKα radiation 30 kV, 15mA at a scanning speed of 0.5 °/min with a scanning range (2θ) from 2° to 35°.

PXRD measurements were carried out to characterize the raw material, to determine the polymorphic purity, and to measure the crystallinity of the diazepam contained in the micropaticles.

The crystallinity was quantified by comparing the intensity of the peak characteristic of diazepam in the microparticles with that of a PEG/diazepam mixture of known concentration. The peak at 2θ=9.5 was exploited for the drug quantification because it showed a detectable intensity at did not overlap with the peaks of PEG (Figure 33).

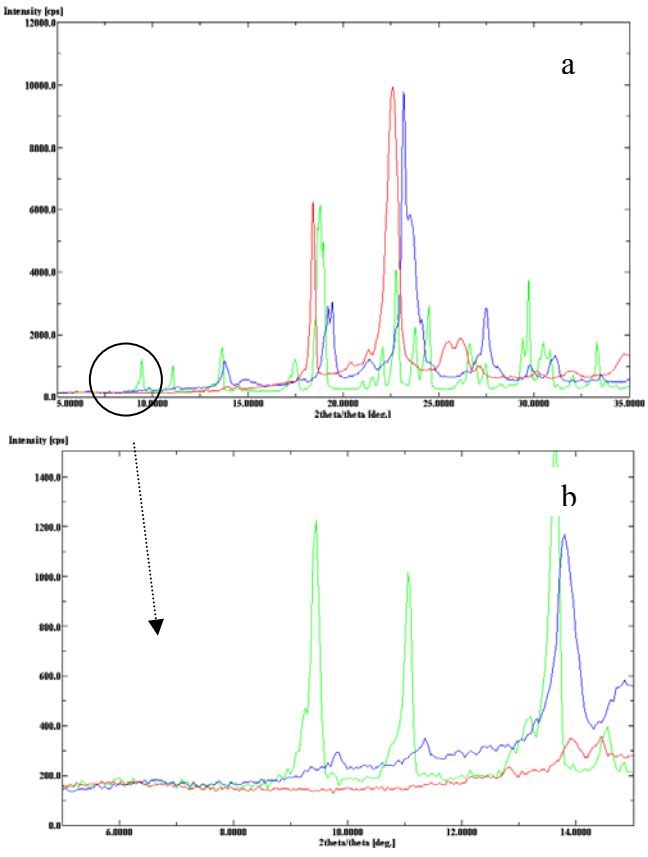

Figure 33. X-ray diffraction patterns on powder of diazepam (green line), PEG (red line) and a diazepam/PEG mixture (blue line) (panel a). Panel b is a zoom of the ringed zone in the panel a

The analyses were carried upon establishing linear relationship between the intensity of the peak at 9.5 2θ and diazepam concentration in PEG (% w/w).
PEG/diazepam mixture of known concentrations were obtained by simple, gentle mixing of the products (both diazepam and PEG 4000) micronized with a vibration mill. The micronization of the products was carried out to obtain the materials with same size to achieve an even distribution of components and to avoid preferential orientation of particles crystals. Noteworthy, it was tested that the micronization of both diazepam and PEG did not change PXRD patterns.

3.2.12 Differential scanning calorimetry (DSC)

DSC is a thermoanalytical technique which measures the amount of energy (heat) absorbed or released by a sample when is heated, cooled, or held at constant temperature.
In a typical experiment both the sample and reference are positioned inside a single furnace and subjected at the same temperature program. The DSC detects the difference in the amount of heat flow between the sample and the reference, due to exothermic or endothermic processes that can occur to the sample during the temperature scanning.
Typical applications include determination of melting point temperature, heat of melting, glass transition temperature, crystallization studies, and identification of phase transformations.
The DSC used in this work to characterize the raw materials was a Mettler Toledo DSC 821e (Mettler Toledo, USA). Scans of PEG 1500 and 4000 were carried out under a flux of dry nitrogen (100 mL min^{-1}) with a temperature program from 20 to 80°C, from 80 to 20 °C and again 20 to 80 °C, at 10 K min^{-1}. Diazepam was scanned from 25 to 150 °C, at 10 K min^{-1}.
Calibration of temperature and enthalpy values was performed with Indium.

3.2.13 Scanning electron microscopy (SEM)

The morphological analyses of the raw materials and particles were carried out by means of a scanning electron microscopy (Jeol 6400, Jeol, Japan). Samples were coated with graphite (0.001 μm thickness) by evaporation under vacuum, and they were analyzed at a distance of 18-21 mm using a tension of 15 KV.

3.2.14 Laser diffraction particle size analysis

The laser diffraction particle size analysis is a technique useful to characterize particles with a dimension ranging from 0.05 to 3500 μm. In this technique a representative cloud or 'ensemble' of particles passes through a broadened beam of laser light which is scattered from the particle with an angle which is inversely proportional to the dimension of particle itself.

The particle size distribution obtained with this technique is expressed as the volume-equivalent diameter which is defined as the diameter of a sphere having the same volume as the particle.

The samples were analyzed by suspending the dry microparticles in a Span 85/cycloexane solution (0.1 % p/v) saturated with diazepam. The suspension was sonicated for 10 minutes before analysis. Measurements were repeated 5 times for each sample and three samples were measured per batch using a randomised sampling procedure.

The analyses were carried out with 100 mm lens corresponding to a dimensional range of 0.2-180 μm. The results are expressed in terms of d_v 0.1, 0.5 and 0.9 which represent the diameters at 10, 50 and 90 % cumulative volumes, respectively.

3.2.15 Aerodynamic assessment using Andersen Cascade Impactor (ACI)

The pulmonary deposition of the raw diazepam and the microparticles obtained by PGSS was analyzed by means of an Andersen Cascade Impactor (ACI) (Copley Scientific, UK) by using Turbospin® as aerosolisation device, following the procedure described in the USP 30.

Turbospin®

The dry powder inhaler device (DPI) used in this work to study the pulmonary deposition was Turbospin (PH&T, Milan, Italy). This is a medium resistance DPI, with a resistance of 0.09 cm ($H_2O^{1/2}$) L min^{-1} (Meakin et al., 1996), that works at 60 L/min.

In Figure 34, a picture of the device with all its components is reported.

a b c d

Figure 34. Picture of Turbospin with its components: a cap, b capsule with drug, c mouthpiece, d body device

The size #2 capsule, containing the powder to be aerosilized, is positioned inside the body of the device in the capsule chamber, and closed with the mouthpiece. After the piercing of the capsule with a needle contained in the body device, the powder is delivered through vacuum induced by the patient's inspiration. The Turbospin utilizes shear during rattling of the capsule, generated by the airflow through vents along the side of the capsule chamber, and jetting of the airstream at the restriction in the mouthpiece to deagglomerate and disperse the powder (Meakin et al., 1996).
Size 2 Hydroxypropyl Methylcellulose capsules were purchased from Qualicaps Europe S.A. (Spain) for use with the Turbospin® device. The capsules were loaded with 10±1 mg of microparticles.

Andersen Cascade Impactor

ACI allowed to know a detailed aerodynamic size distribution (eight different stage) which corresponds to the stage of the vivo deposition (Figure 35).

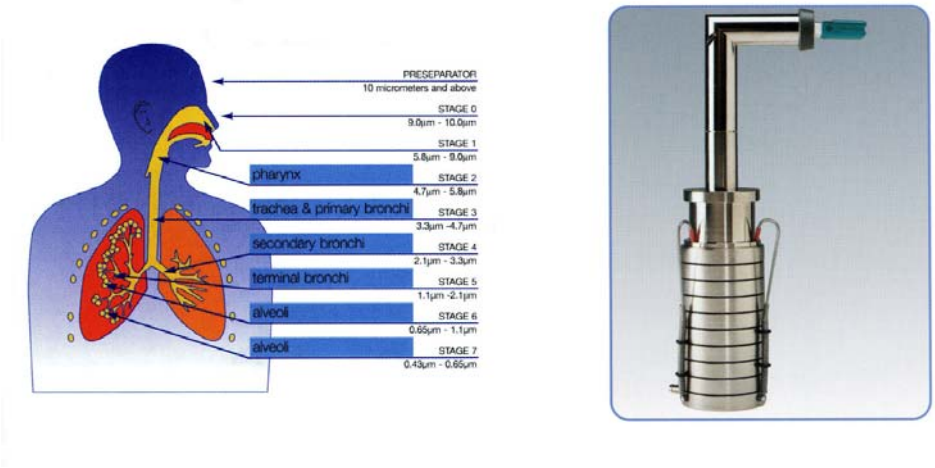

Figure 35. Aerodynamic size distribution of the ACI stages and corresponding areas of the vivo deposition

ACI consists of 8 aluminium stages and a final filter. The stages were clamped together and sealed with O-rings. The aerosolization device was connected to the stages by means of a right-angle bend metal induction port. A suitable mouthpiece adapter was used to provide an air-tight seal between the inhaler and the introduction port.

The analyses were performed at a flow rate of 60 L/min (Q) which produced a pressure drop across the inhaler of 4.0 KPa (TPK 2000, Copley Scientific, UK). Since ACI is calibrated at 28.3 (± 5%) L/min of air, while the aerosolization device requires an air flow of 60 L/min, to work properly, the equation 15 was applied to determine the cutoff diameter of each individual stages of the impactor at 60 L/min:

$$D_{50,Q} = D_{50,Qn} \cdot \left(Qn / Q \right)^{1/2} \qquad [15]$$

where $D_{50,Qn}$ is the cutoff diameter of each stage at the flow rate, Q, employed in the test, and the subscript, n, refers to the nominal values determined when Q_n equals 28.3 L/min.

The test flow duration, T, was calculated by using the equation:

$$T = 240/Q \qquad [16]$$

and it resulted to be 4 seconds. This time was calculated in order that a volume of 4.0 litres of air ± 5 % is withdrawn from the inhaler during the withdrawal of the test dose.

The collection plates of ACI were coated with a solution of span 85 in cycloexane (1 % p/v) to avoid the rebounding of the solid particles inside the instrument.

Each batch was analyzed in triplicate.

Each analysis was carried out by acting the device 10 times through the ACI to obtain a HPLC-detectable amount of drug. Then the impactor was dismantled and each stage was separately washed with a mixture of acetonitrile: water 60:40 v/v. The obtained solutions were filtered (PTFE 0.45 μm, Sartorious, Italy) and analyzed by HPLC with a method described previously for diazepam quantification.

The following parameters were calculated according to the USP:

Recovery. It is defined as the percent of the ratio between the mass of the drug deposited on each stage, induction port, mouthpiece and adapter, and the mass of the drug emitted from the Turbospin®. The recovery value must to be in the 75-125 % range, if the value is outside this range the test must be repeated.

Fine Particle Dose (FPD). It is defined as the mass (mg) of the drug with a particle size less then 5 μm. It is calculated as:

$$FPD = \left(\frac{R}{N} \right) \qquad [17]$$

where R is the total mass of the drug less the 5 μm an N is the number of dose discharged during the experiments.

R was determined by interpolation from a plot which reports the cumulative percentage of drug mass below than stated aerodynamic diameter in probability scale, versus the cutoff diameter in logarithmic scale.

Fine Particle Fraction. It is defined as the % of the mass of the drug less the 5 μm. It was calculated by using the equation:

$$FPF = \left(\frac{R}{\Sigma A} \right) \cdot 100 \qquad [18]$$

where R is the total mass of the drug less the 5 μm an ΣA represents the total mass of the drug recovered from the impactor.

MMAD (Mass Median Aerodynamic Diameter). It is defined as the median particle diameter of the formulation depositing within the ACI. A diagram which reports the cumulative percentage of drug mass less than stated aerodynamic diameter versus the

cutoff diameter was drawn. The MMAD was determined as the diameter which corresponds to 50 % of the cumulative fraction (Figure 36).

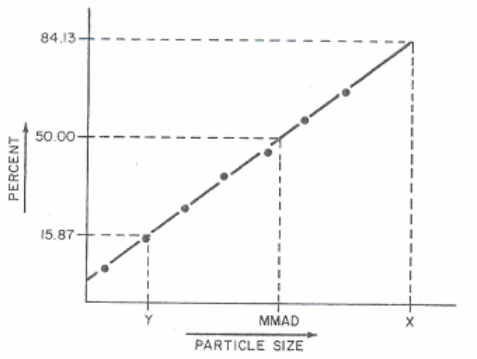

Figure 36. Plot of cumulative percentage of drug mass less than stated aerodynamic diameter versus the cutoff diameter

Delivered Dose. It represents the dose delivered from the Turbospin®, and it is calculated as the weight difference of the device before and after the dose discharging.

3.2.16 Nasal deposition

The microparticles nasal deposition of the microparticles was studied with a silicon cast of the human nasal cavity, using MIAT® as insufflator device .

MIAT®

MIAT® (MIAT S.p.A., Italy) includes a smooth plastic bottle (blue part) with a simple jet outlet (Figure 37).

Figure 37. MIAT® insufflator device

A size #2 gelatine capsule was filled with an exactly weighted amount of microparticles which corresponded to a diazepam dose of 1 mg.
The capsule was positioned inside the jet outlet and pierced with a needle. Then, by pushing the plastic bottle the air inside the container was pressed out of the small nozzle, thereby nebulizing the powder contained in the capsule.
By releasing the pressure again air was drawn inside the bottle.

Silicon cast

The powder contained in a capsule was sprayed in the silicon cast (Figure38).

Figure 38. Silicon cast of the human nasal cavity

The deposited powder was repeatedly washed with a mixture of acetonitrile: water 60:40. The drug amount in the obtained solution (corresponded to the deposited drug) was measured by HPLC with a method described previously.

For each batch, three samples were randomly taken and sprayed inside the cast to analyze the nasal deposition.

The nasal deposition was calculated as the percent of the ratio between the mass of the drug deposited on the cast (analyzed by HPLC) and that emitted from the MIAT®. The dose delivered from the MIAT® was calculated as the weight difference of the device before and after the discharging during the experiment.

3.2.17 Dissolution studies

The rate of drug dissolution from the microparicles was studied by using a flow-through apparatus described in the USP 30.

The apparatus consists in three parts: a reservoir for the dissolution medium, a pump that forces the dissolution medium upwards through the flow-through cell, and the flow-through cell. The dissolution medium was purified water at ambient temperature.

In a typical experiment, by using the pump, water was introduced through the bottom of the cell to obtain a suitable continuous flow through an open circuit at a flow rate of 5 mL/min. After few minutes of equilibration, air starts to escape through the capillary tube and the chamber, and an exactly weighted amount of each samples (corresponding on the basis of the drug content at 10 mg of diazepam) were placed in the flow-through cell.

The microparticles spread through the dissolution medium according to its physico-chemical properties. Samples, at fixed time, were collected at the outlet of the cell and analyzed by HPLC.

The dissolution behavior of pure diazepam, micronized diazepam, and of diazepam from physical mixture and from microparticles prepared by PGSS were analyzed.

The diazepam was micronized by means of a vibration mill for 10 minutes obtaining the microparticles characterized in the section 4.3.

The physical mixture of micronized diazepam and micronized PEG 4000 was obtained by simple gentle mixing. For the binary mixture PEG 4000 micronized was used with a vibration mill until its particles size was close to that of diazepam. The reasons were to achieve a randomly even distribution of components and do not influence the dissolution

behavior. The concentration of the physical mixture investigated was chosen (10 % w/w) to be comparable to that of the microparticles obtained by PGSS.

All the analyses were made in triplicate.

4. Results and Discussion

4.1 HPLC method validation

4.1.1 PEG 1500

The PEG 1500 was quantified by using HPLC according the method described in the section 3.2.1. A calibration curve was drawn using eight PEG 1500 solution in water having different concentrations (Figure 39).

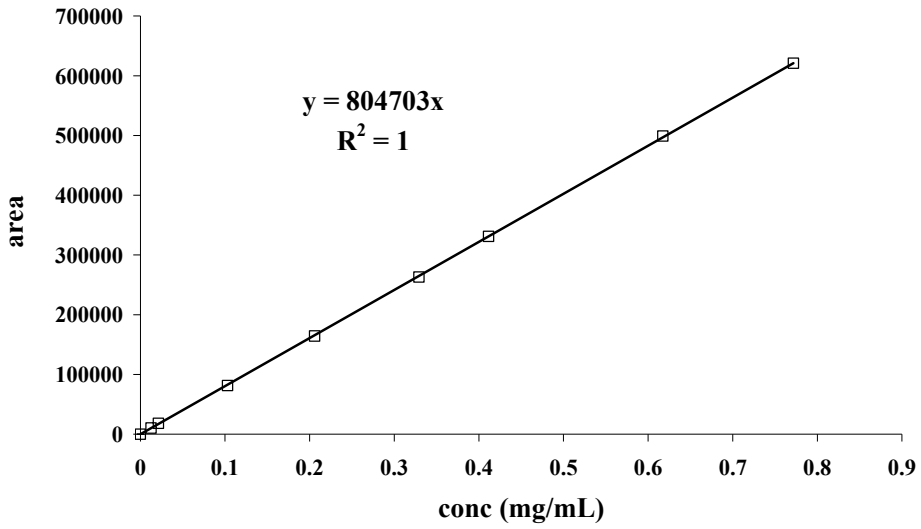

Figure 39. Area of the peaks *vs* diazepam solution concentrations

Each solutions was injected five times and the linearity, precision (expressed as relative standard deviation, RSD %), limit of detection, limit of quantitation, number of theoretical plates and tailing factor of the assay were calculated.

The correlation coefficient (R^2) for the calibration curve was 1 within a range of 0.0127-0.7718 mg/mL which indicates a good linearity.

The reproducibility of the method was considered acceptable as the RSD% values obtained for each standard was < 2%, limit defined by the guidelines ICH Q2 (R1) (Table 5).

Table 5. Standard deviation (n=5) and RSD% values of sample solutions of different concentration samples

Concentration (mg/mL)	mean AUC	standard deviation	RSD %
0.0127	10412	99	0.95
0.0213	18190	285	1.50
0.1029	81367	542	0.67
0.2058	164343	1308	0.80
0.3293	263142	3200	1.22
0.4116	330956	2787	0.84
0.6174	499073	4313	0.86
0.7718	620694	6473	1.04

The limit of detection was 0.0038 mg/mL; the limit of quantitation was 0.0127 mg/mL; the number of theoretical plates was 2038; and the tailoring factor was 1.05.

4.1.2 Diazepam

Diazepam was quantified by using HPLC accordingly with the method described in the section 3.2.1. A calibration curve was drawn using six diazepam solutions at different concentrations dissolved in acetonitrile:water, (60:40) (Figure 40).

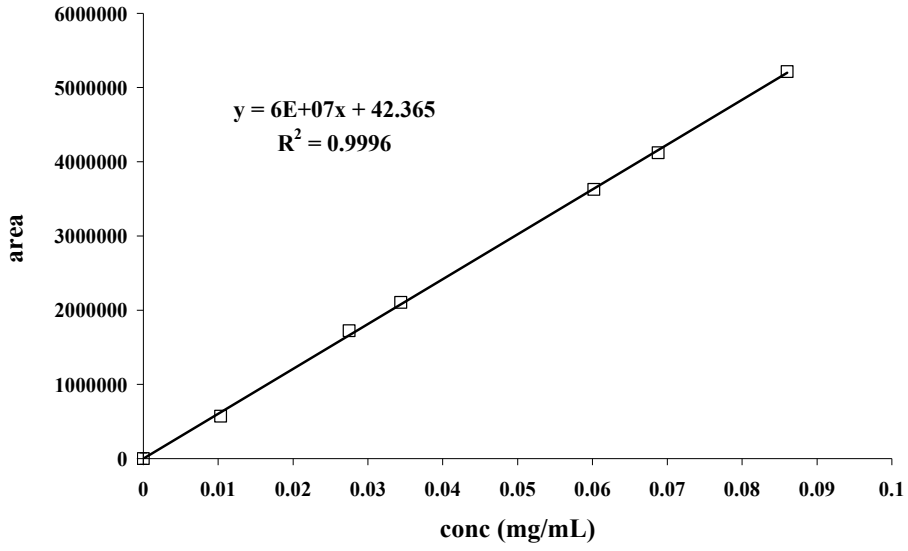

Figure 40. Area of the peaks *vs* diazepam solution concentrations

Each solutions was injected five times and the linearity, precision, limit of detection, limit of quantitation, number of theoretical plates and tailing factor of the assay were calculated. The correlation coefficient (R^2) for the calibration curve was 0.9996 within a range of 0.0103-0.0860 mg/mL which indicates a good linearity also in this case. The reproducibility of the method was considered acceptable (RSD < 2%) (Table 6).

Table 6. Standard deviation (n=5) and RSD% values of different concentration samples

Concentration (mg/mL)	mean AUC	standard deviation	RSD %
0.0103	573224	10466	1.83
0.0275	1723207	7421	0.43
0.0344	2104464	25914	1.23
0.0602	3627897	34841	0.96
0.0688	4121260	68677	1.67
0.0860	5215457	78409	1.50

The limit of detection was 0.75 µg/mL; the limit of quantitation was 2.87 µg/mL; the number of theoretical plates was 12247; and the tailoring factor was 0.94.

4.2 PEG 1500 and 4000 characterization

PEG 1500 and 4000 particles appear like waxy flakes of big dimension (Figure 41).

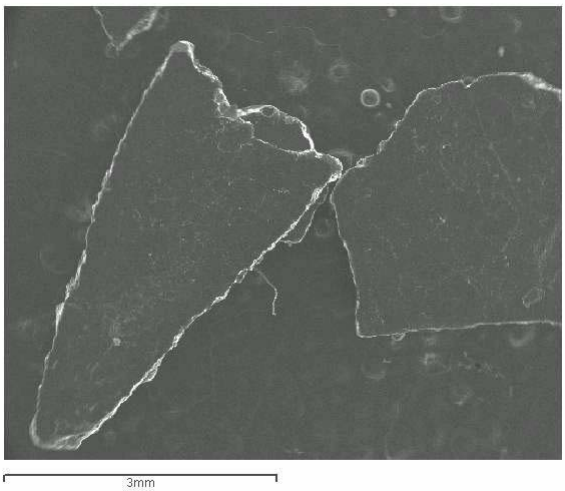

Figure 41. Scanning electron microscopy image of PEG 1500 (20X)

PEG 1500 and 4000 are solid, semicrystalline polymers with a melting point, measured by DSC, of 50.1 and 58.5 °C, respectively. In Figures 42 and 43 the DSC of the PEG 1500 and 4000 are reported.

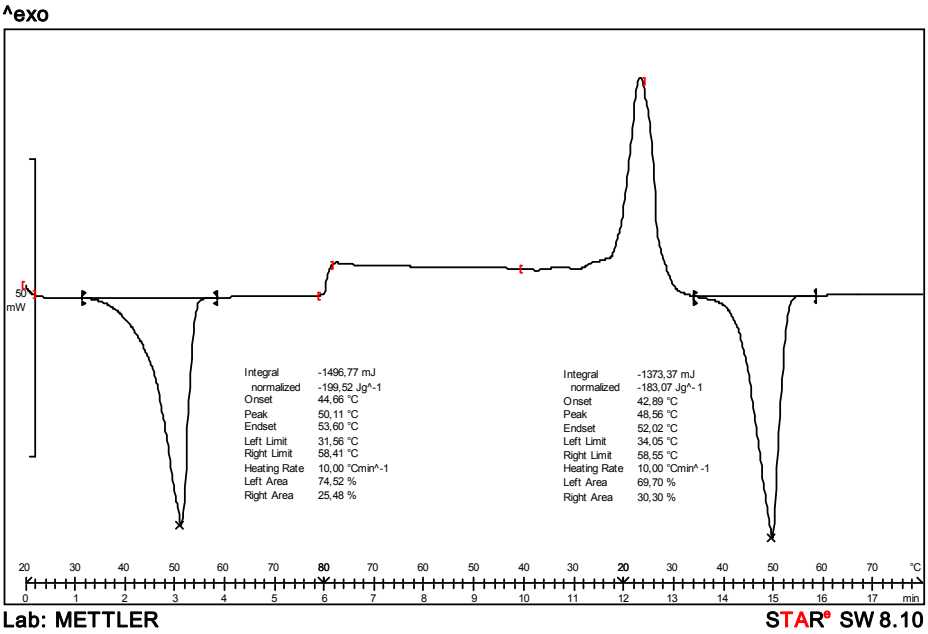

Figure 42. DSC trace of the PEG 1500

The DSC trace of PEG1500 shows an endothermic peak at 50.1 °C indicatives of melting. By temperature decreasing the liquid PEG 1500 recrystallized, and the melting point after recrystallization, was at 48.6 °C.

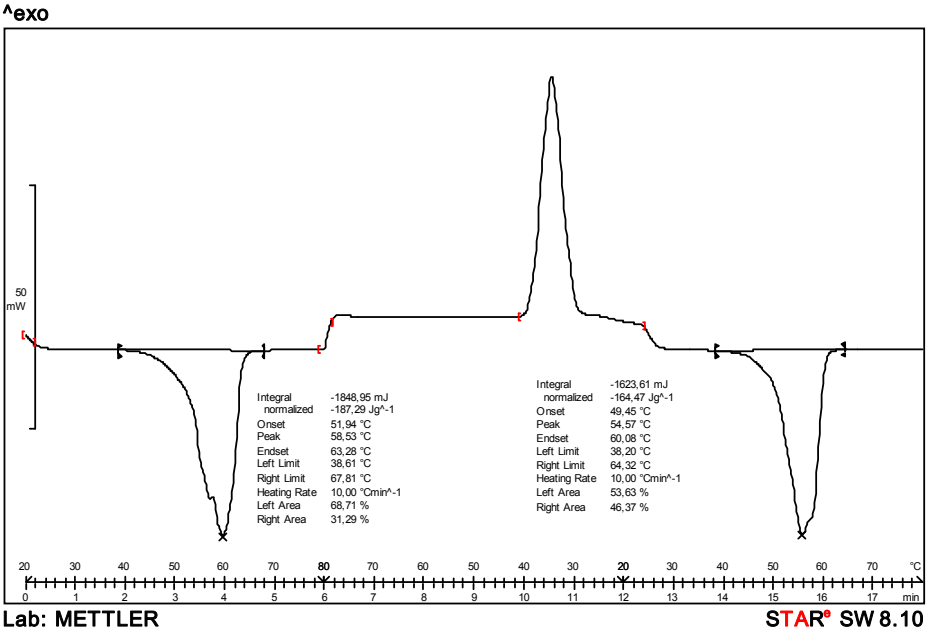

Figure 43. DSC of the PEG 4000

The DSC trace of the PEG 4000 shows a similar trend (Figure 43). The melting point was at 58.5 °C, and the fusion after recrystallization was at 54.6 °C. The melting curve of the PEG 4000 shows a double peak probably due to the polidispersivity of the polymer.

PEG 1500 and 4000 micronized powders were analyzed as well.

In Figure 44 and 45 the DSC of the two micronized polymers were reported.

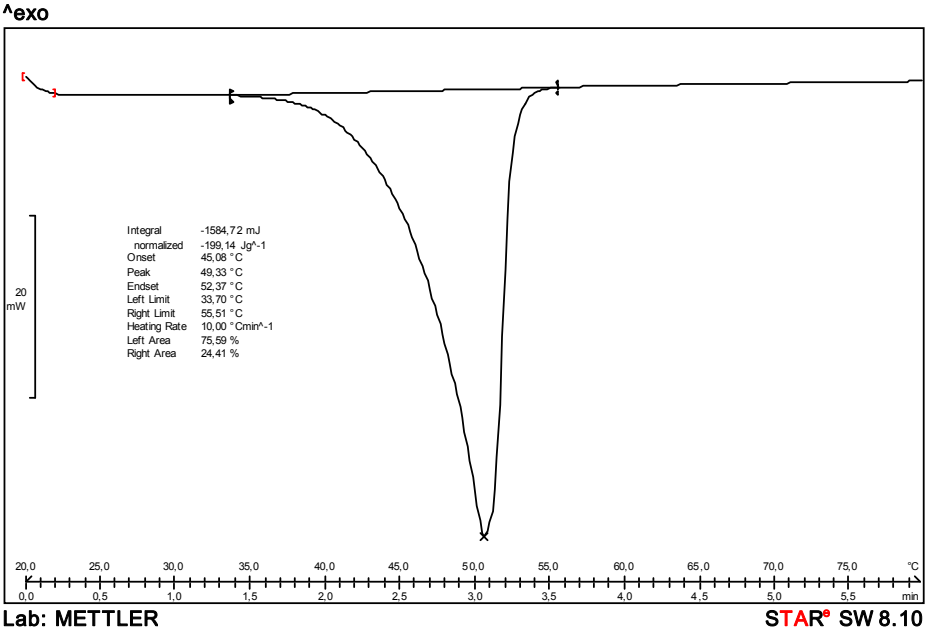

Figure 44. DSC of the micronized PEG 1500

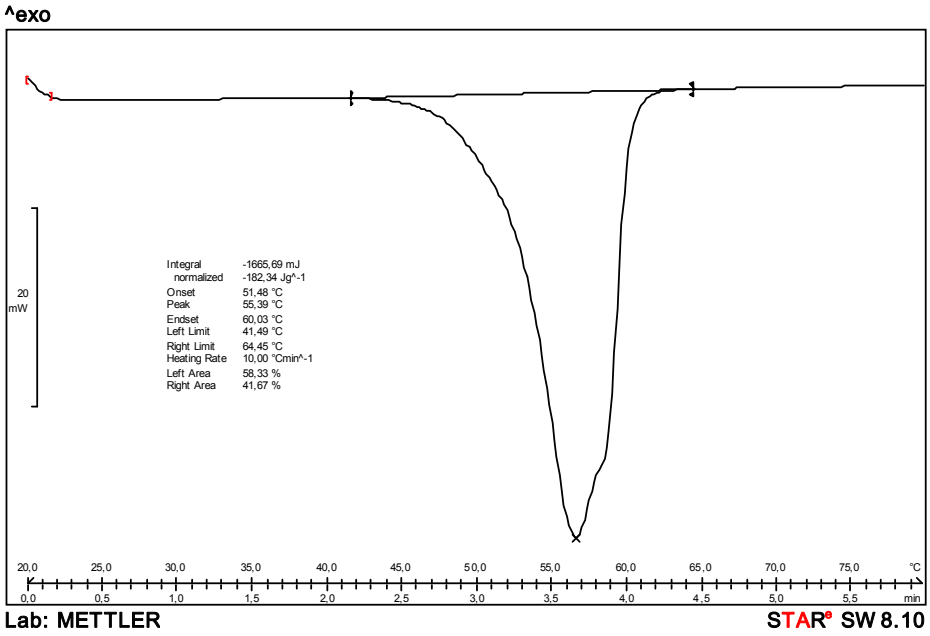

Figure 45. DSC of the micronized PEG 4000

In the case of the micronized polymer the melting points were 49.3 °C for the PEG 1500 and 55.3 °C for PEG 4000. In summary, the recrystallization as well as the milling induce a small reduction of both PEG melting points.

PEG 1500 and 4000 were also characterized by X-ray diffraction. In Figure 46 and 47 the powder X-ray powder diffraction pattern of the PEG 1500 and 4000 as raw, micronized and recrystallized after fusion material are reported.

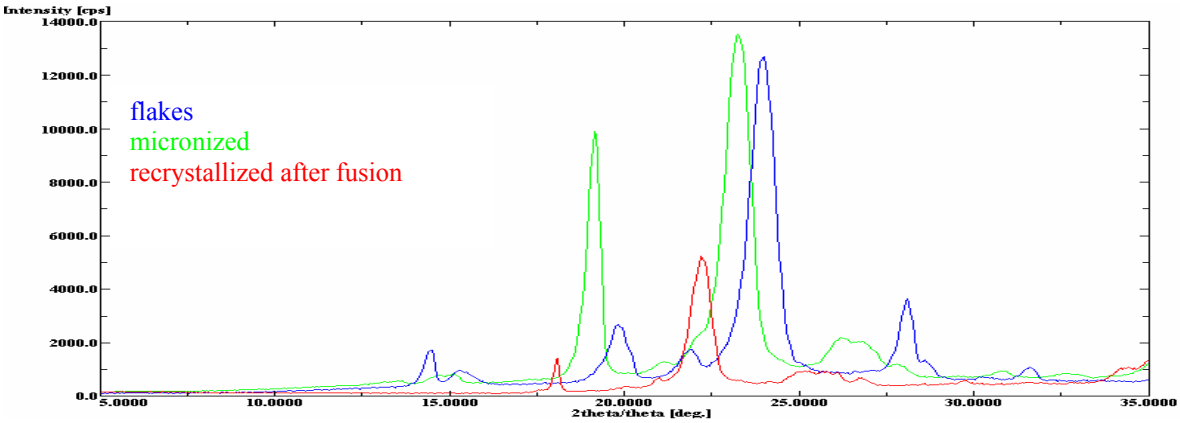

Figure 46. X-ray powder diffraction of PEG 1500 raw material, micronized powder and recrystallized after fusion

The peaks of the micronized and recrystallized PEG 1500 were shifted with respect to that of the raw material. This can be ascribed to the different particle size. The raw material is like flakes of 3 mm in diameter, the micronized polymer are microparticles of 40 μm, and the product recrystallized after fusion is a thin film. Particles with different size and shape may diffract the beam with different orientation eventually leading to a shift of the peaks position.

It is possible to note also that the micronized and recrystallized products are less crystalline (lower peaks intensity) with respect to the raw material. This confirms the observation already made for DSC data.

In Figure 47, the PEG 4000 raw material, micronized powder and recrystallized after fusion are reported.

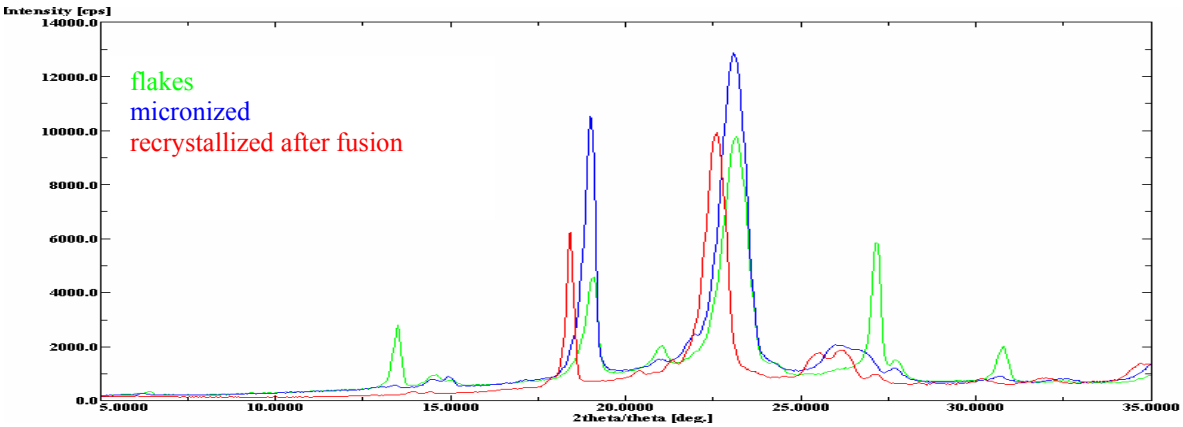

Figure 47. X-ray powder diffraction of PEG 4000 raw material, micronized powder and recrystallized after fusion

In the case of the PEG 4000 it is possible to make the same considerations. The peaks of the micronized and recrystallized PEG 4000 were shifted respect to that of the raw material, although the phenomenon is less evident than in the case of PEG 1500. Furthermore, also in the case of the PEG 4000, the micronized and recrystallized products were less crystalline respect to the raw material.

4.3 Diazepam characterization

Diazepam is a white crystalline powder, as demonstrated by the X-ray difractogram reported in Figure 48, with a melting point of 132.5 °C (Figure 49).

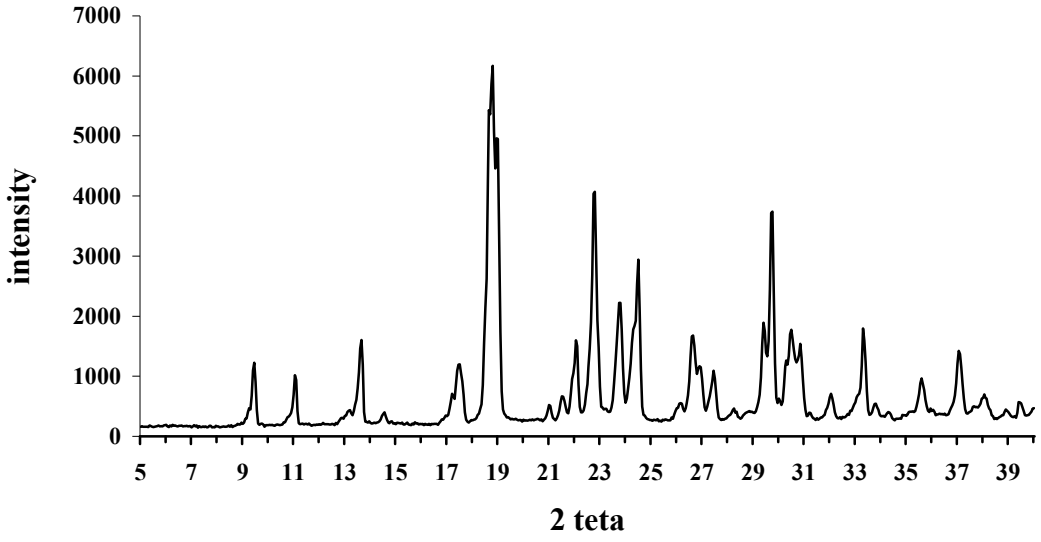

Figure 48. X-ray powder diffraction of diazepam

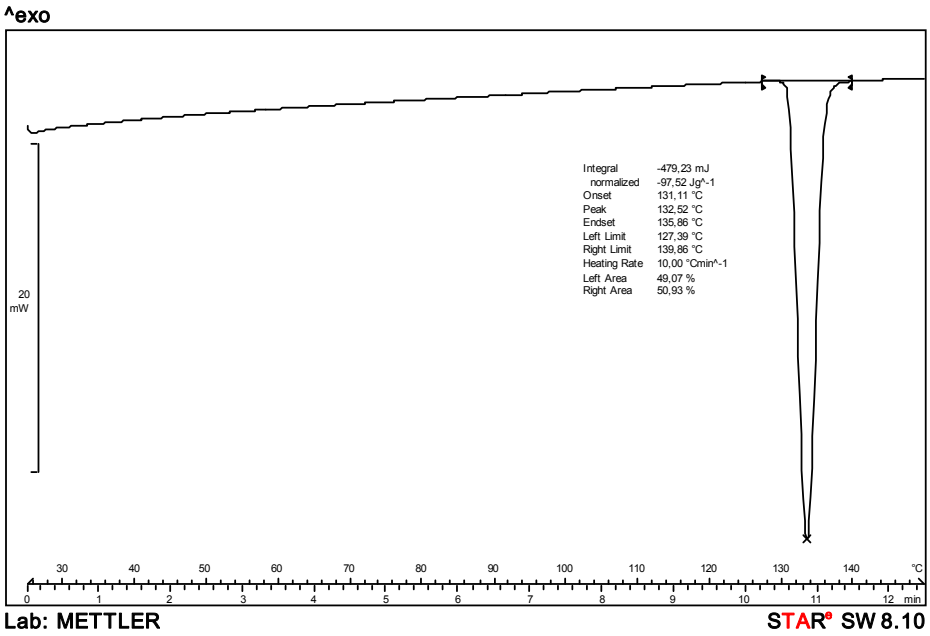

Figure 49. DSC trace of diazepam

The particle size distribution of the diazepam was measured by laser light scattering. In Table 7, the results, expressed as volume diameter are reported.

Table 7. Particle size distribution of diazepam with the standard deviation (n=3)

Material	**d_v 0.1 (μm)**	**d_v 0.5 (μm)**	**d_v 0.9 (μm)**
Diazepam	14.5 (0.29)	42.1 (1.9)	98.0 (9.6)

Furthermore, the morphology of the diazepam particles was analyzed by using SEM (Figure 50).

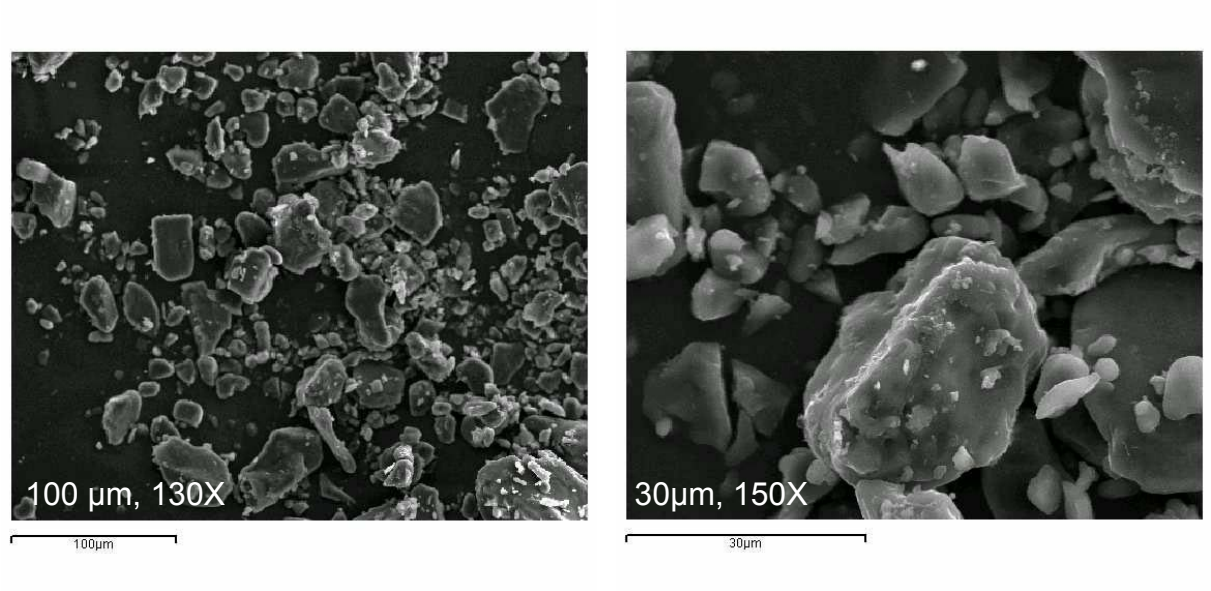

Figure 50. Scanning electron microscope images of diazepam raw material

The SEM images show that the crystals of the raw material were irregular with a dimension varying between 10-40 μm in agreement with the results obtained by the laser diffractometry (Table 7).

It was also produced a batch of diazepam particles micronized by means of a vibration mill in order to obtain particles dimension comparable with that of the microparticles obtained by PGSS (see beyond). The data of the particle size distribution are reported in Table 8.

Table 8. Particle size distribution of diazepam obtained by vibration mill with the standard deviation (n=3)

Material	d_v 0.1 (μm)	d_v 0.5 (μm)	d_v 0.9 (μm)
Vibration mill diazepam	2.1 (0.6)	15.1(1.4)	40.8 (7.8)

It has to be underlined that the dimensional distributional curve obtained with laser diffraction was bimodal, showing the presence of a population of particles with a smaller diameter (Figure 51).

The micronization with the vibration mill led to a poor control of the particle size distribution (demonstrated by the bimodal curve) and to an increase of surface energy with increased tendency to adhesion and agglomeration. Furthermore, the micronized particles showed a high electrostatic charge.

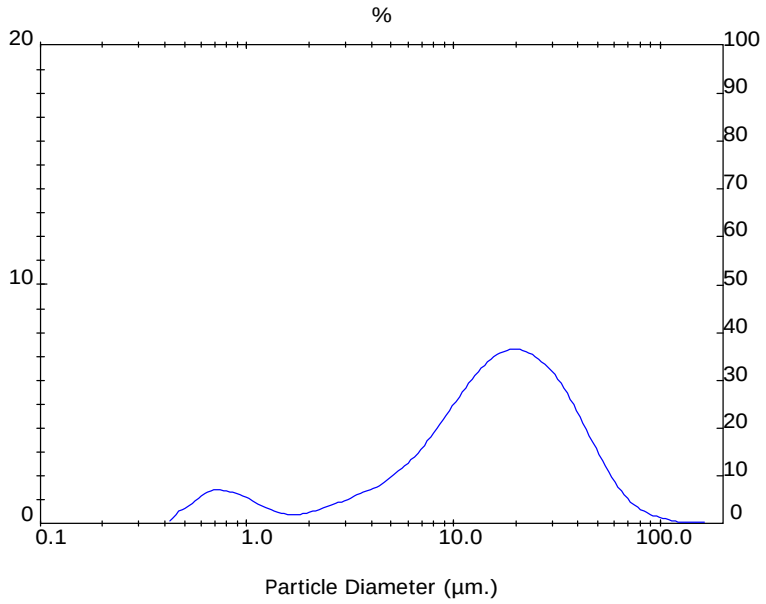

Figure 51. Dimensional distribution curve of diazepam micronized by a vibration mill

The pulmonary deposition of pure and micronized diazepam were carried out by means of ACI and using Turbospin® as device.

Data of the pulmonary deposition with the calculated parameters according to the USP are reported in Figure 52 and 53.

Diazepam raw material

Drug emitted for shot (mg)	8.8 ± 0.41
Recovery (%)	112 ± 12
MMAD (µm)	14.4 ± 2.5
Fine particle fraction (%)	9.7 ± 1.81
Fine particle dose (mg)	0.76 ± 0.08

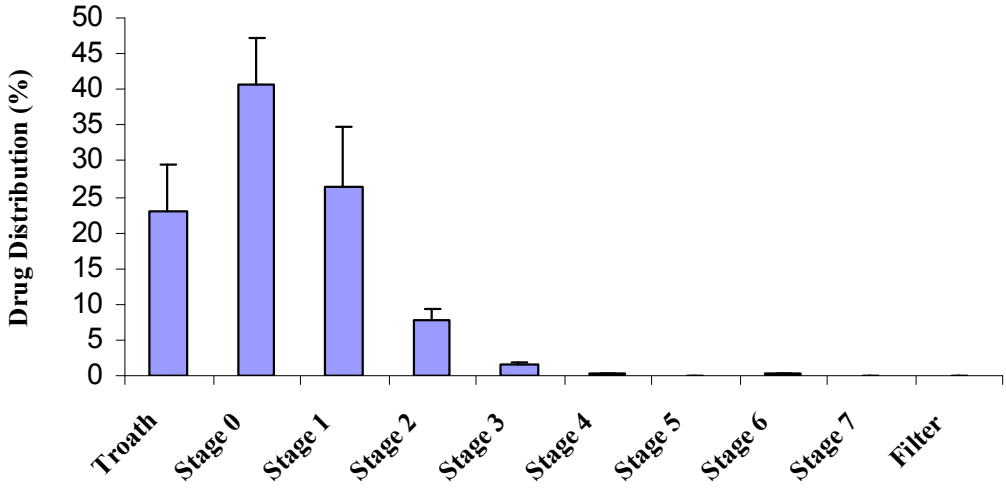

Figure 52. Aerodynamic parameters (Table), and drug distribution % in the ACI

Diazepam obtained with a vibration mill

Drug emitted for shot (mg)	9.9 ± 0.09
Recovery (%)	98.2 ± 11.7
MMAD (µm)	6.7 ± 0.77
Fine particle fraction (%)	25.3 ± 2.9
Fine particle dose (mg)	2.65 ± 0.37

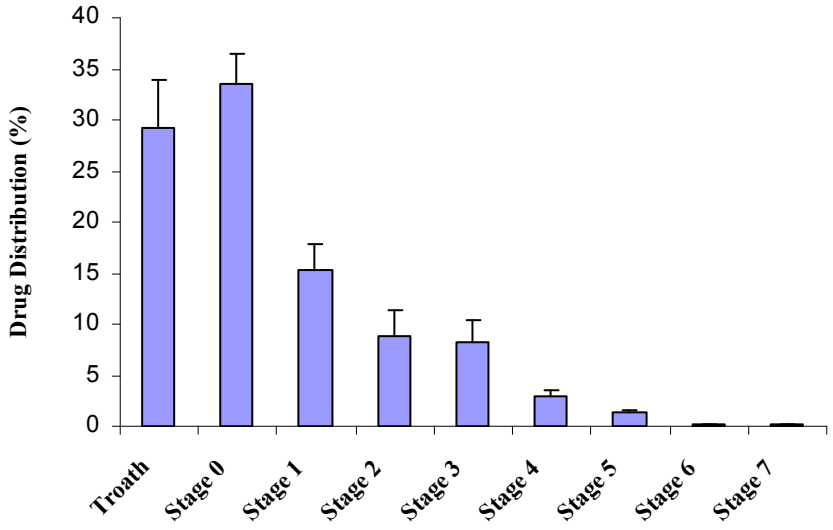

Figure 53. Aerodynamic parameters (Table), and drug distribution % in the ACI

4.4 PEG/CO_2 binary system

To find the most appropriate operative conditions to prepare microparticulate drug delivery systems by PGSS technique, the binary system PEG 1500/CO_2 was studied.
In particular, the PEG 1500 and 4000 melting point variation, and the PEG 1500 swelling under SC-CO_2 were measured. Furthermore, the PEG 1500/CO_2 mutual solubility was performed. The solubility of CO_2 in PEG 1500 was carried out by means of two different techniques: gravimetric, and spectroscopic (ATR-FTIR).

4.4.1 Melting point under Supercritical CO_2

The measurements of the melting points of the PEG 1500 and 4000 under pressure were carried out by means of a high pressure view cell by a method that is a modified capillary method. The obtained data are shown in Figure 54, where the PEG 1500 and PEG 4000 melting points are reported as a function of the CO_2 applied pressure.

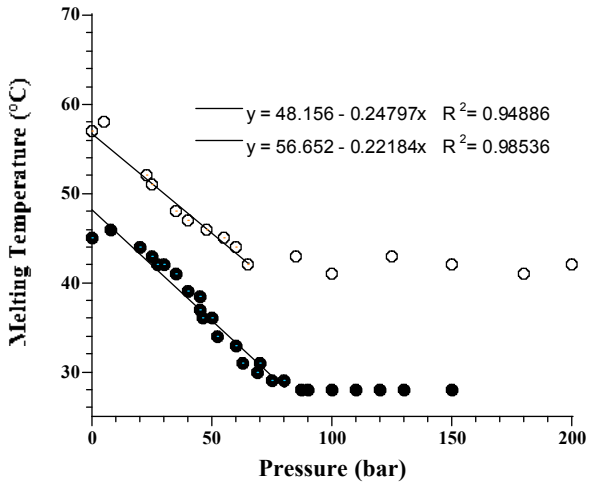

Figure 54. Melting temperature of the PEG 1500 (solid circle) and PEG 4000 (empty circle) in the presence of CO_2 at different pressures, along with the equations of the linear regressions of the experimental data in the 1-80 and 1-65 bar range for PEG 1500 and PEG 4000, respectively

In the 1-2 bar pressure range, the melting point (T_m) of PEG 1500 slightly increased (1 °C), while from 2 to 87 bar a decrease was observed. Then, no further change was observed up to 150 bar.

As already stated by Shieh and Yang (Shieh and Yang, 2005), the first observed phenomenon was probably due to the crystallinity of the polymer, and it might be attributed to an increase in the crystal thickness during CO_2 exposure (Lian et al., 2006).

After 2 bar, the PEG 1500 melting point decreased, and the extent of the melting point depression was directly related to the amount of absorbed CO_2, which, in turn, depended on the applied pressure.

The melting point depression as a function of pressure was determined for PEG 4000 as well. The behaviour of the higher molecular mass polymer paralleled that of PEG 1500: after a slight T_m initial increase, a linear decrease of the melting point was observed up to 65 bar, than T_m levelled off. This indicates that the capability of the CO_2 to reduce the polymer melting point, and therefore to act as a plasticizer, is independent of the polymer molar mass. The shift between the two curves presented in Figure 54 depends, only on the different initial T_m value.

The reported data are in good agreement with those from the literature (Weidner et al., 1997), and are accordingly interpreted in terms of solubility effect, namely as melting point depression of a pure component due to the incorporation of a diluent in a melt (Lian et al., 2006). These authors found that many polymers exhibit, at low pressure, CO_2-induced melting point decrease linearly dependent on pressure, followed by an approximately constant region at higher pressure. By using numerous experimental data (also from literature) they developed a method using the Clapeyron equation for two components, three-phase equilibrium, for predicting the lowest melting temperature for crystalline polymer in the presence of CO_2. These authors, demonstrated that, at low pressure, the simplified form of Clapeyron equation indicates that the melting temperature decreases linearly with pressure. Linear regression was applied to experimental data at low pressure (linear region) in order to determine the slope, dT_m/dP. The melting point variations between the experimental and theoretic data were compared. The obtained melting point variation of PEG 1500, dT_m/dP, was 2.62 and 2.41 for the experimental (Weidner et al., 1997) and the theoretical data, respectively, quite in agreement with the $dT_m/dP = 2.48$ found in the present work. As far as the PEG 4000 is concerned the theoretical, literature (Weidner et al., 1997) and this work figures for dT_m/dP were 2.1, 2.03 and 2.22 respectively.

4.4.2 Polymer swelling under Supercritical CO_2 by using the high-pressure view cell

The absorption of the dense gas into the polymer was also associated to the swelling, in fact the CO_2 solubilizes into the PEG 1500 increasing its volume.
In the Figure 55 the volume equilibrium degree of swelling % reported as function of CO_2 pressure at 35 and 55 °C can be observed.

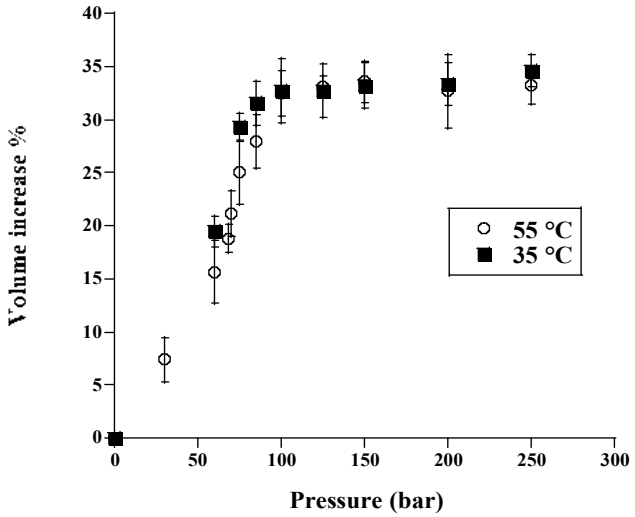

Figure 55. Percentage of swelling (v/v) of the PEG 1500 as function of CO_2 pressure at 35 and 55 °C in the 30-250 bar pressure range. The bars represent the standard deviation (n=3)

At fixed pressure the volume equilibrium degree of swelling, Q, was calculated as:

$$Q = \frac{V_f - V_i}{V_i} \cdot 100 \qquad [19]$$

Where, V_f and V_i are the polymer volume after and before exposure to CO_2 respectively. PEG 1500 swelled with pressure up to 100 bar, thereafter the polymer volume remained practically constant. The maximum Q value was 34.6 and 33.2 % v/v at 35 and 55 °C, respectively. The temperature did not have a significant effect: the two swelling curves were practically superimposed.

4.4.3 Solubility of PEG 1500 in Supercritical CO_2

In Figure 56 the solubility of PEG 1500 in CO_2 at 35 and 55 °C and in the 100-400 bar pressure range are reported as mole fraction *vs* pressure.

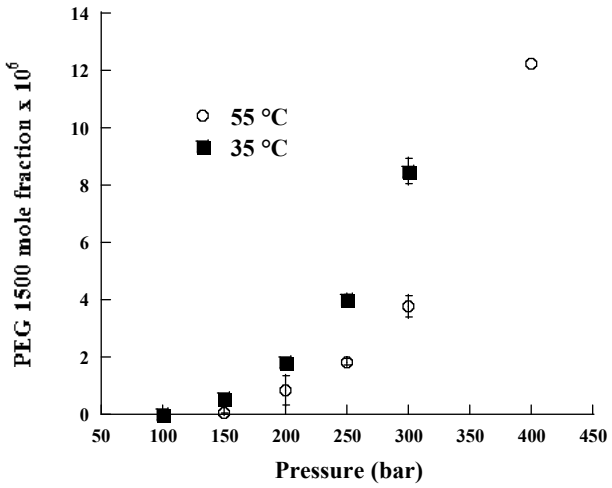

Figure 56. Mole fraction of PEG 1500 dissolved in SC-CO_2 versus pressure at two different temperatures. The bars represent the standard deviation (n = 5)

The PEG 1500 shows a low solubility in SC-CO_2. The solubility increased with the pressure, while it decreased with temperature likely due to the CO_2 density change. It can be observed that the measured solubility values are rather low, although not negligible, due to the fact that the CO_2 is a small molecule with a weak dipolar moment, thus, it cannot easily dissolve large hydrophilic molecule such as PEG 1500. The obtained figures were in the order of 10^{-6} mole fraction, namely one order of magnitude lower than those reported by Dasneshvar et al. (Daneshvar et al., 1990, Duarte, 2006) for PEG 1000 at 50 °C.

Experimental data were correlated with the heuristic model proposed by Giddings and co-workers (Giddings et al., 1968). These authors demonstrated that the solubility of stearic acid, PEG 1000, and PEG 4000 in a very high pressure range (27-190 MPa) can be expressed as a function of the CO_2 solubility parameter and fitted by means of a second degree equation:

$$\log X = a\delta^2 + b\delta + C \qquad [20]$$

where X is the solute mole fraction, a and b are coefficients, C is a constant and δ is the solubility parameter of the CO_2 at a given pressure and temperature.

The solubility parameter, δ, of a given compound can be calculated according to Hildebrand and Scott (Hildebrand and Scott, 1950) from the square root of the cohesive energy, E_{coh}, divided by the molar volume, V:

$$\delta = \sqrt{\frac{E_{coh}}{V}} \qquad [21]$$

Giddings an collaborators (Giddings et al., 1968) stated that the solvent power of a gas depends in part on its state relative to its critical condition. The influence of the state, which depends on pressure and temperature was defined as *state effect*. Besides a *chemical effect*, unique to each chemical species depending on its polarity, acid-base properties, and hydrogen bonding tendency have to be considered. Solvent power differences among liquids depend only on the *chemical effect*, which is expressed by equation 21. Once a dense gas is employed as a solvent reduced density is the principal variable of the *state effect*, which reflects average distances and interactions between molecules.

Thus, the solubility parameter of a compressed gas can be calculated by the equation (Giddings et al., 1968):

$$\delta = 1.25\ Pc^{1/2}\ [\ \rho r / \rho r\ (liq) \qquad [22]$$

where Pc is the critical pressure in atmospheres and the ρr is the reduced density expressed as:

$$\rho r = \frac{\rho a}{\rho c} \qquad [23]$$

here, ρa is the CO_2 density at the given pressure and temperature and ρc is the critical density (for CO_2 = 0.458 g/mL). The parameter ρr (liq) is the reduced density of the liquid that, for CO_2 is 2,66 g/mL. Here the *state effect* can be identified with the second term of the right end side of equation 22, [ρr / ρr (liq)], while the first term, $1.25\ Pc^{1/2}$, is associated with the *chemical effect*.

The density values at given pressures and temperatures, calculated using the Refprop software are reported in Table 9 along with the relevant solubility parameter calculated with equation 22.

The PEG 1500 solubility parameter was calculated with the method of group contributions according to Hildebrand and Scott (Hildebrand and Scott, 1950) as 11.07 $\sqrt{cal/cm^3}$. The difference between the solubility parameters of SC-CO_2 and the polymer justifies the observed low solubility of PEG 1500 at the studied temperatures and pressures. In fact, the solubilization of a solute in a solvent is favoured when the solubility parameters of both solvent and polymer are equal (Hildebrand and Scott, 1950).

Table 9. Density values and solubility parameters of CO_2 at different temperatures and pressures.

Temperature (°C)	Pressure (bar)	Density (g/cm^3)	δ $\sqrt{(cal/cm^3)}$
35	75	0.27	2.38
35	85	0.61	5.38
35	100	0.71	6.21
35	150	0.81	7.10
35	200	0.86	7.54
35	250	0.90	7.84
35	300	0.93	8.12
55	75	0.18	1.59
55	85	0.23	1.98
55	100	0.32	2.83
55	150	0.65	5.69
55	200	0.75	6.57
55	250	0.81	7.06
55	300	0.85	7.45
55	400	0.91	7.89

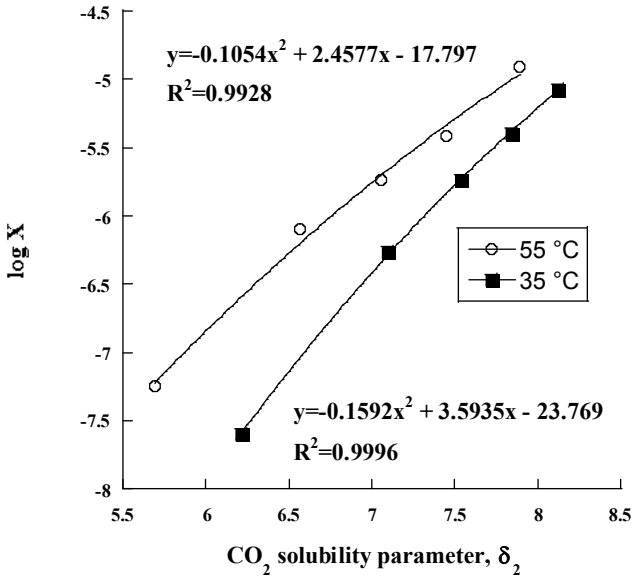

Figure 57. Logarithm of PEG 1500 mole fraction in SC-CO_2 versus the solubility parameter of the solvent

The values of the logarithm of the dissolved polymer mole fraction were plotted versus the relevant δ values (see Table 9) for the two studied isotherms (Figure 57).

The obtained data were fitted to a second degree polynomial equation in order to obtain the a and b coefficients and the constant C of equation 20 (R^2 = 0.993 and 0.999 at 55 and 35 °C respectively). From the data reported in Figure 57 it can be noticed that at lower δ values, namely at lower density, for the same solubility parameter (corresponding the same density) the solubility of PEG 1500 at 55 °C is higher than at 35 °C. This difference decreases with δ increase since, not surprisingly, the two curves tend to a common maximum value that was calculated as –b/2a. At these points the solubility parameter were δ 11.66 $\sqrt{cal/cm^3}$ at 55 °C and δ 11.29 $\sqrt{cal/cm^3}$ at 35 °C. Indeed these figures are very close to that of δ calculated for PEG 1500 (11.07 $\sqrt{cal/cm^3}$).

In agreement with the Hildebrand and Scott theory (Hildebrand and Scott, 1950) as well as with the model proposed by Giddings and co-workers (Czubryt et al., 1970) the maximum of the curves in Figure 57 represents the highest concentration that can be achieved by PEG 1500 in the dense gas. The solubility of the polymer at this point was calculated from equation 20 and resulted $3.23 \cdot 10^{-4}$ and $3.39 \cdot 10^{-4}$ mole fraction at 35 and 55 °C, respectively.

On the other hand, equation 20 can be used also for predicting the solubility of the PEG 1500 in dense CO_2 at those densities (namely temperatures and pressures) at which the solubility is too low to be determined experimentally. In Table 10, the solubility data calculated at 7.5 and 8.5 MPa for the two studied temperatures are reported.

Table 10. Mole fraction of PEG 1500 in carbon dioxide, X_G, and solubility parameter at 35 and 55 °C and 7.5 and 8.5 MPa

T (°C)	P (bar)	δ	X_G
35	75	2.38	$2.85 \cdot 10^{-13}$
35	85	5.33	$2.04 \cdot 10^{-8}$
55	75	1.59	$3.48 \cdot 10^{-19}$
55	85	1.98	$5.27 \cdot 10^{-18}$

It can be noticed that the solubility of PEG 1500 at 55 °C at both pressures is practically negligible, while at 35 °C higher values were obtained. In particular, the solubility value

calculated at 85 bar is comparable to that measured at 100 bar at the same temperature ($2.52 \cdot 10^{-8}$ mole fraction).

4.4.4 CO_2 solubility in PEG 1500 by gravimetric method

Results of the determination of the solubility of CO_2 in PEG 1500 at 35 an 55 °C in a 30-250 bar pressure range are reported in Figure 58 as % w/w *vs* CO_2 pressure.

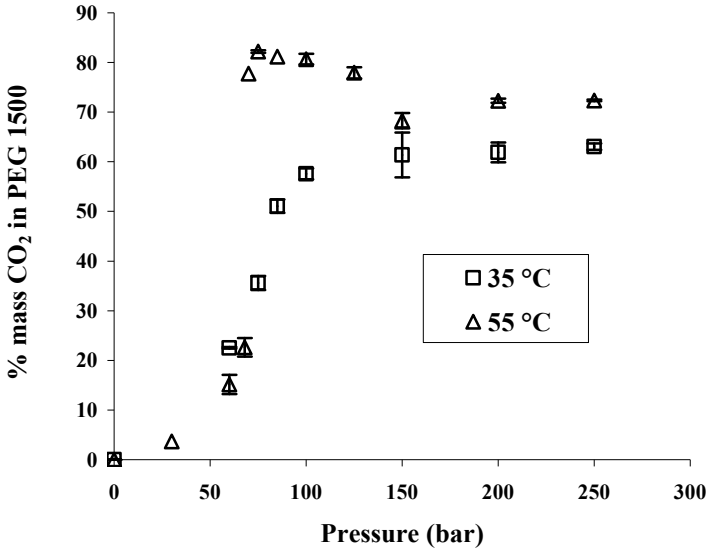

Figure 58. Solubility (%w/w) of CO_2 in PEG 1500 as function of CO_2 pressure at 35 and 55 °C. The bars represent the standard deviation (n=3)

The solubility data increased with the increase of pressure and temperature, but a different trend could be underscored. At 35 °C the solubility dramatically increased up to 100 bar, then it approached a plateau. At 55 °C the solubility of CO_2 increased with pressure up to 75 bar, after that value it remained almost constant up to 100 bar and then it decreased slightly, achieving a constant value similar to that of the plateau observed at the same pressure and 35 °C.

4.4.5 Measurement of CO_2 sorption and PEG 1500 swelling by ATR-FTIR spectroscopy

Principles

Figure 59, shows, as an example, the ATR-IR spectra collected at 55 °C of pure PEG 1500 (ambient pressure) and CO_2 (125 bar). It can be observed that the IR bands relevant to CO_2 and PEG are well separated and clearly distinguishable.

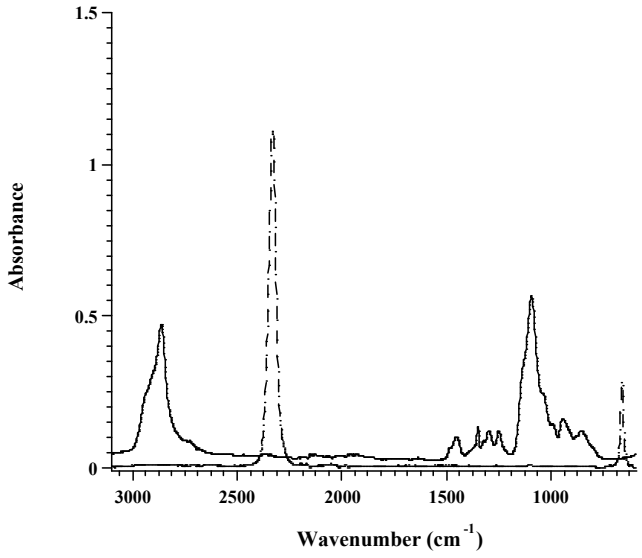

Figure 59. ATR-IR spectra of pure PEG a 55 °C (solid line) before the exposure at the CO_2 and of pure CO_2 at 55 °C and 125 bar (dashed line)

Main characteristic absorption bands are 660 and 2338 cm^{-1} for CO_2 corresponding to the bending and the asymmetric stretching, respectively and 1100 and 2840 cm^{-1} for PEG 1500. Although, all the characteristic bands were studied, the quantitative analysis presented in this work focused on the 2338 cm^{-1} and 1100 cm^{-1} band for CO_2 and PEG, respectively. Upon exposure to CO_2 the PEG spectrum changed (Figure 60).

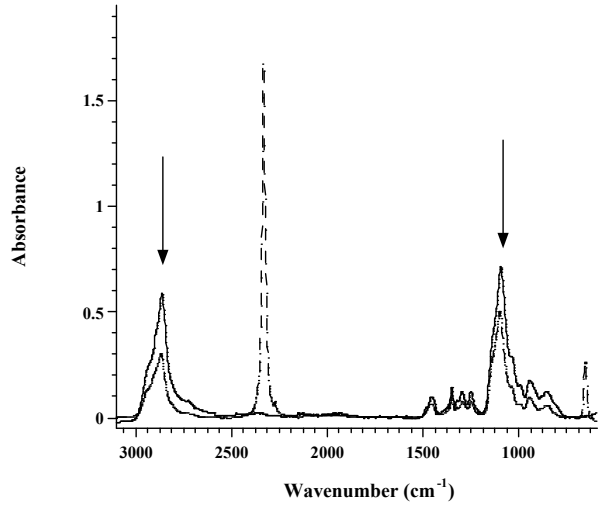

Figure 60. ATR-IR spectra of PEG 1500 at 55 °C before (solid line) and upon (dashed line) exposure to CO_2

In particular, a decrease of the polymers characteristic absorption bands was observed (see arrows in Figure 60).

The intensity of the CO_2 absorption bands was proportional to the amount of carbon dioxide present into the cell which, in turn, depended on the applied pressure. When the polymeric film was placed onto the crystal, obviously, the spectrometer recorded the PEG spectrum as well as the bands of the CO_2. Solely the CO_2 dissolved in the polymer can be detected, owing to the fact that the beam penetration depth (ranging from sub-micrometer to several micrometers) was much smaller than the film thickness. As the CO_2 pressure increased, the intensity of the 2338 cm^{-1} band increased (Figure 61) and, in the same time, the absorbance of the 1100 cm^{-1} band decreased due to a reduction of the polymer density (Figure 62).

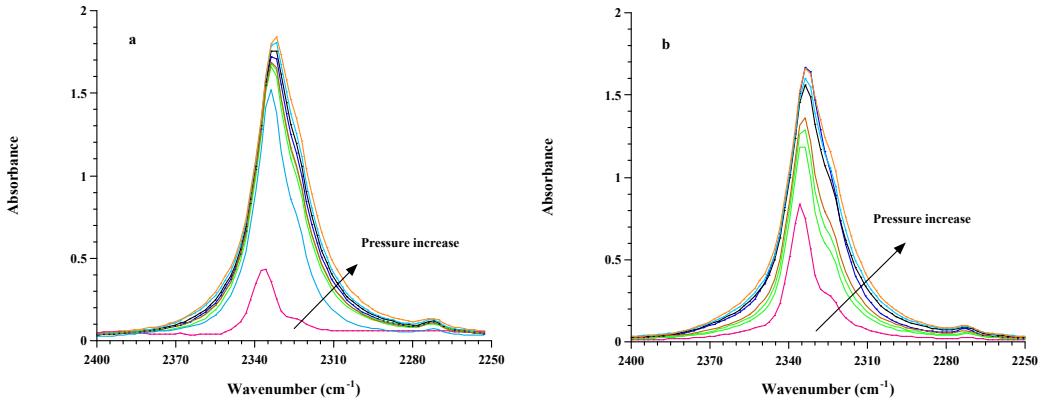

Figure 61. Absorbance of the 2338 cm^{-1} band of CO_2 in a PEG 1500 film at 35 (panel a) and 55 °C (panel b) in the 30-200 bar pressure range

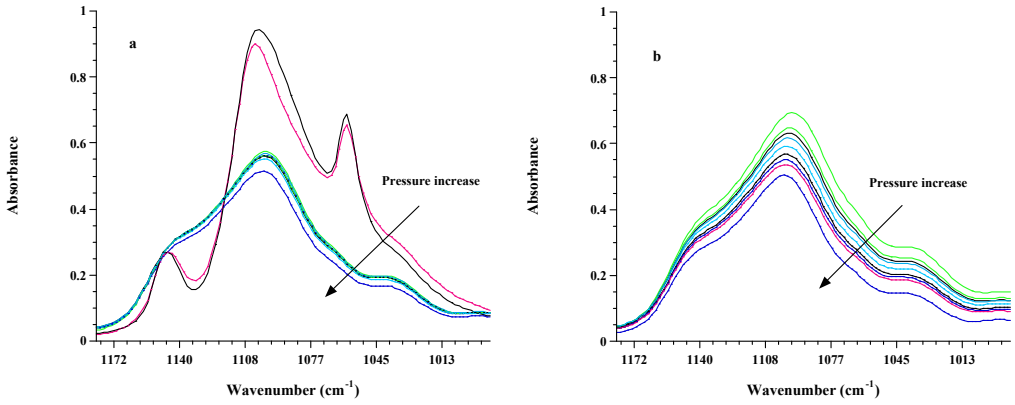

Figure 62. Absorbance of 1100 cm^{-1} band of PEG 1500 at 35 °C (panel a) and 55 °C (panel b) upon exposure to CO_2 in the 1-200 bar pressure range

A remarkable modification of the shape of the 1100 cm^{-1} band at 35 °C was observed by raising the pressure above 30 bar. This effect is due to the solid/liquid transition of the polymer. In fact, at ambient pressure the PEG 1500 melts at 47 °C, while under SC-CO_2 the melting point decreases, as a function of pressure down to 28 °C (see section 4.4.1).

Using infrared spectroscopy, specific weak intermolecular interactions between CO_2 and polymer have been observed for several polymers (Kazarian et al., 1996, Nalawade et al., 2006b). In these papers, it was proposed that Lewis acidity of the CO_2 is responsible for interaction with polymers acting as Lewis's base.

In Figures 63 the spectral shifts of the 660 cm^{-1} band at 35 and 55 °C are reported.

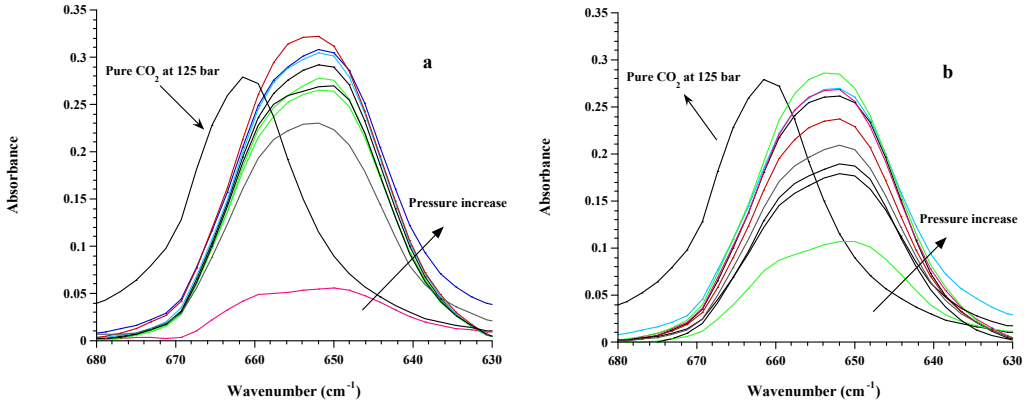

Figure 63. Absorbance at 35 (panel a) and 55 °C (panel b) of the 660 cm^{-1} CO_2 band in a PEG 1500 film in the 30-200 bar pressure range and of pure at 125 bar

At both temperatures a pronounced (about 10 cm^{-1}) shift of the CO_2 bending mode relevant to the CO_2 into the polymer with respect to that of the pure CO_2 can be evidenced. This spectral shift is explained in terms of interaction between CO_2 and PEG 1500. The presence of hydroxyl and ether groups in the PEG molecule is likely responsible for the weak interaction with the CO_2 molecule leading the observed spectral shift to lower wavenumber region. The shape of the band corresponding to the bending mode the CO_2 shows evidence of a possible removal of degeneracy for the bending mode which is indicative of Lewis acid-base interaction as reported previously (Kazarian et al., 1996).

Quantitative analysis

In the ATR-FTIR technique, the beam of infrared radiation traverses a pyramidal crystal of relatively high refractive index and hits the crystal surface at an angle of incidence, θ, greater than the critical angle of the experiment (θ_{crit}).

$$\theta_{crit} = \sin^{-1}(n_s / n_c) \qquad [24]$$

where n_s and n_c are refractive index of the sample and the crystal, respectively.

When θ is higher than θ_{crit} the IR beam is reflected from the internal surface of the crystal creating an evanescent wave projected orthogonally into the specimen positioned in

intimate contact with the ATR crystal. The evanescent electric field created into the sample undergoes an intensity exponential decay (Harrick, 1987):

$$E = E_0 \cdot e^{-z/d_p} \qquad [25]$$

where E is the electric field amplitude at a penetration distance into the sample z, E_0 is the electric field amplitude at the interface, and d_p is the penetration depth given by:

$$d_p = \frac{\lambda}{2\pi\sqrt{(n_1^2\theta - n_2^2)}} \qquad [26]$$

where, λ is the wavelength of the incident beam, θ is the incident angle, n_1 and n_2 are the refractive indexes of the ATR-IR crystal and the sample, respectively.

The solubility of CO_2 in the polymer and the swelling of the PEG was calculated from the intensity of the relevant absorption bands.

To measure the solubility the Lambert-Beer law, which expresses the relation between the absorbance, A, the concentration, c, the beam path length, d, and the absorptivity, ε was used:

$$A = \varepsilon cd \qquad [27]$$

For transmission measurement the beam path length is equal to the thickness of the specimen. When ATR-IR measurements are concerned, it is necessary to use a path length that would give the same absorbance in transmission as that obtained in an ATR-IR experiments. In ATR-IR measurement this path length is called effective thickness (d_e) and it depends on the polarization of the incident light.

The effective thickness for p and s polarized light is defined as complex functions of the wavelength of the incident beam, the refractive index of the ATR crystal and the sample, and the incident angle. The effective penetration for non-polarized light, used in this work to calculate the solubility, is the arithmetical mean between the effective thickness for perpendicular ($d_{e\perp}$) and parallel ($d_{e\parallel}$) polarization (Harrick, 1987):

$$de = (d_{e\perp} + d_{e\parallel})/2 \qquad [28]$$

Harrick et al. presented also the equation for determining the $d_{e\perp}$ and $d_{e\parallel}$. The inputting data necessary for calculate these are: diamond (ATR material) refractive index = 2.42; sample refractive index =1.46; angle of incidence = 43°; wavelength = 2338 cm^{-1}. The amount of CO_2 dissolved in the polymer was calculated with equation 27. The absorbance of the 2338 cm^{-1} band was quantified by measuring the height of the relevant peak. As molar absorptivity of high-pressure CO_2 the value of 1.0×10^6 cm^2 mol^{-1} was used (Maiella et al., 1999). The CO_2 concentration was expressed as g CO_2 per cm^3 of non-swollen polymer.

The swelling of the polymer was calculated by assuming that the absorptivity of the 1100 cm^{-1} band is not affected by the concentration of the dissolved gas. In this case, owing to the above mentioned effect of the CO_2 on the 1100 cm^{-1} band shape, the polymer concentration was determined by using the integrated absorbance, A, as defined by equation 29:

$$\int_{\nu_1}^{\nu_2} A(\nu)d(\nu) = c d_e(\nu)\varepsilon(\nu) \qquad [29]$$

where $d_e(\nu)$ is the optical path length calculated at 1100 cm^{-1} taken as the average value of the interval from 1000 cm^{-1} to 1200 cm^{-1}; $\varepsilon(\nu)$ is the integrated absorption coefficient in the considered frequency range.

The absorbance before (A^0) exposure to the gas is defined by the equation:

$$\int_{\nu_1}^{\nu_2} A^0(\nu)d(\nu) = c^0 d_e^0(\nu)\varepsilon(\nu) \qquad [30]$$

where c^0 and d_e^0 are the polymer concentration and the effective thickness, before the exposure to CO_2 and $\varepsilon(\nu)$ is the integrated absorption coefficient in the considered frequency range.

In both cases the integration range was from 1000 cm^{-1} (ν_1) to 1200 cm^{-1} (ν_2).

The swelling S was calculated by means of the following equation:

$$\frac{c^0}{c} = \frac{V + \Delta V}{V} = 1 + \frac{\Delta V}{V} = 1 + S \qquad [31]$$

where V and ΔV are the polymer volume before and during the exposure to the gas respectively.

By combining equations 29,30, and 31, the polymer degree of the swelling becomes:

$$S = \frac{I^0}{I} \cdot \frac{d_e}{d_e^0} - 1 \qquad [32]$$

where I and I^0 are the intensity of the bands defined as

$$I = \int_{\nu_1}^{\nu_2} A(\nu) d\nu \qquad [33]$$

As mentioned above, the effective thickness depends on the refractive index of the polymer. This last was consider negligibly affected by the polymer interaction with CO_2 in agreement with what reported by Flichy et al. (Flichy et al., 2002) and also considering that all experiments but one (35 °C, 30 bar) were carried out on liquid specimens.

The concentration of CO_2 in the swollen polymer was transformed in mass percentage by using the following equation:

$$\%\text{mass}CO_2 = \frac{c_{gCO_2 \cdot cm^{-3}}}{c_{gCO_2 \cdot cm^{-3}} + \frac{\rho_{pol}}{(1+S)}} \qquad [34]$$

where ρ_{pol} is the density of the polymer in standard conditions (measured with method described in section 3.2.2).

PEG 1500 swelling and CO_2 solubility

As previously stated, for the calculation of the polymer swelling as well as of the solubility of CO_2 in the polymer, the absorbances relevant to the 1100 cm^{-1} band before (A^0) and upon (A) exposure to the gas were compared. At 35 °C and pressure between 1 and 30 bar the shape of the 1100 cm^{-1} band was different to that observed at higher pressures, because of the previously mentioned solid/liquid transition. At 35 °C, above 30 bar the solid/liquid transition implies a change in the 1100 cm^{-1} band. Furthermore, a density decrease from 1.28 to 1.11 g/mL passing from solid to liquid PEG 1500 can be envisaged (see section

3.2.2). This difference in density leads to a difference in the area of the characteristic PEG band. For this reason, for the calculation of the swelling, the absorbance of said band at 35 °C and 30 bar was compared with that at 35 °C and ambient pressure, taking into account the density of the solid PEG. In all other cases the comparison was made using the 1100 cm^{-1} band at 55 °C and ambient pressure considering the density of the liquid PEG 1500.
In Figure 64 the volume swelling % is reported as a function of CO_2 pressure at 35 and 55 °C.

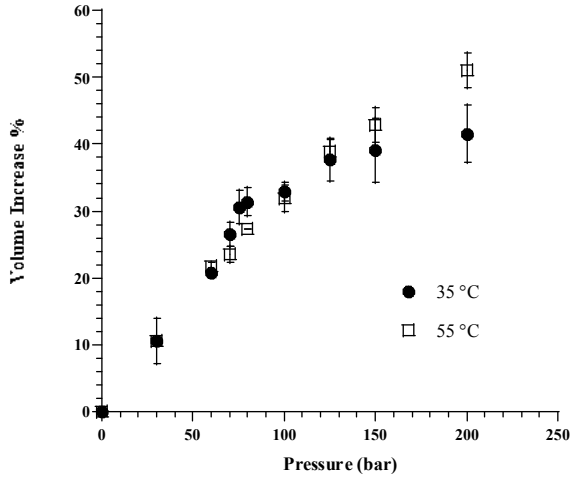

Figure 64. Percentage of swelling (v/v) of PEG 1500 as function of CO_2 pressure at 35 and 55 °C in the 1-200 bar pressure range. Bars represent the standard deviation (n=3)

The polymer swelling increased with pressure, while the temperature did not have a significant effect (Gourgouillon and Nunes da Ponte, 1999): the two swelling curves were practically superimposed. In general, the CO_2 absorption has a remarkable effect on polymer swelling. Up to a pressure close to the CO_2 critical value (70-80 bar), the polymer volume increased linearly with pressure; thereafter, the polymer swelling continued with the pressure increase but with a progressive decrease of the curve slope.
In Figure 65 the solubility of CO_2 in PEG 1500 (as mass percent) at the two studied temperatures is reported as a function of both pressure (panel a) and density (panel b).

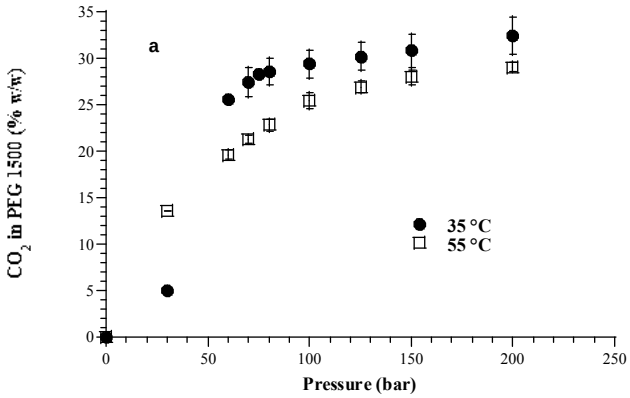

Figure 65. Solubility (% w/w) of CO_2 in PEG 1500 as function of CO_2 pressure (panel a) and density (panel b) at 35 and 55 °C in the 1-200 bar pressure range. The bars represent the standard deviation (n=3)

The reported data were calculated from the height of the 2338 cm^{-1} band taking into account the polymer swelling presented in Figure 64. At both temperatures the solubility dramatically increased with pressure until the CO_2 critical pressure value, then, it approached a plateau. Significantly higher solubility was observed at the lower temperature in the supercritical region ($p < 0.05$ by Student's t-test). This can be mainly ascribed to the effect of the temperature on the CO_2 density as demonstrated by the fact that the solubility data at the two tested temperatures practically overlapped when reported versus the relevant CO_2 density.

4.4.6 Discussion on the solubility and swelling data

In this section, the PEG 1500 swelling and CO_2 solubility data obtained in this study are discuss in comparison to those reported in literature.

In Figure 66, the swelling data at 35 and 55 °C, obtained both with the ATR-IR technique and by means of the visual observation with the high-pressure view cell are reported.

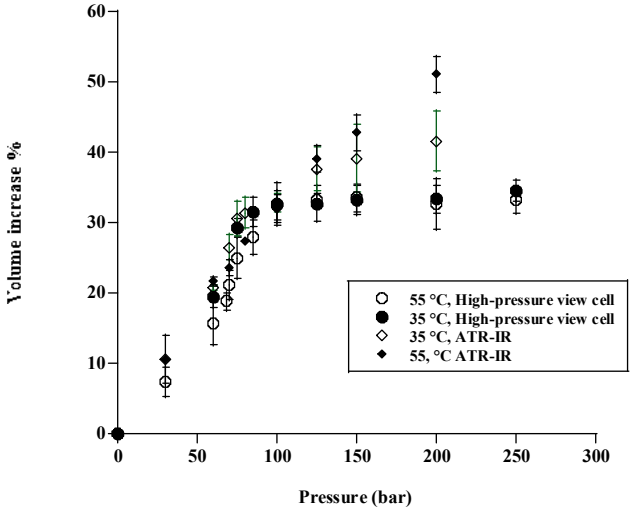

Figure 66. Swelling of the PEG 1500 at 35 and 55 °C. Data obtained both with the ATR-IR technique and by means of the visual observation with the high-pressure view cell

It is possible to note that, up to 100 bar, the curves were practically superimposed. In this pressure range (0-100 bar), different methods gave the same results. Otherwise, for pressure above 100 bar, with the ATR-IR, the swelling increased with the pressure increase, while with the visual observation by view cell the polymer volume remained practically constant.

In the ATR-IR measurements a thin film (1 mm or less in thikness) was used for the measurements, while in the visual observation the samples was composed by a powder contained in cylinder (6-7 mm in thickness). The sample in the ATR-IR was allowed to swell in three dimensions, while in the case of the cylinder sample, only the length along one dimension was measured. This difference can consider responsible for the discrepancy observed in the two cases (Hariharan et al., 1994).

The solubility data collected at 35 °C with the high pressure view cell were compared with those obtained by ATR-IR (Figure 67). It was not possible to compare the data with those of other authors because, in literature, there is no presence of the solubility data at closest experimental condition with respect to those adopted in this work.

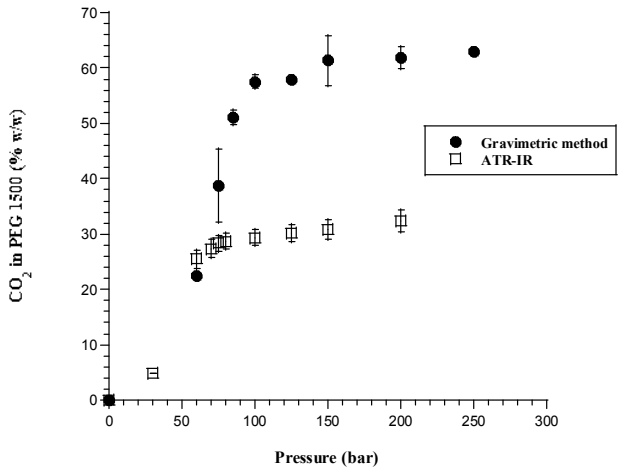

Figure 67. Comparison between the solubility values of CO_2 in PEG 1500 at 35 °C obtained in this work both with ATR-IR, and the gravimetric method

The data obtained by the gravimetric method were comparable with those obtained by ATR-IR up to the critical CO_2 pressure. Thereafter, although the shape of the two curves was comparable, the gravimetric data were significantly higher and the plateau solubility value was almost double relative to ATR-IR data. The solubility data collected at 55 °C, obtained with both the two methods, were compared with those reported by Daneshvar et al. (Daneshvar et al., 1990) and Weidner et al. (Weidner et al., 1997). These authors carried out the CO_2 solubility experiments in the closest experimental conditions with respect to those adopted in the present thesis (Figure 68). Daneshvar et al. measured the high-pressure phase equilibria of PEG 1000 at 50 °C, while Weidner and co-workers carried out the measurements at the same temperature with PEG 1500.

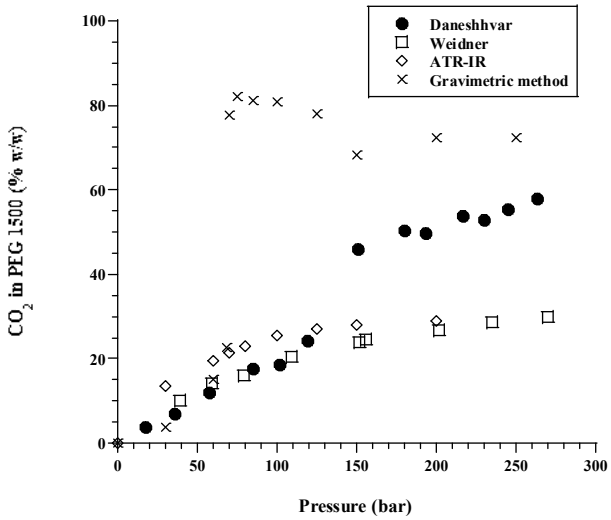

Figure 68. Comparison between the solubility values of CO_2 in PEG 1500 at 55 °C obtained in this work both with ATR-IR, and the gravimetric method, and the data of CO_2 solubility in PEG 1500 (Weidner et al.) and 1000 (Daneshvar et al.) at 50 °C in the 30-280 bar pressure range

Curiously, these solubility data were only partially in agreement to each others. For pressure up to 68 bar the solubility data obtained with the two different methods are in agreement between them and with those reported in literature. For pressure above 68 bar, only Weidner's data and our data obtained by ATR-IR spectroscopy are in agreement, while the data obtained by Daneshvar were significantly higher. The differences of the reported data might be explained considering the different experimental and analytical methods employed. The discrepancy between the data obtained by Weidner and Daneshvar were already discussed by same authors (Weidner et al., 1997, Kazarian, 2000). These autours underlined that the experimental procedure adopted by Daneshvar et al. (Daneshvar et al., 1990) was probably affected by phase equilibrium problems at pressure higher than 150 bar, giving rise to non homogeneous samples which contained large amount of CO_2 as a consequence of foaming. As already stated, sampling procedure and time needed to reach the equilibrium are major issues in phase equilibria studies. Furthermore, it has to be underlined that the high-pressure spectroscopical method is an *in-situ* analysis that did not require any sampling procedure; and the sample used in this analysis was a thin polymeric film that equilibrated in a relatively small time with CO_2.

The curve of the data obtained by the gravimetric method resulted very peculiar. The solubility data showed a jump of solubility between 68 and 70 bar (close to the supercritical region) that led the solubility value up to 82 % w/w. The solubility data at

high pressure resulted much higher even than the solubility data obtained by Daneshavar et al.
The reported data are difficult to interpreter.

4.5 PEG 1500/diazepam/CO_2 system

As it was described above, to prepare microparticulate drug delivery systems by PGSS technique, a mixture of PEG and diazepam was placed in the thermostatic chamber. Then after the interaction with CO_2, PEG 1500 liquefied allowing the diazepam dissolution into the CO_2/liquid PEG mixture. Finally, the solution was expanded through a nozzle.
The knowledge of the diazepam solubility in PEG under SC-CO_2 allowed to fix the right operative conditions to obtain a solution, where diazepam is completely dissolved in the liquid polymer. Consequently, the knowledge of the solubility of diazepam in PEG 1500 under SC-CO_2 at different operative conditions is a necessary prerequisite to identify the diazepam/PEG 1500 ratio to be loaded in the thermostatic chamber.

4.5.1 Quantitative analysis

The quantitative analysis in the FT-IR spectroscopy to measure the solubility of diazepam in PEG 1500 under SC-CO_2 are performed by using the Lambert-Beer law [13].
The characteristic C=O (ketone) stretching band (1680 cm^{-1}) of diazepam was used for the quantification. However, the molar absorptivity of the diazepam in PEG under SC-CO_2 is not known. For this reason, diazepam in PEG 1500 was quantified by comparing the absorbance of the sample with that of known concentration solutions, taking advantage from a previously established linear relationship between absorbance at 1680 cm^{-1} and diazepam concentration in PEG (%w/w).
In Figure 69 the calibration curve of diazepam in PEG 1500 in the presence of SC-CO_2 is presented.

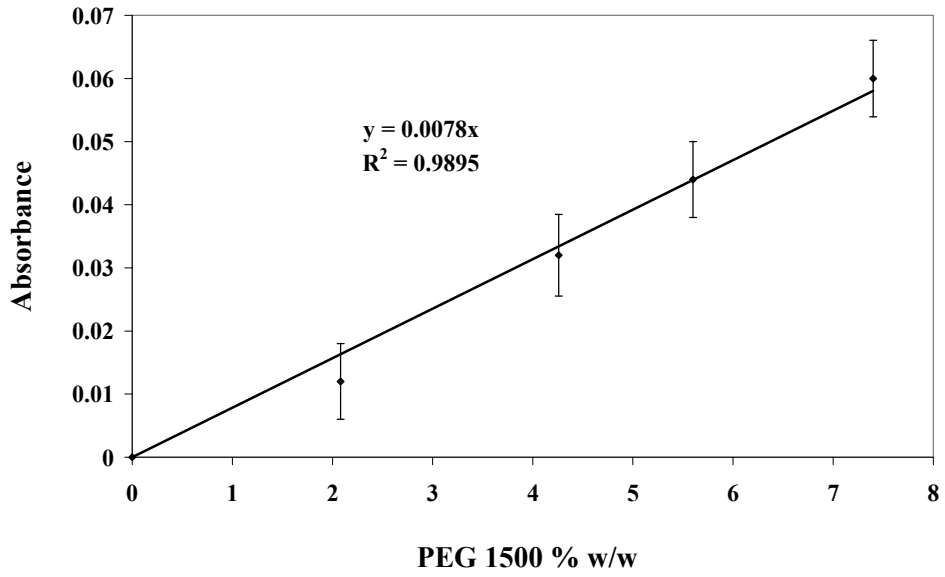

Figure 69. Calibration curve of diazepam in PEG 1500 in the presence of SC-CO_2

In Figure 70, as an example, the ATR-IR spectra of pure PEG 1500 and diazepam, collected at 55 °C in the absence of CO_2 are reported along with the spectrum relevant to CO_2 at 55 °C and 125 bar.

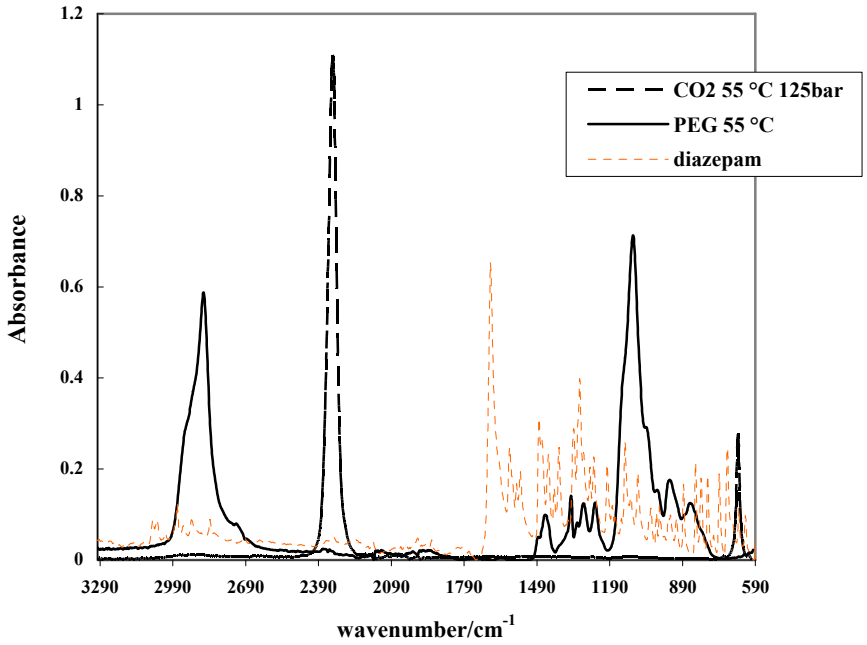

Figure 70. ATR-IR spectra of pure PEG 1500 (solid line) and diazepam (dotted red line) at 55 °C without CO_2 and CO_2 at 55 °C and 125 bar (dashed black line)

The characteristic spectral bands at 2328 cm^{-1} for CO_2, at 1680 cm^{-1} for diazepam and 1100 cm^{-1} for PEG 1500 did not overlap significantly to each other and showed a reasonable absorbance. Thus, they were used to quantify the three components.

In Figure 71 the variation of the intensity of the 1680 cm^{-1} band, relevant to the drug, at 35 °C (panel a) 55 °C (panel b) obtained with MCT detector on the drug containing film (10 % w/w) under CO_2 is reported as a function of pressure.

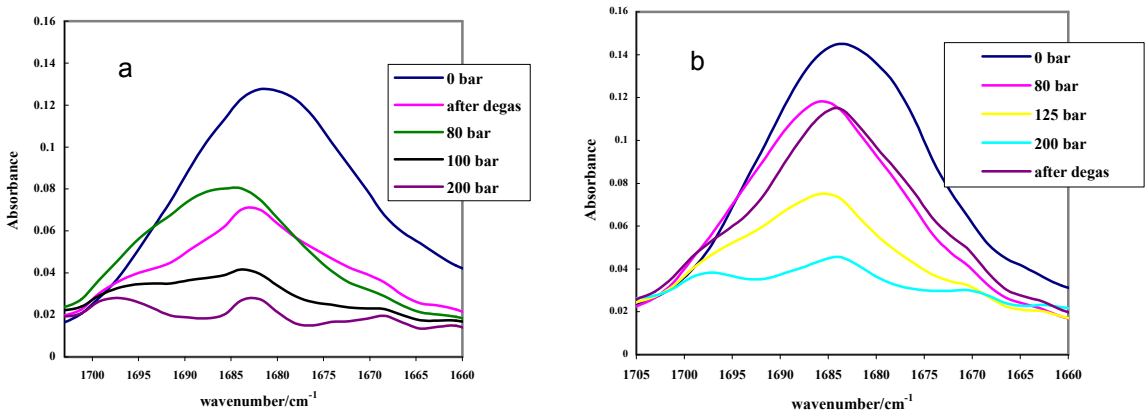

Figure 71. The 1680 cm^{-1} band of the drug at 35 °C (a) and 55 °C (b) and different pressures recorded with the MCT detector on polymeric film containing 10 % w/w diazepam

The intensity of this band decreased with the increase of the pressure at both temperatures. The effect of the temperature was not univocal owing to the not complete equivalence of the sample size. It must be recall that the ATR system could reveal only the drug dissolved into the polymer, namely in intimate contact with the diamond crystal. Therefore, the intensity reduction can be attributed to the drug partitioning between PEG 1500 and CO_2. This was due to the progressive dissolution of the drug into the gas phase as a consequence of the pressure increase. The swelling of the polymer due to the progressive absorption of the CO_2 with the pressure increase can be considered as well to explain the observed phenomenon. Moreover, it must be underlined that upon degassing of the system the drug band intensity recovered a high value, but without reaching the original intensity, namely that registered at 0 bar. In order to quantify the solubility of diazepam in SC-CO_2, transmission NIR experiments were carried out (see section 4.6).

4.5.2 Solubility data

As an example in Figure 72 the images obtained at 80 bar and 35 °C from the film containing diazepam as solid dispersed particles (75% w/v) is presented.

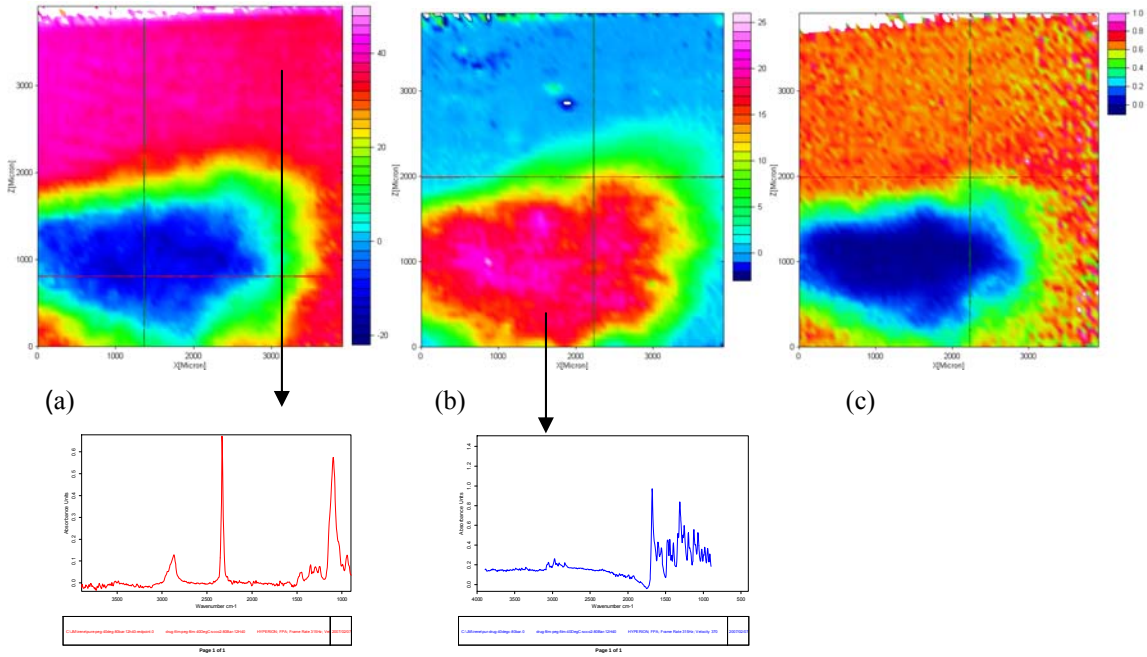

Figure 72. ATR-IR images of a PEG 1500/diazepam thin polymeric film in presence of CO_2 at 80 bar and 35 °C. (a) Spectral band distribution of the PEG 1500 (1100 cm^{-1}), (b) diazepam (1680 cm^{-1}) and (c) CO_2 (2328 cm^{-1}). The spectra were extracted from the images

The images correspond to an area of ca. 820×1140 μm^2, as determined in a previous study (Chan and Kazarian, 2003) and they are accompanied with a scale bar, which associates the colour of the image with the absorbance of a specific band. The band intensity decreases passing from red to orange, to yellow, to green, to blue, being therefore red and blue indicative of very high and low concentration, respectively. Thus the selected ATR-IR spectra from specific location inside the image can be extracted. Differently from the above reported ATR-IR measurements on single component (MTC detector) this system allowed to measure the composition at the equilibrium of multicomponent system in the presence of solid particles, avoiding the risk of misleading results stemming from the measurements of the spectrum relevant to the solid particles instead of that of the solution.

Figure 72 (a) shows the image obtained by integrating the spectral band of PEG 1500 (1100 cm^{-1}). The red region represents a homogeneous area where the polymer is more concentrated. The spectrum extracted from each pixel of this region (panel d) showed the

band of the polymer at 1100 cm^{-1}, the band of the CO_2 at 2328 cm^{-1}, and a small band of the diazepam at 1680 cm^{-1}. This indicates that this sample area is manly composed by PEG 1500 and CO_2, while only a small amount of drug was dissolved into the liquid polymer/CO_2 mixture.

Similarly, images reported in panel (b) and (c) were obtained by integrating the spectral band of diazepam at 1680 cm^{-1}, and CO_2 at 2328 cm^{-1}, respectively.

The red region in panel b represents a diazepam particle; the corresponding area in panel c indicates the practical complete absence of CO_2 evidently due to the fact that the CO_2 did not solubilize into diazepam. On the other hand, the red region in panel c confirmed the high CO_2 solubility in PEG 1500 (red region in panel a) already demonstrated with the analysis of CO_2 solubility in PEG. Finally, it is worthy to underline that in all three images colour (concentration) gradient could be evidenced around the solid drug particle indicating that the system was not yet in equilibrium.

The solubility of diazepam in PEG 1500 in the presence of SC-CO_2 was measured from similar images obtained at the equilibrium. As already stated, the attainment of this last was verified by collecting consecutive spectra until constant intensity of the relevant band was achieved. Furthermore, the spectra extracted from the images, showed that in all regions (red, green and blue), the ratio between the height of the peaks relevant to PEG 1500 and diazepam bands was constant, indicating the achievement of the maximum diazepam concentration in PEG 1500. In this situation the above mentioned drug concentration gradient disappeared.

The obtained solubility values are reported in Table 11 as % w/w.

Table 11. Solubility value of diazepam in PEG 1500 (% w/w) as a function of temperature and pressure

T (°C)	**P (bar)**	**% w/w diazepam in PEG 1500**
35	60	10.86
	80	10.26
	100	9.87
	150	9.49
55	0	16.15
	60	14.74
	80	13.72
	100	14.81
	150	14.36
75	0	19.10
	60	17.95
	100	17.95
	150	17.95
95	0	27.82
	150	26.92

The solubility of diazepam in the PEG 1500 increased with temperature following a hyperbolic trend. As far as the pressure is concerned, no significant influence was evidenced at fixed temperature. Quite surprisingly, at 55 and 75 °C lower diazepam solubility was observed compared to the value measured at ambient pressure. This kind of comparison could not be performed at 35 °C because at this temperature in the absence of CO_2, PEG is solid. On the contrary, no significant difference was evidenced at 95 °C. This can be explained considering that the temperature increase led both to a increase of the diazepam solubility in PEG and to a reduction of the CO_2 solvent power toward diazepam due to the diminution of the supercritical phase density: the overall results its an increase of the diazepam partitioning between PEG and CO_2.

The images at the equilibrium of all samples and experimental conditions show some peculiar features: they did not present a homogeneous aspect as obviously, some areas

pertained to solid diazepam. Beyond this, quite surprisingly the presence of round-shaped areas characterized by very low PEG-diazepam concentration were observed (Figure 73).

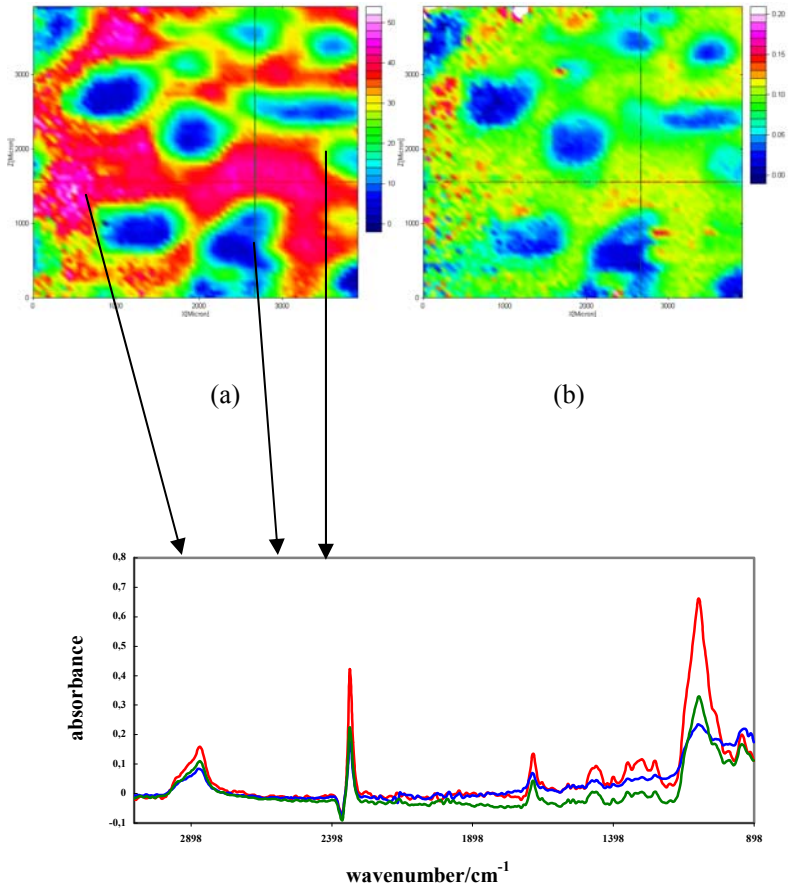

Figure 73. ATR-IR images of the PEG 1500 and diazepam in presence of CO_2 at 80 bar and 55 °C. (a) spectral band distribution of PEG 1500 (1100 cm^{-1}). (b) diazepam (1680 cm^{-1}). Spectra extracted from images

In these areas, weak CO_2 band were detected. However, it must be recall that the ATR-IR system is able to record mainly only substances in solid or liquid state in contact with the crystal. When CO_2 is in the gas phase, due to the different refractive index, the intensity of the CO_2 band is smaller than that recorded when CO_2 is dissolved in the polymer phase. Therefore, we can speculate that these round-shaped areas area might correspond to supercritical CO_2 bubbles entrapped into the polymeric film. This phase separation can be taken as an indication of the fact that in all samples at all tested conditions the PEG films were saturated with CO_2.

4.6 Diazepam/CO_2 system

The solubility of diazepam in pure SC-CO_2 are important data to estimate the potential drug lost into the CO_2 stream during the PGSS particles formation

4.6.1 Quantitative analysis

The solubility of diazepam in SC-CO_2 at 35 and 55 °C in the 30-180 bar range was measured by NIR spectroscopy in transmission. The diazepam concentration was determined by equation 13. The molar absorptivity coefficient (ε) of diazepam was measured in ethanol by assuming that the perfect overlapping of the spectra in the two solvents (CO_2 and ethanol) indicates no change in absorptivity (Liu and Parsons, 1969).
Linearity between drug concentration in ethanol and absorbance at 1485 cm^{-1} was verified (Figure 74).

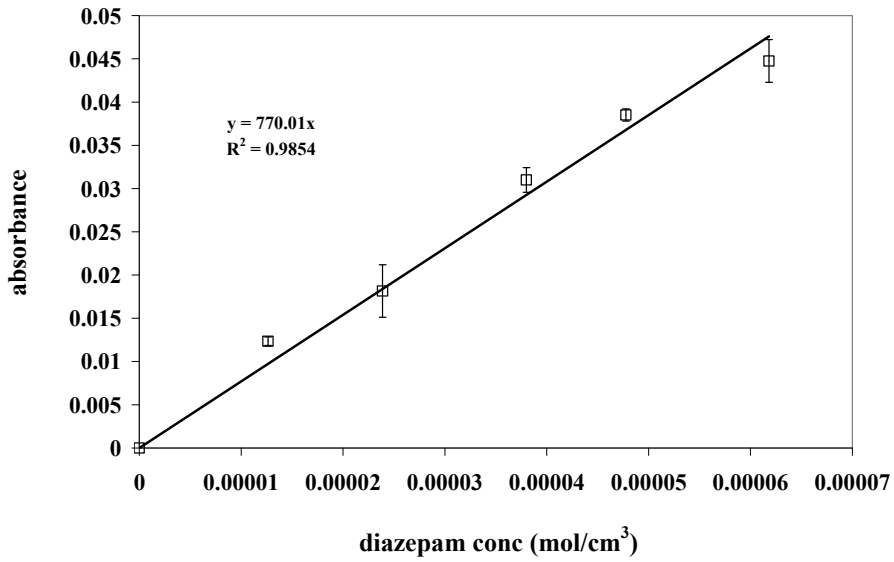

Figure 74. Absorbance of diazepam solutions in ethanol as a function of diazepam concentrations (the error bars represent the standard deviation n=3)

4.6.2 Solubility data

The obtained solubility results are reported in Figure 75 as drug concentration (mole/cm^3) as function of both pressure (panel a) and density (panel b).

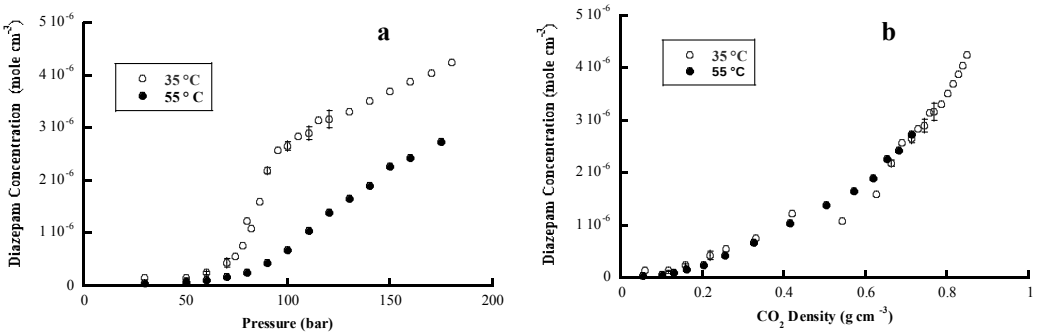

Figure 75. Solubility (mole/cm^3) of diazepam in SC-CO_2 at 35 and 55 °C as function of pressure (panel a) and CO_2 density (panel b)

The solubility of diazepam increased with pressure while it decreased with temperature, likely due to the CO_2 density change (Kompella and Koushik, 2001). In fact, when represented versus CO_2 density (Figure 75, panel b) the two solubility curves were practically superimposed.

Interestingly, a sharp change in drug solubility was observed at 35 °C at pressure close to the critical value (panel a). The phenomenon was less evident at 55 °C. Again this can be attributed to the sudden increase in solvent density around the CO_2 critical point (31.15 °C 73.8 bar).

4.7 Production of the PEG 1500 and 4000 microparticles loaded with diazepam

The preformulation studies described above were employed to set-up the PGSS process. The ability of SC-CO_2 to plasticize the polymer depends on the conditions, namely temperature and pressure, in the thermostatic chamber. For this reason, the knowledge of the phase equilibria of the PEG/CO_2 system is a primary step to applied the PGSS.

Moreover, the solubility data of CO_2 in the polymer allowed to identify at which operative conditions the polymer is less viscous as it has been reported, the higher the solubility and lower the viscosity (Kukova et al., 2003). This last in turn, modifies the capacity of the polymer to be sprayed out through a nozzle. Furthermore, an increase in CO_2 solubility in the polymer may lead to an increase in particles porosity.

Furthermore, the solubility of the diazepam in the polymer in presence of SC-CO_2 may give an indication on the possible drug loading in the particle, while the solubility of the drug in pure CO_2 allowed to estimate the yield of the loading.

In this thesis, the microparticles were obtained both with PEG 1500 and 4000. The melting point reduction under SC-CO_2 was measured for both polymers, while, only the solubility measurements of CO_2 in the PEG 1500 were carried out. Data from literature show that the CO_2 solubility does not change with the molecular weight of PEG, if the same physical state is considered (Daneshvar and Gulari, 1989b, Daneshvar et al., 1990, Gourgouillon et al., 1998, Lopes et al., 2000, Wiesmet et al., 2000). The measurement of the solubility of diazepam in PEG 4000 in the presence of CO_2, was neither carried out. However, it is reasonable to assume that the solubility does not change with the molecular weight of the polymer, if the same physical state is considered.

According to the above reported considerations, the microparticles of PEG 1500 were obtained at 35 and 55 °C, by charging in the thermostatic chamber diazepam/PEG binaries at drug concentrations around 10 % w/w at 35 °C and around 15 % w/w at 55 °C. Such concentrations were chosen on the basis of the temperature, because the solubility of diazepam in PEG in the presence of CO_2 increases with temperature (Table 11).

The pressure used was 100 and 150 bar for the experiments conducted at 35 °C while it was 75, 100 and 150 bar for those at 55 °C.

The microparticles of PEG 4000 were obtained at 55 °C (at 35 °C PEG 4000 is solid at any pressure, Figure 54), in the 100-250 bar pressure range, and by charging in the thermostatic chamber a diazepam/PEG mixture containing around 15 % w/w of drug.

4.7.1 Yield of the precipitation process

The yield of the process is defined as the percentage of the mass of the mixture (PEG/diazepam) loaded in the thermostatic chamber with respect to the mass of microparticles obtained by PGSS.

The obtained values of the microparticles obtained with PEG 1500 and 4000 are reported in the Table 12 for PEG 1500 and 4000 microparticles.

Table 12. Yield of the PGSS process for PEG 1500 and 4000 microparticles containing diazepam

Operative conditions	Yield
PEG 1500	
35 °C, 100 bar	56.5 %
35 °C, 150 bar	42.7 %
55 °C, 75 bar	29.2 %
55 °C, 100 bar	50.0 %
55 °C, 150 bar	63.6 %
PEG 4000	
55 °C, 100 bar	54.4 %
55 °C, 150 bar	59.5 %
55 °C, 200 bar	61.3 %
55 °C, 250 bar	62.2 %

Reported yields varied between 29.2 and 63.6 % although all the material present into the autoclave was sprayed out, giving rise to a theoretical yield of 99.99%. The difference between the measured and theoretical yield can be ascribed to the difficulties in collecting particles.

4.7.2 Drug content of the microparticles

The microparticles theoretical drug content (defined as the percentage by weight of diazepam in PEG 1500 or 4000 loaded in the thermostatic chamber, before the analysis) and the microparticles drug content measured by HPLC were compared (Table 13).

Table 13. Measured and theoretical drug content expressed as % w/w, with the standard deviation (n=3) of the measured drug content

Operative conditions	Theoretical drug content	Measured drug content	ds
PEG 1500			
35 °C, 100 bar	9.1	6.8	0.91
35 °C, 150 bar	9.3	7.1	0.57
55 °C, 75 bar	12.8	11.1	0.40
55 °C, 100 bar	12.9	11.3	0.70
55 °C, 150 bar	13.3	11.7	0.55
PEG 4000			
55 °C, 100 bar	15.5	10.3	0.18
55 °C, 150 bar	15.5	11.6	0.38
55 °C, 200 bar	15.3	13.6	0.73
55 °C, 250 bar	15.3	11.9	0.60

The theoretical drug content was about 3 % w/w higher then the measured one. This difference can be justified by considering the relatively high solubility of diazepam in the supercritical CO_2.

To verify the drug content uniformity three samples of the obtained microparticles were randomly taken and analyzed by HPLC. The mean value with the standard deviation are reported in Table 13. The low standard deviation (between 0.38 and 0.91) indicates a good uniformity of the drug content in the product, which can be expounded considering that particles were obtained starting from a solution.

4.7.3 Particle size distributions and morphology study

The particle size distributions of PEG 1500 and 4000 microparticles containing diazepam are reported in Table 14.

Table 14. Particles size distribution and standard deviation (n=3) of diazepam containing microparticles of PEG 1500 and 4000

Operative conditions	d_v 0.1 (μm)	d_v 0.5 (μm)	d_v 0.9 (μm)
PEG 1500			
35 °C, 100 bar	12.6 ± 0.30	53.1 ± 0.89	181.9 ± 1.9
35 °C, 150 bar	17.5 ± 0.25	48.7 ± 1.21	129.6 ± 2.5
55 °C, 75 bar	17.7 ± 0.18	107.0 ± 1.90	343.8 ± 2.9
55 °C, 150 bar	10.2 ± 0.25	49.5 ± 0.65	262.8 ± 3.4
PEG 4000			
55 °C, 100 bar	3.9±0.07	20.9±0.81	46.6±3.00
55 °C, 150 bar	4.1±0.16	16.4±1.65	40.1±6.27
55 °C, 200 bar	4.3±0.29	18.5±0.04	42.1±1.98
55 °C, 250 bar	4.4±0.06	16.5±0.33	35.4±2.14

Furthermore, the obtained microparticles and the original PEG and diazepam materials were analysed by SEM to assess their morphological characteristics (Figure 76 and 77, respectively).

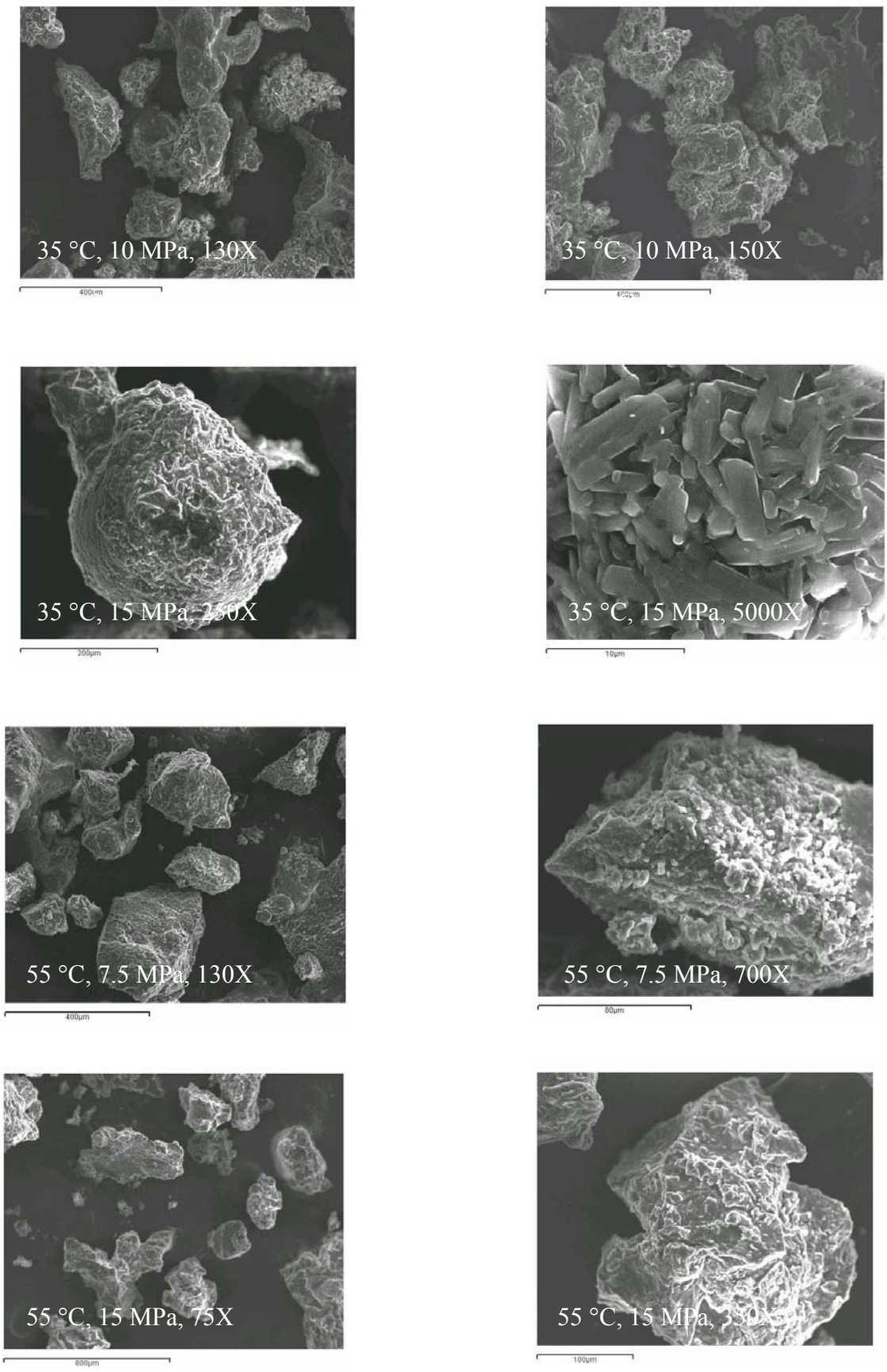

Figure 76. Scanning electron microscope images of PEG 1500 microparticles obtained by PGSS at different pressure and temperature

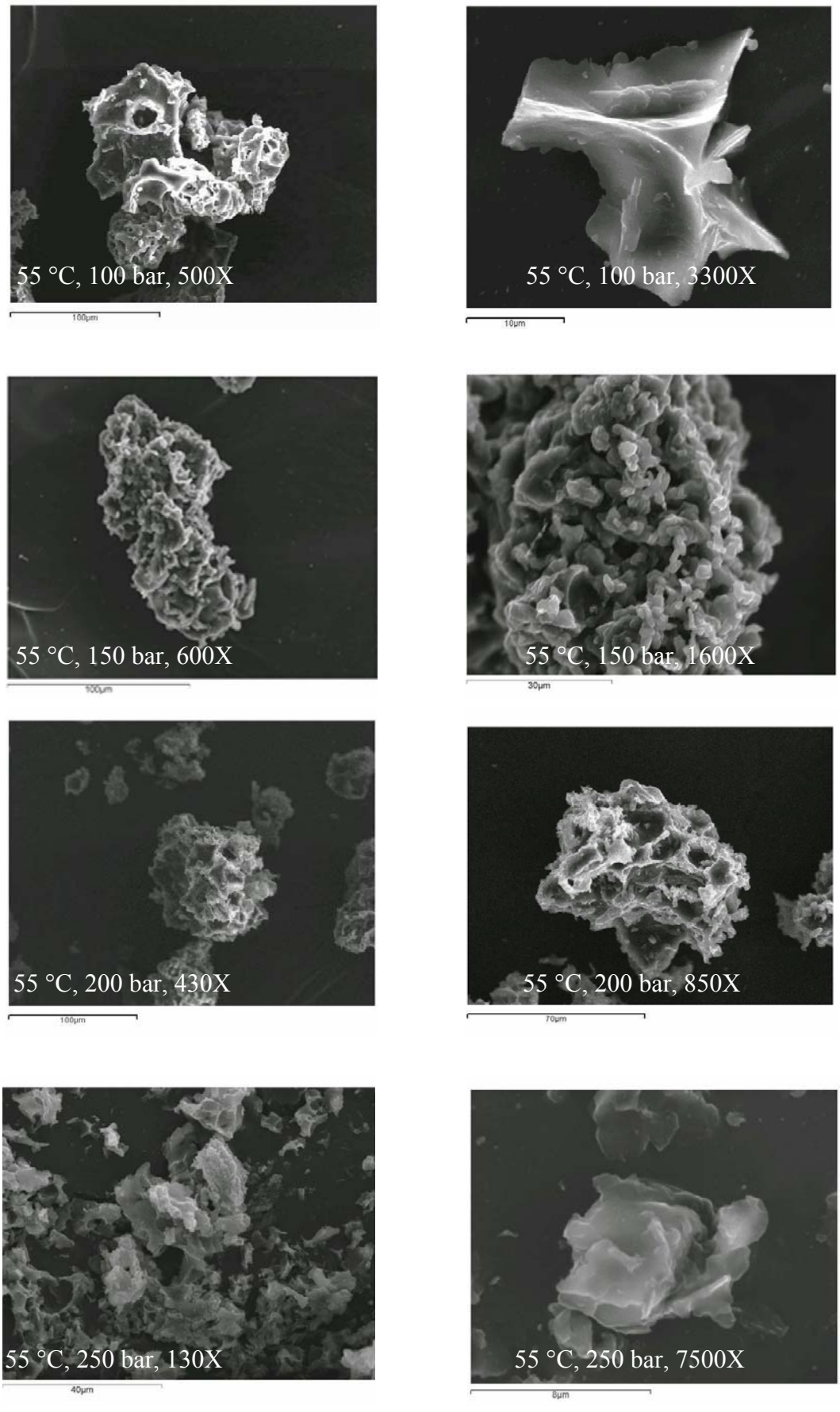

Figure 77. Scanning electron microscope images of PEG 4000 microparticles obtained by PGSS at different pressure and temperature

The microparticles of PEG 1500 show an irregular morphology with a big variation in the dimension (confirmed by laser light diffraction analysis), an they present different shape and size from the raw material (see section 4.2 and 4.3). Furthermore, these microparticles were made by small particles sticked together that form agglomerates difficult to separate. Also macroscopically the particles were sticky and difficult to handle.

The microparticles obtained with PEG 4000 were smaller than the raw material and than microparticles obtained with PEG 1500. The PEG 4000 microparticles obtained at 100 bar were irregular and highly porous. At 150 bar the microparticles were more regular, agglomerate and they assumed a more regular shape. The microparticle regularity increased passing from 150 to 250 bar. This was accompanied by a reduction of a agglomeration. PEG 4000 microparticles were less sticky and more easily to handle than that obtained with PEG 1500.

The morphology, as well as the particle size of the sprayed product in the PGSS technique are primarily determined by two phenomena: *nebulization* and *solidification*. The nebulization occurs when a low viscous material is sprayed trough a nozzle giving rise to a dispersion of very fine droplets; while the solidification occurs when the change in the environmental conditions make the droplets solid. The morphology as well as the particle size changes with the relative rate of these two processes. For example, spherical particles are produced when the nebulised polymer droplets have enough time to adjust their morphology and only after this period of time the solidification process occurs. The nebulization rate is determined by the flow rate of the liquefied polymer through the nozzle, so it can be changed by changing the viscosity of the material (the higher the pressure and temperature and lower the viscosity). The solidification rate can be adjusted by changing the operative conditions: increase of temperature, decrease of pressure, as well as the low molecular mass of the polymer slow down the solidification rate. Furthermore, it has to be considered that if the sprayed particles cannot solidify quickly enough they might fuse together giving rise to agglomerates (Hao et al., 2005, Mooney et al., 1996).

In the case of the microparticles obtained with PEG 1500, agglomerates with irregular shape were obtained because of the low molecular weight of the polymer. Polymer with low molecular weight shows a low melting point (PEG 1500 melting point is nearly 10 °C lower than that of PEG 4000), and low viscosity; these characteristics generate a fast nebulization and slow solidification. Under these circumstances, the nebulized polymer solidifies slowly that the particles fuse together giving rise to the agglomerate reported in Figure 76.

As far as the temperature effect is concern, an increase of temperature decreases the solidification rate. Therefore, at fixed pressure higher temperature results in bigger particles (Table 14). On the other hand an increase in pressure gives rise a viscosity decrease in the polymer/diazepam solution (in the thermostatic chamber) as well as to an increase of the pressure drop at the nozzle. This, in turn, results in a fast solidification rate and nebulization result in smaller particles.

The microparticles obtained with PEG 4000 showed lower agglomeration and particle size distribution, and a more regular morphology than the microparticles obtained with PEG 1500. This higher molecular weight polymer shows a higher viscosity, and melting point temperature, that generates a fast microparticle solidification. Such quickly solidification led to the formation to less agglomerate particles.

The higher porosity of the PEG 4000 microparticles relative to those obtained with PEG 1500 can be ascribed to the faster solidification rate. When a fast solidification occurs, the CO_2 remains entrapped inside the PEG/diazepam mixture affording the formation of micoparticles with high porosity.

It has to be underlined that the influence of the parameters described above is quite complex, especially because the characteristics of the particles obtained stem from the combination of the effect of all above reported factors.

4.7.4 Deposition study by Andersen Cascade Impactor

The pulmonary deposition of the particles obtained with PEG 1500 and 4000 was carried out with ACI by using Turbospin® as device.

Each batch was analyzed in triplicate. Each analysis was carried out by acting the device 10 times through the ACI to obtain a HPLC-detectable amount of drug.

Assuming the dose of 1 mg, the capsule of the device was loaded with nearly 10 mg of microparticles having a drug content ranging 10-15 % w/w.

Although PEG 1500 particles showed non optimal characteristics for aerosolization (large particles with broad particle size distribution) the pulmonary deposition was tested for the particles obtained at 55 °C and 150 bar.

The relevant data are reported in Figure 78.

PEG 1500 microparticles at 55 °C and 150bar

Drug emitted for shot (mg)	0.75 ± 0.14
Recovery (%)	101 ± 9.3
MMAD (µm)	7.8 ± 1.6
Fine particle fraction (%)	32.1 ± 0.86
Fine particle dose (mg)	0.25 ± 0.06

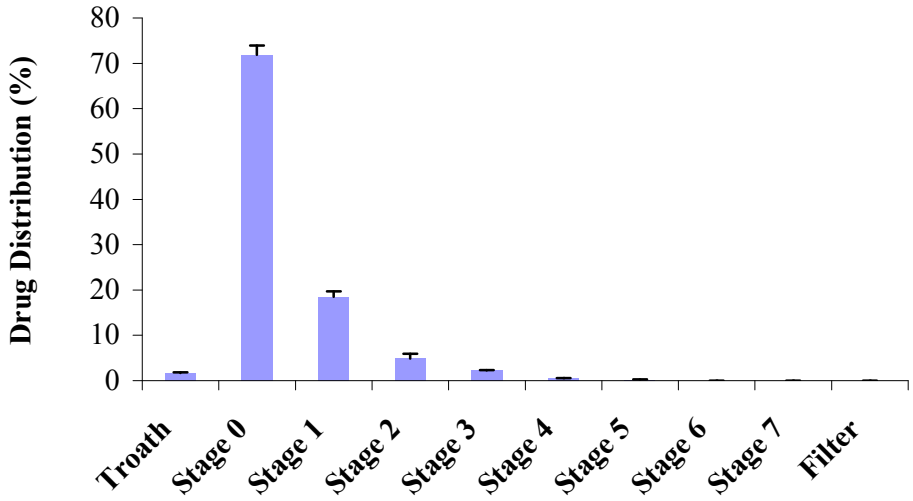

Figure 78. Aerodynamic parameters (Table), and drug distribution % in the ACI

The amount of drug emitted per shot was low and highly variable.

Two shots were necessary to complete emission of the loaded microparticles (44.7±9.1 and 63.2±10.6. emitted with the first and second shot, respectively).

This behavior (pure flowability and difficult handling) reflects the tendency to stick and agglomerate already evidenced when discussing particle size and morphology of these particles.

The aerodynamic behavior of PEG 4000 microparticles prepared at 55 °C and 100, 150, 200, and 250 are reported in Figures 79, 80, 81 and 82, respectively.

PEG 4000 microparticles at 55 °C and 100 bar

Drug emitted for shot (mg)	0.86 ± 0.06
Recovery (%)	96.7 ± 2.81
MMAD (µm)	8.6 ± 0.06
Fine particle fraction (%)	24.7 ± 0.49
Fine particle dose (mg)	0.23 ± 0.01

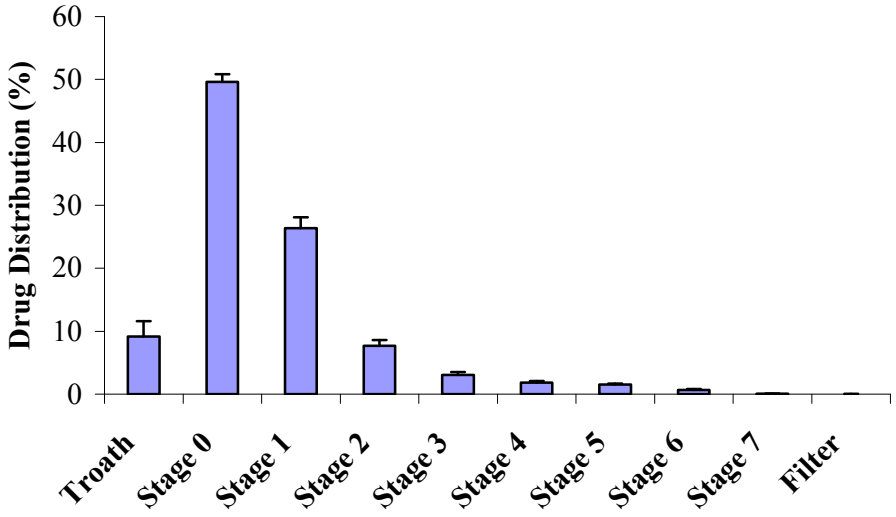

Figure 79. Aerodynamic parameters (Table), and drug distribution % in the ACI

PEG 4000 microparticles at 55 °C and 150 bar

Drug emitted for shot (mg)	0.96 ± 0.02
Recovery (%)	88.42 ± 4.34
MMAD (µm)	7.16 ± 0.54
Fine particle fraction (%)	29.52 ± 4.63
Fine particle dose (mg)	0.36 ± 0.08

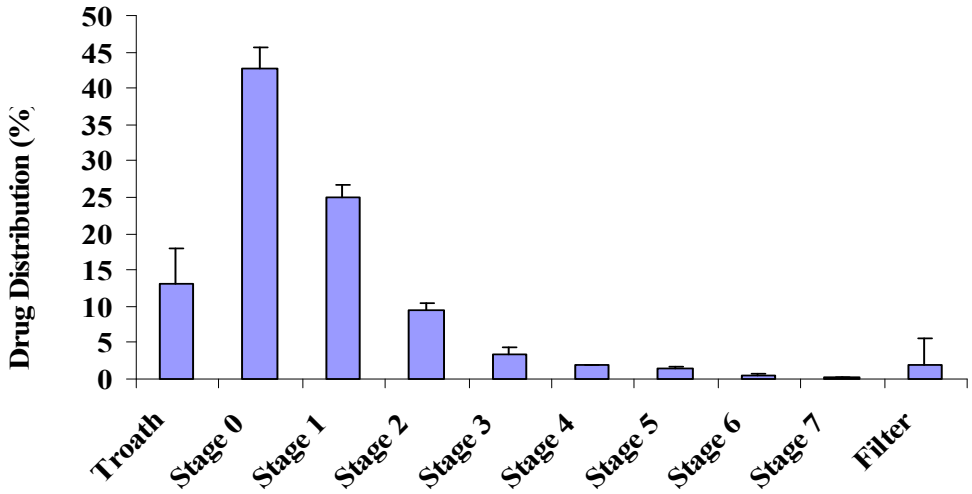

Figure 80. Aerodynamic parameters (Table), and drug distribution % in the ACI

PEG 4000 microparticles at 55 °C and 200 bar

Drug emitted for shot (mg)	0.91 ± 0.07
Recovery (%)	85.30 ± 4.34
MMAD (µm)	6.40 ± 0.77
Fine particle fraction (%)	31.90 ± 5.80
Fine particle dose (mg)	0.48 ± 0.09

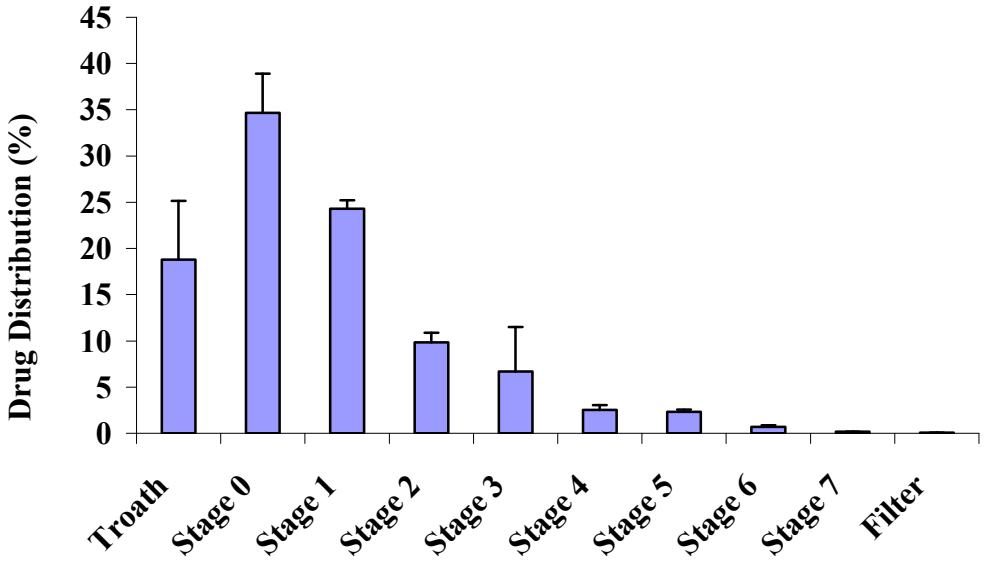

Figure 81. Aerodynamic parameters (Table), and drug distribution % in the ACI

PEG 4000 microparticles at 55 °C and 250 bar

Drug emitted for shot (mg)	0.99 ± 0.02
Recovery (%)	80.95 ± 4.97
MMAD (µm)	6.80 ± 0.36
Fine particle fraction (%)	32.17 ± 2.23
Fine particle dose (mg)	0.47 ± 0.05

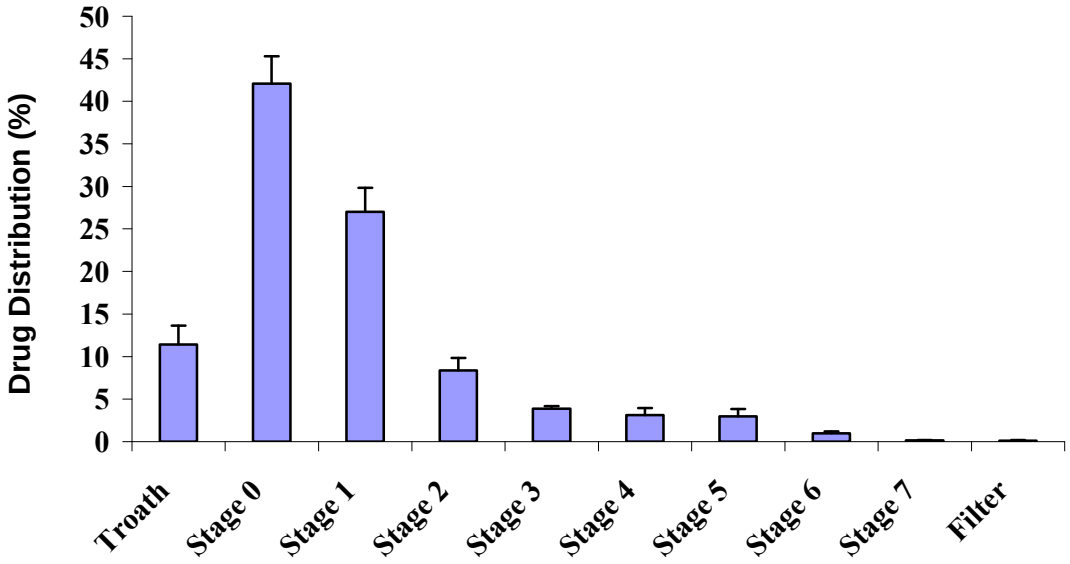

Figure 82. Aerodynamic parameters (Table), and drug distribution % in the ACI

All the obtained microparticles showed a better pulmonary deposition with respect to the raw material and the microparticles obtained with PEG 1500. The best results were obtained with PEG 4000 at 55 °C, 200 and 250 bar. In these cases the microparticles emitted with one single shot were 91 and 99 %, the mass median aerodynamic diameter were 6.4 and 6.8 µm, and the fine particle fraction were 31.9 and 32%, respectively. Interestingly, the fine particles dose was around 0.5 mg in both cases.

Therefore, the targeted dosing (1 mg) can be achieved by two shots each one performed with a different capsule.

4.7.5 Nasal deposition

To study the microparticles nasal deposition, a cast of the human nasal cavity, and a MIAT® insufflator were used. One shot per nostril was performed.
The nasal deposition was calculated as the percentage of the mass of the drug deposited on the cast (measured by HPLC) with respect to that emitted from the device. The microparticles delivered were calculated as the weight difference of the device before and after the discharging. The obtained results are reported in Table 15.

Table 15. % microparticles delivered, and % nasal drug deposition of the microparticles obtained at different pressures and temperatures

Operative conditions	% microparticles delivered	% nasal drug deposition
PEG 1500		
35 °C, 100 bar	93.9± 1.85	27.63 ± 6.82
35 °C, 150 bar	81.4 ± 5.3	20.85 ± 1.43
55 °C, 75 bar	73.4 ± 4.7	36.50 ± 11.90
55 °C, 150 bar	91.3± 2.6	40.33 ± 2.31
PEG 4000		
55 °C, 100 bar	91.2± 10.9	20.01 ± 0.57
35 °C, 150 bar	94.7± 2.8	24.78 ± 4.64
55 °C, 200 bar	100 ± 0	29.70 ± 0.99
55 °C, 250 bar	100 ± 0	21.71 ± 1.96

As expected, the microparticles obtained with PEG 1500 showed a better nasal deposition relative to PEG 4000 microparticles. The trend was somewhat opposite to the trend observed for pulmonary deposition. This can be mainly ascribed to the effect that optimal nasal deposition can be obtained with particles in the 50-150 μm range (De Ascentiis et al., 1996).

4.7.6 Crystallinity of the microparticles

PXRD measurements were carried out to calculate the crystallinity of the embedded active substance. Drug crystallinity plays a key role in aqueous solubility ad stability of solid dosage form.

The drug crystallinity in the microparticles was calculated on the basis of peak intensity at 9.5 2θ and quantified by comparing the peak intensity (area) of diazepam in microparticles with that of a PEG/diazepam mixtures of known concentrations taking into account the drug content in the microparticles. The linearity between the intensity and the concentration of the drug in such mixture was previously checked (Figure 83 and 84).

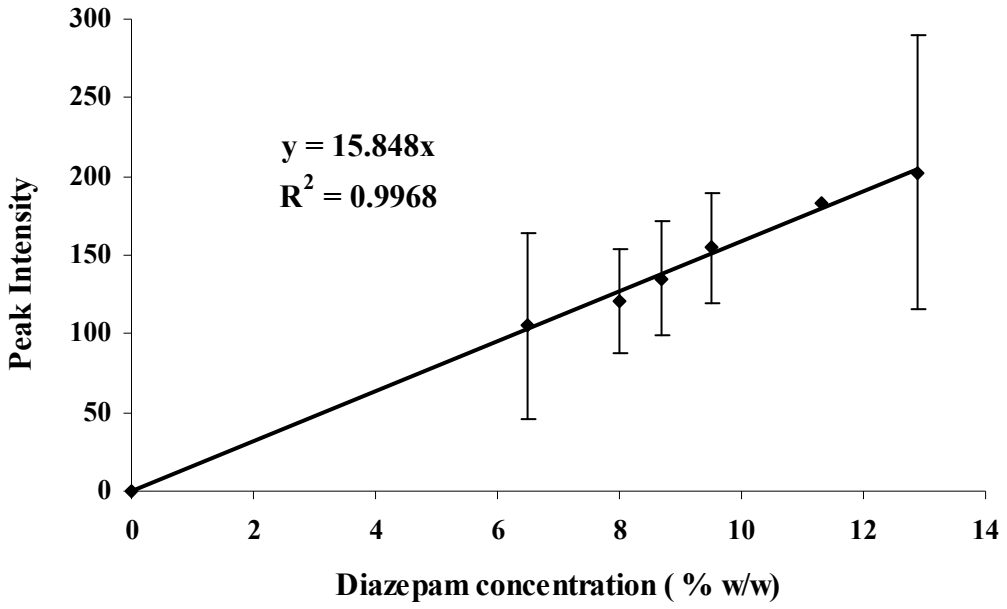

Figure 83. Peak intensity of diazepam *vs* drug concentration in PEG 1500/diazepam binary mixture

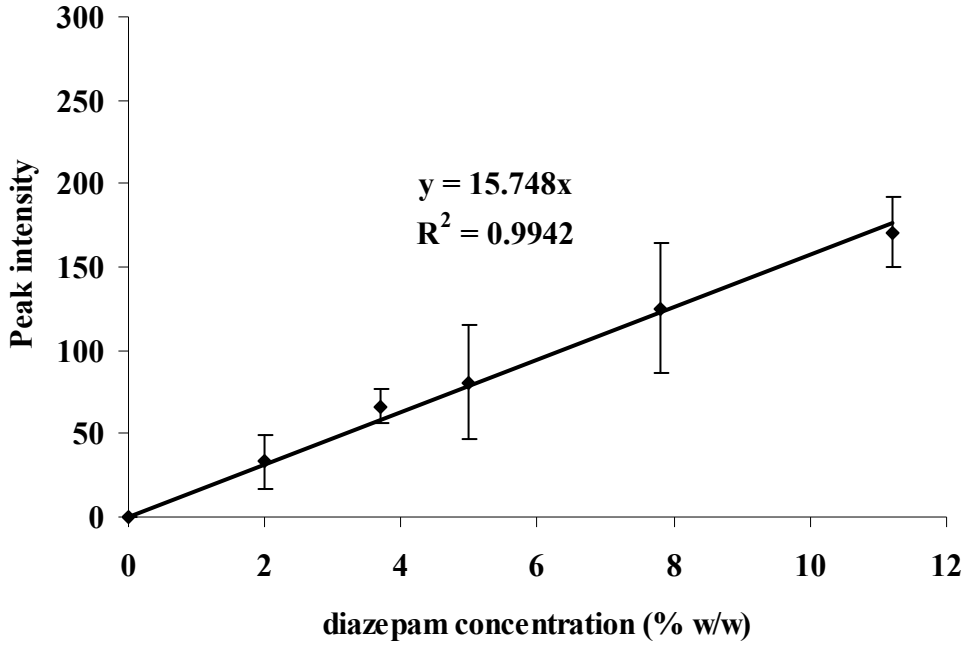

Figure 84. Peak intensity of diazepam *vs* drug concentration in PEG 4000/diazepam binary mixture

The slope of the two calibration curves were practically the same. In fact, it is reasonable to assume that the intensity of diazepam peak does not change with the change of the molecular weight of the polymer.

The crystallinity values of the diazepam embedded in microparticles are reported in Table16.

Table 16. Crystallinity of diazepam in the PEG 1500 and 4000 microparticles obtained at different temperature and pressure

Operative conditions	crystallinity (%)
PEG 1500	
35 °C, 100 bar	68.3 ± 9.8
35 °C, 150 bar	100 ± 11
55 °C, 75 bar	43.4 ± 8.6
55 °C, 150 bar	21.2 ± 0.3
PEG 4000	
55 °C, 100 bar	56.7 ± 0.9
55 °C, 150 bar	47.1 ± 5.4
55 °C, 200 bar	56.9 ± 3.3
55 °C, 250 bar	54.4 ± 3.8

Crystallinity of embedded drug ranged between 21.2-100 %. For the PEG 1500 it is possible to note that the crystallinity was higher for the microparticles obtained at 35 °C relative to those at 55 °C. This can be ascribed to the higher solubility of diazepam in SC-CO_2 at low temperature (see section 3.2.7). If the diazepam solubility is high a drug partioning between polymer and SC-CO_2 occurs (see section 4.5.1). When the system is suddenly depressurized the drug precipitates on the surface of the microparticles in form of microcrystal.

4.7.7 Dissolution

Dissolution studies of the microparticles obtained with PEG 4000 were conducted with a flow-through dissolution apparatus (USP 30) using distilled water at ambient temperature as dissolution medium.

Pure diazepam as raw material or micronized was compared with PEG 4000 particles, prepared with PGSS and a physical mixture (10 % w/w) prepared with micronized PEG 4000. The dissolution data expressed as mg of diazepam released in water as function of the time are reported in Figure 85.

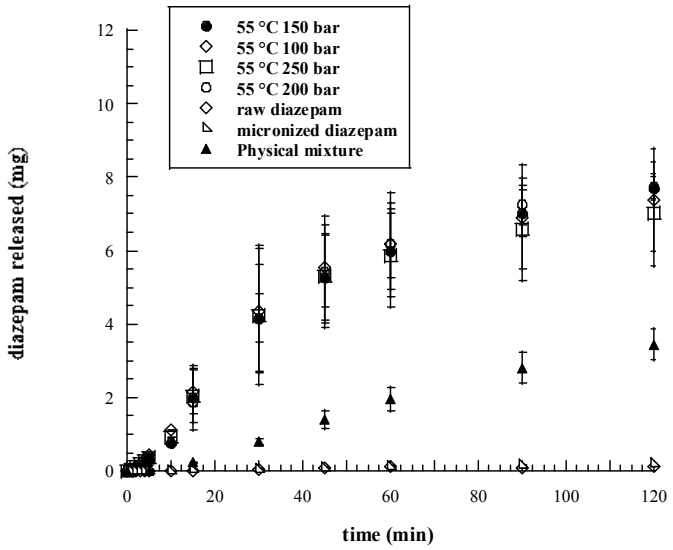

Figure 85. Amount of diazepam released from the microparticles (prepared at 55 °C and different pressure), physical mixture, raw and micronized diazepam as function of time

As expected by considering the low diazepam solubility in water, the amount of drug dissolved in two hours from raw material was practically negligible (dissolution rate ~ 0.15 mg/hour). No significant micronization effect could be observed. It is worthy to note that the dissolution profiles of the raw material (micronized and not micronized) were linear, indicating the achievement of the steady state. These conditions are generated when an active ingredient dissolves at a constant rate giving rise a solution with a constant concentration. Since the experiments were carried out in perfect sink conditions, the above reported amount of drug dissolved per unit time represent the highest dissolution rate achievable from pure diazepam in this conditions.

A better dissolution rate, nearly 2 mg per hour, was obtained with the physical mixture, due to the solubilising effect of the PEG (Doshi et al., 1997).

A dramatic increase of the diazepam dissolution rate was observed for all prepared particles. All microparticles released 60 % of the dose (10 mg) in 60 minutes and nearly 80 % of the dose in two hours. No significant difference was observed among the microparticles prepared with various experimental conditions.

The great improvement of the drug dissolution with microparticles relative to the physical mixture can not be samply ascribed to a difference in the particle size, in fact with the raw material the reduction of the particles proved to have a significant effect. Therefore, the observed difference should be attributed to the embedding of a drug with a reduced crystallinity into a highly porous particles.

5. Conclusions

In this work a preformulation study was carried out to set-up the PGSS process which allowed the production of microparticulate drug delivery system.
The phase behaviour of the binary systems PEG/CO_2, diazepam/CO_2 and the ternary system PEG/CO_2/diazepam were studied to find the appropriate process conditions to carried out the PGSS.

Both PEG 1500 swelling under pressurized CO_2, and the CO_2 solubility in PEG 1500 were measured. It was found that the polymer swells upon CO_2 absorption. While the pressure increase determines an increase in the polymer volume, the temperature does not have a significant effect.
The solubility of CO_2 in PEG 1500 was influenced by both pressure and temperature; in general the CO_2 showed a great affinity for the molten PEG. In particular, its solubility in the polymer remarkably increases with pressure until the CO_2 critical value, then it approaches a plateau.
The in situ high-pressure measurement using ATR-IR spectroscopy proved to be a powerful tool for measuring directly and simultaneously the degree of swelling of the polymer and the absorption of CO_2. The depression of the melting point of the polymer under the action of the SC-CO_2 as well as the interaction between polymer and CO_2 are put into evidence.

The melting point depression was measured both for PEG 1500 and 4000 with the high pressure view cell. In the 1-2 bar pressure range, the melting point of both polymers slightly increases, while from 2 to 87, and to 65 bar for PEG 1500 and PEG 4000, respectively, a decrease of melting point can be observed. Then, no further change is observed up to 200 bar.

The PEG 1500 shows solubility in SC-CO_2 in the order of 10^{-6} mole fraction in the pressure interval 100-400 bar. Isothermal solubility increases with pressure, while at fixed pressure it decreases with temperature, likely due to CO_2 density changes. At the same density, temperature exhibits a positive effect on PEG 1500 solubilization in the SC gas.
The heuristic model proposed by Giddings and co-workers proved to be a useful and simple tool to predict the maximum concentration achievable by the polymer in the dense

gas at a given temperature, as well as to quantify the polymer concentration at low pressures, where its experimental determination can be extremely difficult.

Diazepam shows a relatively high solubility (in the order of 10^{-4} mole fraction at 180 bar) in supercritical CO_2 in particular at the lower studied temperature (35 °C).
This high solubility implies a remarkable partitioning effect between the drug dissolved into the polymer and in supercritical phase.

The diazepam solubility in PEG 1500 under SC-CO_2 varies between 10 to 27 % w/w in the 35-95 °C temperature range.
These figures suggest the suitability of a supercritical CO_2 process for preparing microparticles of PEG and diazepam with adequate drug dosage.

PEG plasticization by CO_2 can be exploited to carry out the PGSS process. The measurement of the solubility of diazepam in PEG in the presence of CO_2 made possible the production of PEG microparticles loaded with 10-15 % w/w of diazepam.
The microparticles obtained showed a different behaviour when tested for nasal, and pulmonary deposition *in vitro*. Suitable pulmonary deposition was obtained with the PEG 4000 microparticles due to their high porosity, low agglomeration, and small size. Better nasal deposition was obtained with PEG 1500 microparticles relative to PEG 4000, because of the greater particles dimensions of the PEG 1500 microparticles.
Furthermore, the diazepam embedded into the microparticles shows a higher dissolution rate with respect to the raw, micronized material, and physical mixture.
Finally, it ca be concluded that, from the reported data, the PGSS is a good technique for the production of microparticulate drug delivery systems of PEG and diazepam with adequate drug dosage, for administration via transmucosal or transepitelial route characterized by an improved drug dissolution rate and, likely, to a rapid onset of action.

References

ALAVI, S. H., RIZVI, S. S. H. & HARRIOTT, P. (2003a) Process dynamics of starch-based microcellular foams produced by supercritical fluid extrusion. I: model development. *Food Res. Int.,* 36**,** 309-319.

ALAVI, S. H., RIZVI, S. S. H. & HARRIOTT, P. (2003b) Process dynamics of starch-based microcellular foams produced by supercritical fluid extrusion. II: numerical simulation and experimental evaluation. *Food Res. Int. ,* 36 321-330.

BAE, Y. C. (1996) Gas plasticization effect of carbone dioxide for polymeric liquid. *Polym.,* 37**,** 3011-3017.

BALDWIN, D. F., PARK, C. B. & SUH, N. P. (1996) A microcellular processing study of poly(ethylene terephthalate) in the amorphous and semicrystalline states. Part I: Microcell nucleation. *Polym. Eng. Sci.,* 36**,** 1437-1445

BETTINI, R., BONASSI, L., CASTORO, V., ROSSI, A., ZEMA, L., GAZZANIGA, A. & GIORDANO, F. (2001) Solubility and conversion of carbamazepine polymorphs in supercritical carbon dioxide. *Eur J Pharm Sci,* 13**,** 281-6.

BRISTOW, S., SHEKUNOV, T., SHEKUNOV, B. Y. & YORK, P. (2001) Analysis of the supersaturation and precipitation process with supercritical CO_2. *J. Supercrit. Fluids* 21**,** 257-271.

BRUNNER, E. (1904) Reaction velocity in heterogeneous systems. *Z. Phys. Chem. ,* 47**,** 56-102.

BRUNNER, G. (1994) *Gas Extraction,* New York, Steinkopff Darmstadt Springer.

BYRAPPAB, K., OHARAA, S. & ADSCHIRIA, T. (in press) Nanoparticles synthesis using supercritical fluid technology - towards biomedical applications *Adv. drug del. rev.*

CAGNIARD DE LATOUR, C. (1822) The hydrodynamic properties of an SCF also lie between those of a liquid and a gas. *Ann.Chim.Phys,* 21127-178.

CHAN, K. L. & KAZARIAN, S. G. (2003) New opportunities in micro- and macro-attenuated total reflection infrared spectroscopic imaging: spatial resolution and sampling versatility. *Appl Spectrosc,* 57**,** 381-9.

CHARBIT, G., BADENS, E. & BOUTIN, O. (2004) *Methods of particle production , in: Supercritical fluid technology for drug product development,* New York,, P. York, U.B. Kompella, B.Y. Shekunov

CZUBRYT, J. J., MYERS, M. N. & GIDDING, J. C. (1970) Solubility in dense carbon dioxide gas in the range 270-1900 atmospheres. *J. Physic. Chem. ,* 74**,** 4260-4266.

DANESHVAR, M. & GULARI, E. (1989a) Partition coefficients of poly(ethylene glycol)s in supercritical carbon dioxide. IN SOICIETY, A. C. (Ed.) *ACS symposium series 406.* Washington, DC, American chemical soiciety.

DANESHVAR, M. & GULARI, E. (1989b) Supercritical fluid science and technology. *ACS Symposium Series 406; America Chemical Society: Washington DC***,** 72-85.

DANESHVAR, M., KIM, S. & GULARI, E. (1990) High-pressure phase equilibria of poly(ethylene glycol)-carbon dioxide systems. *J. Phys. Chem. ,* 94**,** 2124-2128.

DE ASCENTIIS, A., BETTINI, R., CAPONETTI, G., CATELLANI, P., PERACCHIA, M. T. & COLOMBO, P. (1996) Delivery of nasal powders of b-cyclodextrin by insufflation. *Pharm Res,* 13**,** 734-738.

DOSHI, D. H., RAVIS, W. R. & BETAGERI, G. V. (1997) Carbamazepine and polyethylene glicol solid dispersion preparation, in vitro dissolution, and characterisation. *Drug Dev Ind Pharm,* 23**,** 1167-1176.

DUARTE, A. R., COSTA, M. S., SIMPLICIO, A. L., CARDOSO, M. M., DUARTE, C. M., (2006) Preparation of controlled release microspheres using supercritical fluid technology for delivery of anti-inflammatory drugs. *Int J Pharm,* 308**,** 168-74.

FLICHY, N. M. B., KAZARIAN, S. G., LAWERENCE, C. J. & BRISCOE, B. J. (2002) An ATR-IR study of poly(dimethylsiloxane) under high-pressure carbon dioxide: simultaneous measurement of sorbtion and swelling. *J. Phys. Chem. ,* B 106 654-759.

FOLIE, B. & RADOSZ, M. (1995) Phase equilibria in high-pressure polyethylene technology *Ind. Eng. Chem. Res.,* 34**,** 1501-1516.

FRICKE, J. & TILLOTSON, T. (1997) Aerogels: production, characterization, and applications. *Thin Solid Films,* 297**,** 212-223.

FRUIJTIER-PÖLLOTH, C. (2005) Safety assessment on polyethylene glycols (PEGs) and their derivates as used in cosmetic products. *Toxicology,* 214**,** 1-38.

FUNAMI, E., TAKI, K. & OHISHIMA, M. (2007) Density measurament of polymer/CO_2 single-phase solution at high temperature and pressure using a gravimetric method *J. Appl. Polym. Sci,* 105**,** 3060-3068.

GALIA, A., ABDULJAWAD, M., SCIALDONE, O. & FILARDO, G. (2006) A novel gas chromatographic method to measure sorption of denses gases into polymers. *AIChE,* 52**,** 2243-2253.

GALLAGHER, P. M., COFFEY, M. P., KRUKONIS, V. J. & KLASUTIS, N. (1989) *Gas antisolvent recrystallization: new process to recrystillize compounds insoluble in supercritical fluids,* Washington, DC, American chemical society.

GIDDINGS, J. C., MYERS, M. N., MCLAREN, L. & KELLER, R. A. (1968) High pressure gas chromatography of non-volatile species, compressed gas is used to cause migration of intractable solutes. *Science,* 162**,** 67-73.

GOURGOUILLON, D., AVELINO, H. M. N. T., FARELEIRA, J. M. N. A. & NUNES DA PONTE, M. (1998) Simultaneous viscosity and density measurement of supercritical CO2-saturated PEG 400. *J. Supercrit. Fluids* 13**,** 177-185.

GOURGOUILLON, D. & NUNES DA PONTE, M. (1999) High pressare phase equilibria for poly(ethylene glicol)s + CO2: experimental results and modelling. *Phys. Chem. Chem. Phys. ,* 1**,** 5369-5375.

GRASER, F. & WICKENHAEUSER, G. (1982) Conditioning of finely divided crude organic pigments.

GREF, R. (2001) Pegylated polymers for "stealth" nanoparticles. *New trends in polymers for oral and parenteral administration fron design to receptors.* Paris.

GREF, R., DOMB, A., QUELLEC, P., BLUNK, T., MÜLLER, R. H., VERBAVATZ, J. M. & LANGER, R. (1995) The controlled intravenous delivery of drugs using PEG-coated sterically stabilized nanospheres. *Adv. drug del. rev.,* 16**,** 215-233.

GROSS, J., CORONADO, P. R. & HRUBESH, L. W. (1998) Elastic properties of silica aerogels from a new rapid supercritical extraction process. *J. Non-Cryst. Solids,* 225 282-286.

GUADAGNO, T. & KAZARIAN, S. G. (2004) High-pressure CO_2-expanded solvents: simultaneous measurement of CO_2 sorption and swelling of liquid polymers with in-situ near-IR spectroscopy. *J. Phys. Chem. B,* 108**,** 13995-13999.

HANNA, M. & YORK, P. (1995) WO 95/01221.

HANNAY, J. B. & HOGARTH, J. (1879) On the solubility of solids in gases. *Proc. Roy Soc.,* 29**,** 324-327.

HAO, J., WHITAKER, M. J., SERHATKULU, G., SHAKESHEFF, K. M. & HOWDLE, S. M. (2005) Supercritical fluid assisted melting of poly(ethylene glycol): a new solvent-free route to microparticles. *J Mater Chem,* 15**,** 1148-1153.

HARIHARAN, D., PEPPAS, N., BETTINI, R. & COLOMBO, P. (1994) Mathematical analysis of drug delivery from swellable systems with partial physical restrictions or impermeable coatings. *Int J Pharm,* 112**,** 47-54.

HARRICK, N. J. (1987) *Internal Reflection Spectroscopy,* New York, Harrick Scientific Corporation, John Wiley and Sons, Inc.

HAY, J. N., KHAN, A. & (2002) Environmentally friendly coatings using carbon dioxide as the carrier medium *J. Mater. Sci.,* 37**,** 4743-4752.

HILDEBRAND, J. H. & SCOTT, R. L. (1950) *The solubility of Nonelectrolytes,* New York, Reynolds.

HILLMANN, R. & BÄCHMANN, K. (1995) Extraction of pesticides using supercritical trifluoromethane and carbon dioxide. *Short Communication J. Chrom. ,* A 695**,** 149-154.

HTTP://RSB.INFO.NIH.GOV/IJ/.

HTTP://WWW.NIST.GOV/DATA/NIST23.HTM.

JUNG, J. & PERRUT, M. (2001) Particle design using supercritical fluids: Literature and patent survey. *J. Supercrit. Fluids* 20**,** 179-219.

KAMIYA, Y., HIROSE, T., MIZOGUCHI, K. & NAITO, Y. (1986) Gravimetric study of high pressure sorption of gases in polymers. *J. Polym. Sci. Part B: Polym. Phys.,* 24**,** 1525-1539.

KAYRAK, D., AKMAN, U. & HORTAÇSU, Ö. (2003) Micronisation of ibuprofen by RESS. *J. Supercrit. Fluids* 26**,** 17-31.

KAZARIAN, S. G. (2000) Polymer processing with supercritical fluids. *Polym. Sci. Ser. C* 42**,** 78-101.

KAZARIAN, S. G. (2002) Polymers and supercritical fluids: opportunities for vibrational spectroscopy. *Macromol. Symp. ,* 184**,** 215-228.

KAZARIAN, S. G., SAKELLARIOS, N. & GORDON, C. M. (2002) High-pressure CO_2-induced reduction of the melting temperature of ionic liquids. *Chem Commun (Camb)***,** 1314-5.

KAZARIAN, S. G., VINCENT, M. F., BRIGHT, F. V., LIOTTA, C. L. & ECKERT, C. A. (1996) Specific intermolecular interaction of carbon dioxide with polymers. *J. Am. Chem. Soc. ,* 118**,** 1729-1736.

KIBBE, A. H. (2000) *Handbook of pharmaceutical excipients,* London, Pharm. Press.

KING, M. B. & BOTT, T. R. (1993) *Extraction of natural products using near-critical solvents,* Glasgow, U.K., Blackie Academic and Professional.

KLEINRAHM, R. & WAGNER, W. (1986) Measurament and correlation of the equilibrium liquid and vapour densities and the vapour pressure along the coexistence curve of methane *J. Chem. Thermodyn.,* 18**,** 739-760.

KNEZ, Z., SKERGET, M., SENCAR-BOZIC, P. & RIZNER, A. (1995) Solubility of nifedipine and nitredipine in supercritical CO_2. *J. Chem. Eng. Data,* 40**,** 216-220.

KOGA, T. Ù., JEROME, J., RAFAILOVICH, M. H., CHU, B., DOUGLAS, J. & SATIJA, S. (2006) Supercritical fluid processing of polymer thin films: an X-ray study of molecular-level porosity. *Adv. coll. inter. sci.,* 128**,** 217-226

KOMPELLA, U. B. & KOUSHIK, K. (2001) Preparation of drug delivery systems using supercritical fluid technology. *Crit. Rev. Therap. Drug Carrier Systems* 18**,** 173-199.

KRUKONIS, V. (1984) Supercritical fluid nucleation of difficult-to-comminute solids. *Proc. Annual Meeting AIChE,* paper 140 f, T-214

KUKOVA, E., PETERMAN, M. & WEIDNER, E. (2003) Phase behaviour (S-L-G) and fluiddynamic properties of high viscous polyethylene glycols in the presence of compressed carbon dioxide. *International symposium on supercritical fluids.* Versailles, 1547-1552.

LIAN, Z., EPSTEIN, S. A., BLENK, C. W. & SHINE, A. D. (2006) Carbon dioxide-induced melting point depression of biodegradable semicrystalline polymers *J. Supercrit. Fluids* 39**,** 107-117.

LIU, K. & KIRAN, E. (1999) Kinetics of pressure-induced phase separation (PIPS) in solutions of polydimethylsiloxane in supercritical carbon dioxide: crossover from nucleation and growth to spinodal decomposition mechanism. *J. Supercit. Fluids,* 16**,** 59-79.

LIU, K. & PARSONS, J. L. (1969) Solvent effects on the preferred conformation of Poly(ethylene glycols). *Macromolecules,* 5**,** 529-533.

LOPES, J. A., GOURGOUILLON, D., PEREIRA, P. J., RAMOS, A. M. & NUNES DA PONTE, M. (2000) On the effect of polymer fractionation on phase equilibrium in CO2 + poly(ethylene glycol)s systems. *J. Supercrit. Fluids* 16**,** 261-267.

MAIELLA, P. G., SCHOPPELEREI, J. W. & BRILL, T. B. (1999) Spectroscopy of hydrothermal reaction. Part XI: infrared absorptivity of CO_2 and N_2O in water at elevated temperature and pressure. *Appl. Spectr. ,* 53**,** 351-355.

MEAKIN, B. J., WOODCOCK, P. M., SEGU, A., NICCOLAI, F. & VECCHIO, C. (1996) Evaluation of the resistance to airflow through Turbospin in comparison with dry powder inhalers available on the market. *Boll. Chim. Farmaceutico-Anno* 135**,** 107-109.

MEZIANI, M. J., PATHAK, P., BEACHAM, F., ALLARD, L. F. & SUN, Y.-P. (2005) Nanoparticle formation in rapid expansion of water-in-supercritical carbon dioxide microemulsion into liquid solution. *J. Supercrit. Fluids* 34**,** 91-97.

MOONEY, D. J., BALDWIN, D. F., SUH, N. P., VACANTI, J. P. & LANGER, R. (1996) Novel approach to fabricate porous sponges of poly(D,L-lactic-co-glycolic acid) without the use of organic solvents. *Biomaterials,* 17**,** 1417-22.

MOREL, G. & PAUL, D. R. (1982) CO2 sorption and transport in miscible poly(phenylene oxide)/polystyrene blends. *J. Membr. Sci.,* 10**,** 273-282.

MOSHASHAEE, S., BISRAT, M., FORBES, R. T., QUINN, E. A., NYQVIST, H. & YORK, P. (2003) Supercritical fluid processing of proteins: lysozyme precipitation from aqueous solution. *J Pharm Pharmacol,* 55**,** 185-92.

NAKATANI, T., OHGAKI, K. & KATAYAMA, T. (1989) Solubilities of Indole Derivatives in Supercritical fluids *J. Supercrit. Fluids* 2**,** 9-14.

NALAWADE, S. P., PICCHIONI, F. & JANSSEN, L. P. B. M. (2006a) Supercritical carbon dioxide as a green solvent for processing polymer melts: processing aspects and application. *Prog. Polym. Sci.,* 31**,** 19-43.

NALAWADE, S. P., PICCHIONI, F., MARSAM, J. H. & JANSSEN, L. P. B. M. (2006b) The FT-IR studies of the interaction of CO_2 and polymers having different chain groups. *J. Supercrit. Fluids,* 36**,** 236-244.

NERNST, W. (1904) Theory of reaction velocity in heterogeneous systems. *Z. Phys. Chem.,* 47**,** 52-55.

NISHIKAWA, K. & MORITA, T. (2000) Inhomogenity of molecular distribution in supercritical fluids. *Chem. Phys. Lett.,* 316**,** 238-242.

NOYES, A. A. & WHITNEY, W. R. (1897) The rate of solution of solid substances in their own solutions. *J. Am. Chem. Soc. ,* 19 930-934.

PALAKODATY, S. & YORK, P. (1999) Phase behavioral effects on particle formation processes using supercritical fluids. *Pharm. Res.,* 16**,** 976-985.

PARCHER, J. F. (1982) Trace pulse chromatography: a review and prospects. *J. Chromatogr.,* 251**,** 281-288.

PASQUALI, I., ANDANSON, J.-M., KAZARIAN, S. G. & BETTINI, R. (in press-a) Measurament of CO_2 sorption and PEG 1500 swelling by ATR-IR spectroscopy. *J. Supercit. Fluids, in press*.

PASQUALI, I., BETTINI, R. & GIORDANO, F. (2006) Solid-state chemistry and particle engineering with supercritical fluids in pharmaceutics. *Eur J Pharm Sci,* 27**,** 299-310.

PASQUALI, I., BETTINI, R. & GIORDANO, F. (in press-b) Supercritical fluid technologies: an innovative approach for the manipulation of the solid-state of pharmaceuticals. *Adv. drug del. rev.,* in press.

PASQUALI, I., COMI, L., PUCCIARELLI, F. & BETTINI, R. (in press-c) Swelling, melting point reduction, and solubility of PEG 1500 in supercritical CO_2. *Int J Pharm*.

PERRUT, M. (2000) Supercritical fluid applications: industrial development and economic issue. *Ind. Eng. Chem. Res.,* 39**,** 4531-4535.

PERRUT, M. (2003) Supercritical fluid applications in materials science. *Curr. Opin. Solid State Mater Sci.,* 7**,** 319

PERRUT, M. & REVERCHÔN, E. (2000) Proc. of the 7th Meeting on Supercritical Fluids.

PERRUT, M. & SUBRA, P. (1998) Proc. of the 5th Meeting on Supercritical Fluids.

PHILLIPS, E. M. & STELLA, V. J. (1993) Rapid Expansion from supercritical solutions: application to pharmaceutical processes. *Int. J. Pharm. ,* 94**,** 1-10.

POLIAKOFF, M., GEORGE, M. W. & HOWDLE, S. M. (1999) Proc. of the 6th Meeting on Supercritical Fluids.

PRAJAPATI, D. & GOHAIN, M. (2004) Recent advances in the application of supercritical fluids for carbon-carbon bond formation in organic synthesis. *Tetrahedron* 60**,** 815-883.

REVERCHÔN, E. (2002) Supercritical-assisted atomization to produce micro- and/or nano particles of controlled size and distribution. 41**,** 2405-2411.

RIZVI, S. S. H. (1994) *Supercritical fluid processing of food and biomaterials,* London U.K., Blackie Academic& Professional.

SAKO, S., SHIBATA, K., OHGAKI, K. & KATAYAMA, T. (1989) Solubilities of indole, skatole, and 5-Methoxyindole in supercritical fluids. *J. Supercrit. Fluids,* 2**,** 3-8.

SARRADE, S., GUIZARD, C. & RIOS, G. M. (2003) New applications of supercritical fluids and supercritical fluids process in separation. *Sep. Purif. Technol. ,* 32**,** 57-63.

SHEKUNOV, B. Y., HANNA, M. & YORK, P. (1999) Crystallization process in turbulent supercritical flows, . *J. Cryst. Growth,* 198/199 1345-1351.

SHIEH, Y.-T. & YANG, H.-S. (2005) Morphological changes of polycaprolactone with high-pressure CO2 treatment *J. Supercrit. Fluids,* 33**,** 183-192.

SIEVERS, R. E. & KARST, U. (2000) Methods and apparatus for fine particle formation.

STASSI, A., BETTINI, R., GAZZANIGA, A., GIORDANO, F. & SCHIRALDI, A. (2000) Assessment of solubility of ketoprofen and vanilic acid in supercritical CO2 under dynamic conditions. *J. Chem. Eng. Data,* 45**,** 161-165.

VAN KONYNENBURG, P. H. & SCOTT, R. L. (1980) *Phil. Trans. R.* London.

VASUKUMAR, K. & BANSAL, K. A. (2003) Supercritical fluid technology in pharmaceutical research. *CRIPS* 4**,** 8-12.

VENTOSA, N., SALA, S. & VECIANA, J. (2001) Depressurization of an expanded liquid organic solution (DELOS): a new procedure for obtaining submicron- or micron-sized crystalline particles. *Cryst. Growth Des. ,* 1**,** 299-303.

VENTOSA, N., SALA, S. & VECIANA, J. (2003) DELOS process: a crystallization technique using compressed fluids 1. Comparison to the GAS crystallization method. *J. Supercrit. Fluids* 26**,** 33-45.

WEIDNER, E., PETERMANN, M., BLATTER, K. & REKOWSKI, V. (2001) Manufacture of powder coatings by spraying of gas-enriched melts. *Chem. Eng. Technol.,* 24**,** 529-533.

WEIDNER, E., WIESMET, V., KNEZ, Z. & SKERGET, M. (1997) Phase equilibrium (solid-liquid-gas) in polyethylenglicol-carbon dioxide systems. *J. Supercrit. Fluids* 10**,** 139-147.

WERLING, J. O. & DEBENEDETTI, P. G. (1999) Numerical modelling of mass transfer in the supercritical antisolvent process. *J. Supercrit. Fluids,* 16 167-181.

WIESMET, V., WEIDNER, E., BEHME, S., SADOWSKI, G. & ARLT, W. (2000) Measurement and modelling of high-pressure phase equilibria in the systems polyethyleneglycol (PEG)-propane, PEG-nitrogen and PEG-carbon dioxide. *J. Supercrit. Fluids* 17**,** 1-12.

WISSINGER, R. G. & PAULAITIS, M. E. (1987) Swelling and sorption in polymer-CO_2 mixtures at elevated pressures. *J. Polym. Sci. Part B: Polym. Phys.,* 25**,** 2497-2510.

XIONG, Y. & KIRAN, E. (2000) Kinetics of pressure-induced phase separation (PIPS) in polystyrene+methylcyclohexane solutions at high pressure. *Polym.,* 41**,** 3759-3777.

YORK, P. (1999) Strategies for particle design using supercritical fluid technologies. *PSTT* 2**,** 430-440.

YORK, P., HANNA, M., SHEKUNOV, B. Y. & HUMPHREYS, G. O. (1998) Microfine particle formation by SEDS (Solution Enhanced Dispersion by Supercritical Fluids): scale up by design. *Proc. Resp. Drug Delivery VI* 169-175.

ZHUANG, W. & KIRAN, E. (1998) Kinetics of pressure-induced phase separation (PIPS) from polymer solutions by time-resolved light scattering. Polyethylene+*n*-pentane. *Polym. ,* 39**,** 2903-2915.

Acknowledgements

This work would not have been possible without the help of many people.
Many thanks to Professor Ruggero Bettini, my supervisor, who supported me with an invaluable assistance, support and guidance during the research work and thesis revision.

I wish to express my sincere thanks to Professor Ferdinando Giordano for sharing with me his great knowledge and expertise.

I gratefully thank Prof. Sergei G. Kazarian for giving me the opportunity to carry out part of this research work (ATR-FTIR spectroscopy) at Department of Chemical Engineering and Chemical Technology, Imperial College of Science, Technology and Medicine of London as well as Dr. Jean-Michel Andanson for his kind assistance.

Stefania, Lidia, Francesca, Letizia, and Roberta are kindly acknowledge for their help in data collection.

This work was supported in part by a grant from MUR through its PRIN 2006 program.